Relationship Between Cortical Acetylcholine, Neurophysiologic Complexity, and the Level of Consciousness

by

Michael A. Brito

A dissertation submitted in partial fulfillment
of the requirements for the degree of
Doctor of Philosophy
(Neuroscience)
in the University of Michigan
2021

Doctoral Committee:

Professor George A. Mashour, Chair
Assistant Professor Omar Ahmed
Associate Professor Cynthia Chestek
Associate Professor Shelly Flagel
Assistant Professor Dinesh Pal

Michael A. Brito

brito@umich.edu

ORCID iD: 0000-0002-0352-2598

Dedication

This dissertation is dedicated to my those who have loved me, nurtured me, and otherwise guided me thus far through this painful, blissful, and humbling journey of self-actualization.

To my family, who have been the source of both immense love and many difficult lessons in life. Generations have worked through poverty, sickness, incarceration, and suffering, sacrificing to build the path that led me to the unlikely world of science. This degree is a testament to the strength and internal will instilled in me by you, and above all else I pray that it marks the beginning of something better for us all.

To Sophia, a wonderful partner who has supported me unconditionally and shown me a love greater than I could have ever hoped for in this world. You have been the single greatest source of joy in my life, and I couldn't have done this without you. And of course, to our furry children Hannibal and Nai Palm, who have been the source of much affection and levity in difficult times.

Acknowledgements

I must first acknowledge the scientific mentors who supported my unlikely entrance into academia. Dr. Jonathan Schooler and Dr. Aaron Ettenberg, without your guidance, kindness, and genuine acceptance of me in this alien world, I would never have made it this point. To all my friends in the CCS and NGP – particularly Jon Dean, who was the source of much laughter and strangeness all over the world – I am so grateful for the gracious love and positivity you have all provided me over these years. Dr. Tiecheng Liu and Dr. Duan Li, you have been incredible teachers of the craft and your work ethic is inspiring. Chloe Rybicki-Kler and Christopher Fields, you were the backbone of some of the most difficult work that went into this degree, and I hope I have given you half as much as you've given me. This degree would not have been possible without the kindness, guidance, and genuine investment that my committee members Drs. Shelly Flagel, Cynthia Chestek, and Omar Ahmed have given me. Finally, to my mentors Drs. George Mashour and Dinesh Pal, I am eternally indebted to you two for having the patience to nurture this very rough and unformed human being under your tutelage. I wish I could properly express the gratitude I hold and the hope looking forward that this degree has given my family and I, it means the world to us.

I would like to thank the administrators within the Neuroscience Graduate Program, Department of Anesthesiology, and Rackham Graduate School, who have literally kept me fed, clothed, and paid throughout these years. This research was made possible by the generous funding of the National Science Foundation Graduate Research Fellowship DGE 1256260, the National Institutes of Health R01 GM111293, the University of Michigan Department of Anesthesiology, and the Rackham Merit Fellowship.

Dearest in my heart, I would like to acknowledge the sacrifice of the laboratory rats whose lives were taken for this research. Science has given me the perspective to better appreciate their value as sentient beings one and the same, and I pray that their sacrifice may in some way contribute to the greater benefit of all sentient beings.

Table of Contents

List of Tables

List of Figures

Abstract

Contemporary theories have argued that the level of consciousness can be approximated by cortical complexity or the strength of frontoparietal connectivity. In support of this, studies have demonstrated suppressed brain state repertoire and frontoparietal connectivity during loss of consciousness. Comparatively little focus has been placed on understanding the neurobiological mechanisms relating to these computational measures of consciousness, leaving their relationship to underlying neurochemical processes unknown. Levels of acetylcholine in the cortex have been shown to relate to the capacity for consciousness, but a relationship between cortical acetylcholine and cortical dynamics such as neurophysiologic complexity has not been investigated. We therefore tested the hypothesis that cortical cholinergic tone would correlate with neurophysiologic complexity.

A prior study from our laboratory assessed the effects of cholinergic or noradrenergic stimulation of the prefrontal or parietal cortices in anesthetized rats, finding that only cholinergic stimulation of the prefrontal cortex restored wakefulness during anesthesia. While only prefrontal cholinergic neurotransmission was implicated in regulating the level of consciousness, all stimulation cohorts displayed an activated electroencephalogram (EEG) and elevations in cortical acetylcholine relative to the pre-stimulation anesthetized state. Therefore, in our first data chapter we used EEG data from Pal et al. 2018 to test if prefrontal cholinergic neurotransmission regulates the level of consciousness through changes in neurophysiologic complexity and frontoparietal connectivity. As expected, sevoflurane anesthesia suppressed neurophysiologic complexity and corticocortical connectivity relative to wakefulness. Unexpectedly, however, the strength of frontoparietal connectivity remained suppressed in all cohorts following stimulation, notwithstanding the presence or absence of wakefulness. In contrast, complexity was elevated in all cohorts, correlating instead with spectral features such as EEG activation and periods of elevated cortical acetylcholine. We conclude that prefrontal cholinergic neurotransmission does not regulate the level of consciousness through

frontoparietal connectivity, and that neurophysiologic complexity may instead index EEG activation or cortical acetylcholine.

In our next data chapter, we explored the relationship between EEG complexity, spectral contents of the signal, and the level of consciousness by contrasting the effects of ketamine and propofol anesthesia over three bandwidths (0.5-175 Hz, 65-175 Hz, and 0.5-55 Hz). We demonstrate bandwidth-dependent properties of both ketamine and propofol on complexity, demonstrating that ketamine anesthesia suppresses complexity in the 65-175 Hz bandwidth, while propofol does not. Using a normalization method to average out spectral influence on the signal, we demonstrate comparable effects of ketamine and propofol anesthesia on 0.5-175 Hz and 0.5-55 Hz complexity that are dissociable from spectral EEG properties.

In our final data chapter, we leveraged the dose-dependent properties of the dissociative anesthetics ketamine and nitrous oxide to characterize the relationship between cortical acetylcholine levels, neurophysiologic complexity, and frontoparietal connectivity (25-55 Hz, 85-125 Hz, 125-175 Hz). During subanesthetic ketamine and nitrous oxide induction, we report periods of elevated prefrontal and parietal cortical cholinergic tone, neurophysiologic complexity, and frontoparietal connectivity in the 125-175 Hz bandwidth. During nitrous oxide sedation, cortical acetylcholine levels and neurophysiologic complexity were concomitantly suppressed with the level of arousal. Our findings demonstrate a correlation between cortical acetylcholine levels, neurophysiologic complexity, and frontoparietal connectivity in the high gamma bandwidth.

In sum, our findings establish acetylcholine as a neurochemical correlate of cortical dynamics purported to relate to consciousness. While future causal studies are necessary, we offer preliminary evidence suggesting a role for cortical cholinergic neurotransmission in supporting neurophysiologic complexity and the capacity for consciousness.

Chapter 1 Introduction

1.1 Consciousness: From Philosophy of Mind to Neural Correlates

The question of where consciousness resides and how it emerges has been the subject of philosophical and scientific inquiry throughout recorded history. Although early luminaries such as Democritus, G.W. Leibniz, Immanuel Kant, David Hume, and René Descartes wrote extensively on the philosophy of mind,[1,2] attempts to empirically address the relationship between the mind and brain were not undertaken until the 19th century.[3,4] The advent of clinical anesthesia in the mid-19th century would mark a significant advancement in these efforts. While American Dentist William Morton's use of ether for a tooth extraction in 1846 is widely credited as the first public demonstration of general anesthesia,[5–7] other notable applications of anesthesia appear to predate this event. Horace Wells – a mentor to Morton – used nitrous oxide in dentistry as early as 1844,[8] and Crawford Long was documented successfully using sulfuric ether in the removal of a neck tumor in 1842.[9,10] Regardless of its origins, the value of general anesthesia as a tool to study consciousness would be recognized by 20th century physicians such as Henry Beecher,[11] as it provided a model system wherein consciousness could be safely and reliably modulated to study its underlying neural mechanisms.

The 19th and 20th centuries set the foundation for the neuroscientific study of consciousness, as this period yielded several critical discoveries illustrating that perceptual contents and states of arousal could be related to neurophysiological and neurochemical processes within the brain. The early neurophysiologic investigations of David Ferrier in 1876 demonstrated that electrical stimulation of the motor cortex in animals induced movement, while stimulation of parietal and temporal cortices induced behaviors that were suggestive of visual, tactile, auditory, and olfactory experiences.[12] In the 1920's and 1930's, Wilder Penfield expanded upon this work in human epileptic patients, topographically mapping loci of movement in the cortex and obtaining detailed verbal reports of somatosensory and perceptual experiences following site-specific cortical stimulation.[13,14] Hans Berger – a contemporary of Penfield – invented electroencephalography (EEG) in 1924,[15–17] which enabled the objective

recording of distinct sleep-wake states by Loomis and colleagues in the 1930's.[18,19] The work of Giuseppe Moruzzi, Horace Winchell Magoun, and Donald Lindsley further established the presence of specific subcortical loci governing cortical activation, demonstrating that stimulation of the brainstem reticular formation produced wake-like EEG patterns, while lesions of reticular formation produced a coma-like state.[20,21] Neurophysiologic processes were linked to neurochemical action in the early 1900s by the discoveries of Henry Dale – who first isolated acetylcholine in 1914 – and Otto Loewi, who would go on to identify acetylcholine as a neurotransmitter in 1921.[22–25] Dale and Loewi's findings ultimately contributed to the discovery that nerve impulses could be transmitted by chemical messengers, catalyzing decades of ensuing discovery linking neurochemical processes to perception, cognition, and behavior. [26,27]

While the 20th century was not lacking in theoretical and empirical efforts to explicitly study neurobiological mechanisms related to consciousness,[28–35] the field of consciousness science did not mature to the point of widespread acceptance until the 1990s.[36] This period was marked by the publication of several landmark articles, most notably Nobel-Laureate Francis Crick and Christof Koch's *Towards a neurobiological theory of consciousness*,[37] wherein the scientific framework to characterize the "neural correlates of consciousness" (i.e. the minimal neural activity necessary to explain a given conscious percept) was formally conceptualized. While advances in neuroimaging, neurophysiology, and computational neuroscience allowed for substantial progress in identifying neural processes contributing to perception and arousal,[38–41] decades of research since have not yielded a consensus on the precise neurobiological regions that are both necessary and sufficient to describe the minimal neural correlates of consciousness.[42–44] However, developments in clinical and basic neuroscience during this time have led to substantial progress and empirically testable theories of consciousness as well as the emergence of global network-level correlates of consciousness such as cortical complexity and anterior-posterior connectivity that have shown substantial promise in clinical and basic research applications.[45] Before discussing correlates of consciousness, however, it is first necessary to describe two dimensions of consciousness that are scientifically and clinically dissociable – namely, level and content.

1.2 Distinctions Between Level and Contents of Consciousness

Neuroscientific efforts to study consciousness have commonly drawn a conceptual distinction between dimensions of "level" and "contents" of consciousness. When scientists refer to the "level" of consciousness, they are often referring to the general behavioral arousal state of the animal or human under observation, i.e. whether the subject being observed is awake, asleep, responsive to stimuli, or unresponsive to stimuli. Importantly, level of consciousness can be determined almost exclusively by behavioral assessment, which facilitates its study in animals. Investigations into the level of consciousness have commonly utilized pharmacologic (anesthetic), pathologic (coma, unresponsive wakefulness syndrome, minimally conscious states), and physiologic (sleep states) models of unconsciousness to inform the neural correlates of arousal.[3,45,46] The "contents" of consciousness refer to the experiential qualities that an animal or human may perceive, such as the shape of a visual stimulus, the specific auditory tone associated with a given frequency, the odor associated with an olfactory cue, etc. Studies of the contents of consciousness have often employed perceptual tasks or passive "no-report" paradigms to attempt to localize stimulus-specific activity in the brain.[47]

In clinical and basic neuroscience, the level and contents of consciousness have been conceptualized to scale together in a simplified two-dimensional framework – a heuristic construct that has nonetheless often made valid experimental predictions in discriminating wakefulness from conditions such as sleep, coma, anesthesia, and psychedelic states. Indeed, studies of general anesthesia and disorders of consciousness have demonstrated that the level of arousal, behavioral responsivity, and contents of consciousness are more likely to be degraded in a correlated manner.[48–51] However, prior studies have identified pharmacologic, pathologic, and physiologic conditions in which behavioral responsiveness and the contents of consciousness have been demonstrated to dissociate.[52] While general anesthesia induced by traditional GABAergic anesthetics such as propofol is associated with a very low incidence of dream recall,[53] the anesthetic state induced by the N-Methyl-D-aspartate (NMDA) antagonist ketamine has often been associated with the presence of dream-like conscious content. During rapid-eye-movement (REM) sleep, the level of consciousness as assessed by behavior or responsiveness to external stimuli is low,[54] and yet the phenomenologically rich state of dreaming occurs predominantly during this stage of sleep.[55–57] Furthermore, neurophysiologic and neuroimaging paradigms have utilized neural activity to detect responsivity to verbal command or retention of sensory processing in minimally conscious patients,[40,58] patients with

locked-in syndrome,[59,60] unresponsive wakefulness syndrome,[61] and healthy subjects given propofol titrated to the loss of responsiveness.[62]

In sum, while the presence of consciousness is often inferred from behavioral responsivity, responsiveness can be decoupled from consciousness during sleep states, disorders of consciousness, and in pharmacologically-induced states such as dissociative anesthesia. Furthermore, while basic and clinical neuroscience often separate and simplify the interaction between the level and contents of consciousness as a matter of heuristic convenience, the level and contents of consciousness have been demonstrated to possess complex, nonlinear, and multi-dimensional interactions. In the following sections, we will briefly discuss leading contemporary theories of consciousness and examine experimental evidence for the network-level correlates of consciousness that they propose.

1.3 Network-Level Correlates of Consciousness: Computational Measures of Complexity and Corticocortical Connectivity

1.3.1 Theories of Complexity

Prevailing theories of consciousness – such as the Integrated Information Theory (IIT)[63,64] and the Entropic Brain Hypothesis[65,66] – have posited that the level of consciousness may scale with nonlinear dynamic features such as the complexity or entropy (i.e. diversity) of spatiotemporal brain networks. Specifically, IIT proposes a mathematical framework wherein consciousness emerges from nested hierarchies of neural processing, such that the informational whole that emerges (i.e. consciousness) is irreducible to the sum of its parts (i.e. the brain regions or brain networks generating it).[63,64,67] The Entropic Brain hypothesis predicts that consciousness depends on the entropy of spontaneous brain activity within a critical band, such that too little or too much entropy within the cortex results in the ablation of awareness.[65,66,68] In IIT, measures of complexity are thought to relate to consciousness in the sense that they index the differentiation of information throughout spatiotemporal brain networks,[64] while in the Entropic Brain Hypothesis cortical complexity is posited to reflect the amount of entropy and informational richness within the brain.[64,66] Within this framework, it is predicted that unconscious states should be characterized by constrained signal complexity relative to wakefulness, while states

characterized by rich conscious contents – such as the psychedelic state – should show enhanced signal complexity relative to spontaneous wakefulness.

Empirical data from EEG,[69–81] MEG,[82–84] fMRI,[85–87] and spike[88,89] studies have extensively supported theories suggesting that neural signal complexity relates to the level of consciousness. Most studies to date have relied on the application of Lempel-Ziv complexity to stimulus-evoked or spontaneous neural data. Lempel-Ziv complexity is a measure of algorithmic complexity that computes the compressibility of finite sequences, using the number of unique patterns within time-series as a surrogate measure for the amount of information contained within the signal.[90] A landmark study by Casali and colleagues (2013) introduced Perturbational Complexity Index (PCI),[73] which computes the averaged Lempel-Ziv complexity of repeated TMS-evoked EEG potentials across the cortex, demonstrating significant reductions in cortical complexity during anesthesia, non-REM sleep, and disorders of consciousness relative to wakefulness.[73] A follow-up study by Sarasso and colleagues (2015) applied PCI to subjects administered propofol, xenon, or ketamine titrated to loss-of-responsiveness, showing that reductions in PCI are a conserved trait across major anesthetic classes.[69] Of note, however, is the fact that PCI could not distinguish between waking and REM sleep, which was confirmed to be associated with conscious contents in the form of self-reported dreaming.[73] Furthermore, the follow-up study by Sarasso et al. found that subjects treated with ketamine were distinguished by insignificant reductions in PCI relative to wakefulness – a dynamic phenotype that was accompanied by a very high incidence of dream reports relative to propofol or xenon anesthesia. These results suggest that PCI may broadly predict the presence of conscious contents independent of behavioral arousal, but pending further study the implications of these findings are not yet clear when placed in the context of assessing the level of consciousness in clinical settings.

Lempel-Ziv complexity has also been computed from spontaneous neural data, a paradigm that is more readily applicable in clinical and basic research studies as it does not require the use of concurrent TMS or the perturbation of endogenous neural activity. These studies have found constrained complexity in spontaneous neural activity during states marked by low levels of arousal and reductions in conscious contents, such as anesthesia,[70,71,75,78,79,91,92] coma,[82,93,94] and non-REM sleep.[76,88] Conversely, Lempel-Ziv complexity is elevated during states associated with the presence of phenomenal content, such as wakefulness or REM

sleep.[76,88] Recent studies have also investigated the complexity of spontaneous neural data in the context of the psychedelic state. These studies have demonstrated that pharmacologically disparate psychedelics such lysergic acid diethylamide, psilocybin, dimethyltryptamine, and subanesthetic ketamine increase cortical complexity relative to spontaneous wakefulness.[79,80,83] A subset of these studies have demonstrated a correlation between the degree of increase in signal complexity during the psychedelic state and the subjectively reported intensity of alterations to conscious contents, indicating that neural signal complexity may not only reflect the level of arousal, but perhaps could broadly index dynamics pertaining to the richness of conscious experience.[80,83]

Although complexity-based approaches to measuring the level of consciousness show promise, caution is warranted in the interpretation of results derived from clinical and basic research pending further study. "Type-I" based complexity measures such as Lempel-Ziv complexity are purported to capture nonlinear features of neural signals, but traditional implementations of the Lempel-Ziv complexity algorithm have been shown to be susceptible to bias from linear properties of the signal, e.g. excessive low/high frequency content.[95,96] In the case of dissociative anesthesia with ketamine, this has been reported to result in inaccurate measurements of the depth of anesthesia,[97] as ketamine anesthesia results in the maintenance of low gamma oscillations[69,97–99] that have been associated with cortical complexity values comparable to wakefulness.[69,97] Studies dissecting the role of linear and nonlinear signal components in driving changes in Lempel-Ziv complexity – as well as how to control for spectral influence during different states of consciousness – are warranted. Furthermore, while complexity measures are capable of broadly discriminating states of consciousness, their clinical utility in discriminating finer dimensions of conscious states – for example in detecting disconnected states of consciousness or tracking the recovery of consciousness following traumatic brain injury – are still a matter of debate.[100] Finally, given the relative novelty of these measures in consciousness science, few studies have focused on understanding the biological processes underlying changes in complexity. A richer understanding of how computational measures of complexity relate to underlying neurophysiological or neurobiological processes will be necessary to advance their implementation in clinical and basic neuroscience as indices of the level of consciousness.

1.3.2 Theories of Consciousness Involving Frontoparietal Connectivity

Other prominent theories of consciousness, such as the Global Neuronal Workspace Theory (GNW),[101] suggest that consciousness depends on reverberant connectivity between key nodes in anterior and posterior cortices. Within this framework, primary sensory processing is amplified and broadcast across the cortex via reciprocal long-range feedforward and feedback projections across posterior and anterior cortical regions. Given its neuronal density and rich reciprocal connections to other cortical and subcortical areas, the prefrontal cortex (PFC) is postulated to be a higher order hub that "ignites" this reverberant network, which allows sensory representations to be sustained and accessible by an array of cognitive processors, resulting in conscious awareness.[102] Studies supporting the GNW hypothesis have included measures of directed connectivity such as Granger Causality or transfer entropy.[103–105] Compared to the correlative properties of measures of functional connectivity such as corticocortical coherence or cross correlation, these measures are employed to approximate the directionality of information flow within brain networks and – in the case of transfer entropy – can be readily applied to non-Gaussian data.[106–109]

In support of GNW, a wealth of studies have demonstrated that anterior-posterior connectivity is disrupted during loss of consciousness induced by a broad range of pharmacologic, pathologic, and non-pathologic causes. Studies of anesthesia have demonstrated that perturbations to anterior-to-posterior connectivity are a pharmacologically invariant consequence of anesthetic-induced unconsciousness.[110] Neurophysiologic and neuroimaging studies in humans have demonstrated that GABAergic anesthetics such as propofol, sevoflurane – as well as dissociative anesthetics such as ketamine – interrupt connectivity patterns between frontal and parietal cortices.[111–115] Similar anesthetic-induced reductions in connectivity have been replicated in non-human primates[116–118] and rodents,[119,120]as well as in *Drosophila melanogaster*[121] – in which attenuated connectivity between central nuclei involved in abstract behavioral computation[122] and peripheral sensory nuclei[123] has been demonstrated during isoflurane anesthesia. Studies of disorders of consciousness have likewise demonstrated substantial reductions in frontoparietal connectivity,[124–126] and corticocortical connectivity between these regions has been used to successfully discriminate between coma, unresponsive wakefulness syndrome, minimally conscious states, and wakefulness.[127,128]

Impaired frontoparietal connectivity has been observed during sleep in humans[129,130] and rodents.[120] Work by Pal and colleagues (2016) demonstrated disruptions in frontoparietal EEG connectivity within high gamma bandwidths (85-155 Hz) as a phenotype conserved across both sleep and anesthetic-induced unconsciousness.[120] In the same study, REM sleep was distinguished from non-REM sleep (and wakefulness) by further a reduction in frontoparietal connectivity within high gamma bandwidths.[120] These studies distinguish measures of directed frontoparietal connectivity from measures of signal complexity based upon Lempel-Ziv complexity, which have failed to differentiate the activated cortical state of REM sleep from waking.[73,76,88] Studies of lucid dreaming – a disconnected state of consciousness marked by awareness of dreaming and partial retention of executive control – have pointed to comparably increased gamma coherence and spectral power in the dorsolateral prefrontal cortex during lucid dreaming compared to non-lucid dream states,[131] as well as increased connectivity between anterior PFC and temporoparietal regions during dreaming.[132]

In summary, these studies broadly support measures of directed frontoparietal connectivity as a network-level correlate of the level of consciousness across physiologic, pathologic, and pharmacologic states of unconsciousness. However, the neural correlates regulating changes in frontoparietal connectivity are poorly characterized. Given the association between frontoparietal connectivity and the level of consciousness, previous studies have assessed the role of arousal-promoting neuromodulators on frontoparietal networks, finding a relationship between measures of frontoparietal connectivity and levels of neurotransmitters such as acetylcholine.[120,133] It is uncertain, however, to what degree changes in corticocortical connectivity reflect the presence of consciousness and the neurochemical state of the cortex, as opposed to pharmacology-specific or state-dependent effects on neurophysiology, motivating the development of novel paradigms to study the interaction between neuromodulatory influence and cortical dynamics. In the next section, we will discuss in further depth previous research that has identified cortical acetylcholine as a neurochemical correlate of dynamics supporting consciousness.

1.4 Acetylcholine as a Neurochemical Correlate of Dynamics Supporting Consciousness

While empirical studies supporting GNW, IIT, and the Entropic Brain Hypothesis have advanced our understanding of network-level correlates of consciousness, comparatively little

focus has been placed on relating the proposed computational markers to underlying neurobiological or neurochemical processes. To address this, future inquiry can draw on decades of studies into neurotransmission, which have implicated a pharmacologically diverse milieu of neuromodulators – including acetylcholine - in regulating the level of consciousness.[134] The pedunculopontine tegmental nucleus, lateral dorsal tegmental nucleus, and basal forebrain serve as central nodes of cholinergic transmission throughout the brain, with bidirectional cholinergic projections to the basal ganglia, thalamus, striatum, reticular formation, cerebellum, and cerebral cortex.[134–136] Among these cholinergic nuclei, the basal forebrain serves as the predominant source of acetylcholine to the cortex, forming a complex network of efferent and afferent projections with topographically-mapped cortical targets.

Neurochemical research has demonstrated that cortical acetylcholine levels appear to track with the cortical activation and the capacity for phenomenal consciousness. Cortical acetylcholine levels are high during states associated with an activated EEG, high cortical complexity, and the presence of conscious contents, such as in the case of wakefulness or REM sleep[120,136–140] – during which disconnected conscious contents are common in the form of dreaming. In the context of the psychedelic state, increases in cortical acetylcholine release beyond basal wakefulness have been demonstrated following the administration of the classical serotonergic psychedelics mescaline and DOI, as well as subanesthetic doses of the dissociative NMDA-antagonists ketamine,[141] nitrous oxide,[142]and xenon.[143] Conversely, cortical cholinergic tone is suppressed during non-REM sleep, a state in which EEG dynamics are slow, hypersynchronous, and dreaming is comparatively uncommon and less rich in content.[120,140,144,145] A broad range of anesthetics including sevoflurane,[120,142] isoflurane,[146] propofol,[120,147] pentobarbital,[148] and midazolam[149] reduce cortical acetylcholine release relative to wakefulness, demonstrating that cortical cholinergic circuits are implicated in anesthetic-induced unconsciousness.[150] Furthermore, cortical cholinergic dysfunction has also been demonstrated in the context of pathologic disorders of consciousness following traumatic brain injury in humans,[151] as well as in experimental models of coma in animals.[152,153]

In addition to its broad relation to phenomenal consciousness, cortical acetylcholine release is known to produce neurophysiological features conducive to high levels of neurophysiologic complexity. For example, the release of acetylcholine in the cortex promotes spectral features known to accompany a diverse brain state repertoire, such as the reduction of

slow oscillatory power, enhancements in theta-gamma coupling, and the promotion of gamma oscillations.[98,120,154] Furthermore, cortical acetylcholine release promotes the amplification of sensory feedback between the cortex and thalamus, as well as the desynchronization of thalamocortical dynamics during wakefulness.[155–157] A study by Pal et al. in 2018[158] demonstrated that cholinergic (but not noradrenergic) stimulation of the prefrontal cortex was sufficient to reverse clinical levels of sevoflurane anesthesia in rats. This phenotype was not replicated with cholinergic or noradrenergic stimulation of posterior or parietal cortical regions, suggesting that prefrontal cholinergic circuits may serve as a key cortical hub in regulating arousal and dynamics related to the level of consciousness.

In summary, there is a large body of literature to support a role for acetylcholine as a neurochemical correlate of behavioral and cortical arousal. However, pending further study it is unknown if the release of acetylcholine in the cortex supports cortical dynamics thought to relate to the capacity for consciousness, such as neurophysiologic complexity.

1.5 Summary and Central Hypothesis

Despite decades of modern neuroscientific research, there is yet to be a consensus on the precise neural correlates of consciousness. However, prominent theories of consciousness have converged upon network-level correlates of consciousness, such as cortical complexity or frontoparietal connectivity, which are grounded in neuroscience and have shown promise in assessing the level of consciousness in clinical and basic research applications. Questions remain about these measures, however, which limit their interpretation in the neuroscientific study of consciousness. 1) It is a matter of debate as to what extent changes in computational measures such as complexity or corticocortical connectivity truly index behavioral arousal and the level of consciousness as opposed to drug-specific effects on the cortex 2) To speak to the latter possibility, commonly employed metrics of complexity such as Lempel-Ziv complexity show at least some degree of dependence on linear spectral features of the signal, calling into question their utility in assessing the level of consciousness in exceptional cases such as ketamine anesthesia or disorders of consciousness wherein conscious contents are decoupled from electrocortical activation and responsivity. This warrants study of the unique spectral-dependent or bandwidth-specific properties of pharmacologically disparate anesthetics on Lempel-Ziv complexity, which have not yet been characterized. 3) Little is understood about the precise

neurochemical correlates that underlie changes in computational measures of the level of consciousness. While a relationship between cortical complexity, connectivity, and cortical acetylcholine levels may be inferred from previous neurochemical research, there is a remarkable paucity of studies assessing concurrent changes in dynamic signatures of consciousness and changes in neurochemistry.

In the following chapters of this dissertation, we attempt to empirically address these questions, **with a central hypothesis that neurophysiologic complexity correlates with cortical cholinergic tone**. In Chapter 2, we use data from Pal et al., 2018, to investigate cortical dynamics – including neurophysiologic complexity and frontoparietal connectivity – following cholinergic or noradrenergic stimulation of prefrontal and parietal cortices during sevoflurane anesthesia. In Chapter 3, we utilize EEG data during pharmacologically disparate states of ketamine and propofol anesthesia to investigate their state-dependent and bandwidth-specific effects on Lempel-Ziv complexity. Finally, in Chapter 4, we utilize a novel experimental approach in rodents that enables us to combine multi-site cortical microdialysis and high-density EEG, permitting thorough exploration of the relationship between cortical acetylcholine levels and neurophysiologic complexity.

Chapter 2 The Level of Consciousness is Dissociable from Electroencephalographic Measures of Cortical Connectivity, Slow Oscillations, and Complexity[159]

2.1 Introduction

The biological basis of consciousness is considered to be among the most fundamental questions in science. A number of prominent theories of consciousness focus on the integration of neural information in cortical networks as measured via the strength or repertoire of functional brain connections.[64,66,101,160] Studies across multiple species and from multiple laboratories, including our own, suggest that (1) disruption of frontal-parietal functional connectivity,[112,113,115,120,161–170] (2) increase in spectral power of slow oscillations,[171–174] and (3) reduced spatiotemporal complexity[69,73,75,79,85,175] are correlates of anesthetic-induced unconsciousness. However, it is not clear whether the anesthetic-induced disruption in cortical connectivity, increase in the spectral power of slow oscillations, and reduction in cortical complexity correlate with unconsciousness (i.e., a state effect) or reflect the presence of anesthetic drugs in the brain (i.e., a drug effect). A primary reason for this gap in our understanding is that, normally, the presence of anesthetic drugs in the brain at clinically relevant concentrations is associated with the absence of wakefulness. Conversely, wakefulness normally occurs in the absence of anesthetic drugs or when these drugs reach subanesthetic concentrations in the brain. In a recent study,[158] we demonstrated that cholinergic stimulation, via local carbachol delivery, of prefrontal cortex (PFC) in sevoflurane-anesthetized rat was sufficient to restore wakefulness despite the continuous presence of sevoflurane at concentrations (1.9%–2.4%) associated with surgical anesthesia. If preserved frontal parietal connectivity, low power

Published as: Dinesh Pal, Duan Li, Jon G. Dean, Michael A. Brito, Tiecheng Liu, Anna M. Fryzel, Anthony G. Hudetz, George A. Mashour. Level of Consciousness Is Dissociable from Electroencephalographic Measures of Cortical Connectivity, Slow Oscillations, and Complexity. *Journal of Neuroscience*. 40, 605–618 (2020). doi: 10.1523/JNEUROSCI.1910-19.2019

Contributions: M.A.B. performed the high-density EEG studies utilized for spatiotemporal Lempel-Ziv complexity analysis and edited the paper. D.P., J.G.D., T.L., and A.M.F. performed all other EEG studies; D.P. and G.A.M. designed the original research; D.P., D.L., J.G.D., analyzed data; D.P., D.L., and G.A.M. wrote the paper; D.P., D.L., J.G.D., A.G.H., and G.A.M. edited the paper; A.G.H. contributed unpublished reagents/analytic tools.

of slow oscillations, and/or high spatiotemporal complexity are indeed correlates of wakefulness, then these should be restored during carbachol-induced wakefulness despite the presence of anesthetic in the brain. Conversely, if disruption of frontal-parietal connectivity, enhanced power of slow oscillations, and/or reduced spatiotemporal complexity correlate with the presence of anesthetics in the brain, then pharmacological restoration of wakefulness in the presence of sevoflurane will not be associated with restoration to baseline wake levels. Interestingly, in our previous study,[158] we also demonstrated that cholinergic stimulation of parietal cortex or the noradrenergic stimulation of either prefrontal or parietal cortices in sevoflurane-anesthetized rats activated the electroencephalogram (EEG) but failed to reverse general anesthesia and restore wakefulness, creating alternative models for understanding the state- and drug-related effects of general anesthetics.

In the current study, we analyzed the EEG datasets collected as part of these experiments[158] and demonstrate that (1) functional cortical gamma connectivity remains suppressed during ongoing sevoflurane exposure despite the concurrent induction of wakefulness following carbachol delivery into PFC; and (2) the changes in slow oscillations and cortical complexity correlate with changes in EEG activation rather than behavior. These findings suggest that the level of consciousness can be dissociated from EEG measures of connectivity and dynamics, prompting a reevaluation of the precise role in the mechanism and monitoring of consciousness.

2.2 Materials and Methods

2.2.1 Experimental Model and Subject Details

All experiments were conducted in adult male Sprague Dawley rats (300–350 g, Charles River Laboratories) maintained on a 12 h light/12 h dark cycle (lights on at 6:00 A.M.) with ad libitum food and water. The experiments were approved by the Institutional Animal Care and Use Committee (University of Michigan, Ann Arbor, Michigan) and were in compliance with the *Guide for the care and use of laboratory animals* (Ed 8, National Academies Press) as well as the ARRIVE guidelines.[176]

2.2.2 Surgical Procedures

The procedures for the surgical implantation of electrodes to record EEG and the guide tubes for microdialysis delivery of carbachol or noradrenaline (NA) are reported in detail in our recently published study[158] that generated the EEG data for analysis in the current study, as well as in 2.2 Materials and Methods. The EEG data were collected from five cortical sites: one frontal (from bregma: anterior 3.0 mm and mediolateral 2.5 mm), two parietal (from bregma: posterior 4.0 mm and mediolateral 2.5 mm), and two occipital (from bregma: posterior 8.0 mm and mediolateral 2.5 mm). One subset of rats was implanted with a microdialysis probe in PFC (from bregma: anterior 3.0 mm, mediolateral 0.5 mm, ventral 4.0 mm, and contralateral to the frontal EEG electrode) for microdialysis sample collection and local delivery of carbachol or NA, whereas the other subset was implanted with a microdialysis probe in parietal cortex (from bregma: posterior 3.6 mm, mediolateral 2.6 mm, ventral 2.0 mm, and at an angle of 40 degrees) for microdialysis sample collection and local delivery of carbachol or NA. All stereotaxic coordinates were based on the rat atlas by Paxinos and Watson.[177] A limitation of the conventional EEG recording montage as used in the previous study[158] is that, in the absence of high-density spatial data, it allows only temporal complexity analysis or the measurement of the diversity of the EEG signal only in the temporal domain. To overcome this limitation and examine the changes in spatiotemporal complexity, in the current study, we surgically prepared another group of rats (n = 7) for intracranial high-density EEG recording (thirty cortical sites). To the best of our knowledge, this approach to sample EEG data from across the cortical surface in combination with microdialysis delivery and sample collection has not been reported previously. The same procedures for the surgical implantation of electrodes to record EEG and the guide tubes for microdialysis delivery of carbachol or NA in our five cortical site studies[158] were adopted for the high-density EEG cohort in the current study.

2.2.3 Electroencephalographic Recordings

Monopolar EEG signals were recorded with reference to a stainless-steel electrode over nasal sinus, as has been reported previously in studies from our[98,120,178] and other[179,180] laboratories. The signals were amplified (5000X) and bandpass filtered between 0.1 and 300 Hz using a Grass model 15 LT bipolar portable physiodata amplifier system (15A54 Quad Amplifier, Natus Neurology), and digitized at 1 kHz using MP150 data acquisition unit (Acq*knowledge* software version 4.1.1, Biopac Systems). The high-density EEG dataset was

recorded on a Scout Grapevine Neural Processor (Ripple Neuro) using a bandpass filter of 0.1–300 Hz and sampling rate of 1 kHz. The raw EEG data were exported into MATLAB (version 2015a; The MathWorks) and downsampled to 500Hz(resample.m function in MATLAB signal processing toolbox) for further analysis.

2.2.4 Experimental Design

We used the intracranial EEG data from Pal et al., 2018[158] to analyze the changes in functional cortical gamma connectivity (25–155 Hz), spectral power of slow oscillations (0.5–1 Hz), and Lempel–Ziv complexity (<175 Hz), before, during, and after reverse dialysis delivery of carbachol and noradrenaline (NA) into the PFC and parietal cortex of sevoflurane-anesthetized rats.[158] The experimental design is the same as outlined in Figure 2.1. The detailed methodology for reverse dialysis delivery of carbachol and noradrenaline, cortical acetylcholine quantification, and histological confirmation of the microdialysis sites are outlined in detail in Pal et al., 2018.[158] In brief, on the day of the experiment, the rats were connected to the EEG recording cable, and a microdialysis probe being continuously perfused (2 μL/min using a CMA/400 syringe pump, CMA Microdialysis, Harvard Apparatus) with Ringer's solution (147 mM NaCl, 2.4 mM CaCl2, 4.0 mM KCl, 10 μM neostigmine; pH6.0±0.2), was lowered into either prefrontal (CMA/11, 1-mm-long cuprophane membrane, 0.24-mm-diameter, 6 kDa membrane cutoff) or parietal cortex (CMA/11, 2-mm-long cuprophane membrane, 0.24-mm-diameter, 6 kDa membrane cutoff) for carbachol or NA delivery and simultaneous collection of microdialysis samples. The EEG data were collected during baseline wake state for 75 min. To hold the behavioral state constant during the baseline condition, the rats were kept awake by introduction of novel objects and gentle tapping on the recording chamber. At the completion of 75 min of baseline wake recording, sevoflurane exposure (1.9%–2.4%) was started and titrated to maintain (1) loss of righting reflex, which is a widely accepted behavioral surrogate for anesthetic-induced unconsciousness in rats, and (2) high amplitude, slow-wave EEG. The anesthetic exposure was continued for 75 min, after which either carbachol (5 mM) or NA (20mM) was reverse dialyzed for 12.5 min into the PFC (n = 10 rats for carbachol and n = 8 rats for NA) or the parietal cortex (n = 11 rats each for carbachol and NA) while the rats were still inhaling the same concentration of sevoflurane anesthesia. At the end of carbachol or NA delivery, the EEG recordings continued under sevoflurane anesthesia for another 50 min.

Thereafter, sevoflurane exposure was stopped and EEG data were collected for 37.5 min during the post-sevoflurane recovery wake state. The use of reverse dialysis delivery allowed us to restrict the spatial spread of carbachol or NA, thereby avoiding nonspecific effects associated with activation or inhibition of spatially distinct brain regions. Importantly, administration of carbachol and NA through reverse dialysis allowed us to simultaneously monitor the changes in local acetylcholine levels, which have been reported in our previous study.[158] In the current study, the new cohort of male Sprague Dawley rats (n = 7) prepared for intracranial high-density EEG recordings was also implanted with a microdialysis probe in PFC for measuring acetylcholine levels during local reverse dialysis delivery of 5 mM carbachol. The following EEG segments, visually inspected and free of any artifacts, were selected for analysis: (1) baseline wake condition: last 300 s of the baseline wake state before exposure to sevoflurane anesthesia; (2) sevoflurane anesthesia: last 300 s of the sevoflurane exposure before pharmacological stimulation with carbachol or NA; (3) carbachol: 300 s from the point of first visible change in EEG after the start of carbachol delivery during sevoflurane anesthesia; (4) NA: 90–220 s from the point of first visible change in EEG after the start of NA delivery during sevoflurane anesthesia; and (5) post-sevoflurane recovery wake state: 300 s from the recovery of righting reflex, which occurred within 750 s after the cessation of sevoflurane anesthesia. The emergence time from sevoflurane anesthesia, as indicated by the return of righting reflex, was variable among rats, but all the rats recovered within 750 s of sevoflurane discontinuation. The epoch selection and the data analysis scheme for the high-density cohort were the same as that followed for the five-channel prefrontal-carbachol group described above and reported previously.[158]

2.2.5 Corticocortical Coherence Analysis

Corticocortical coherence was measured by the magnitude squared coherence method using the mscohere.m function in MATLAB signal processing toolbox (The Math-Works). The EEG data were segmented into nonoverlapped 10 s windows, which were further divided into 2 s subwindows with 80% overlap. Each subwindow was multiplied with a Hamming window, and the coherence was estimated from the cross-spectra and auto-spectra of the two EEG signals using Welch's averaged-modified periodogram method. The coherence for each window was estimated as a function of frequency (0.5–250 Hz) and between each pair of the five EEG

channels. The mean global coherence was obtained by averaging the coherence for individual channel pairs for each animal in the following gamma frequency bands: low gamma (25–55 Hz), medium gamma (85–125 Hz), and high gamma (125–155 Hz). The choice of these frequency bands was based on our recent rat study in which we demonstrated high gamma (85–155 Hz) corticocortical coherence and frontal-parietal connectivity as a correlate of wakefulness that is disrupted during general anesthesia and sleep.[120]

2.2.6 Frontal-parietal Directed Connectivity: Normalized Symbolic Transfer Entropy Analysis

Normalized symbolic transfer entropy is an information theoretic measure that is considered a surrogate for directed cortical communication. Our previous findings with normalized symbolic transfer entropy as a surrogate for frontal-parietal directed connectivity changes in human subjects[112,161] and rats[120,168,178] have been supported by reports from other laboratories that have used methodologically different approaches.[163,165] In the current study, we analyzed the EEG data for changes in directed connectivity between ipsilateral frontal and parietal channels in the gamma frequency bandwidth: low gamma (25–55 Hz), medium gamma (85–125 Hz), and high gamma (125–155 Hz). We used a Butterworth filter of order 4 (butter.m and filtfilt.m, MATLAB signal processing toolbox) to filter the raw EEG data for the frequency bands of interest (i.e., low, medium, and high gamma), and segmented the filtered data into nonoverlapped 10 s windows. The calculation of normalized symbolic transfer entropy requires three parameters: embedding dimension, time delay, and prediction time. We fixed the embedding dimension at 3, and time delay at 5, 2, and 1, corresponding to low, medium, and high gamma, respectively. For each window, we searched the prediction time between 1 and 50 (corresponding to 2–100 ms) and selected the one that yielded maximum normalized symbolic transfer entropy in the frontal-to-parietal and parietal-to-frontal direction. These parameters for normalized symbolic transfer entropy have been used in our previous rat studies.[120,168,178]

2.2.7 Spectral Power Analysis

The absolute power for the slow EEG oscillations was assessed in the temporal domain by applying a bandpass filter (0.5–1 Hz) to the EEG data using the eegfiltnew function in the

EEGLAB toolbox.[181] The power values were calculated for each non-overlapped 10 s window, and the averaged power across all the windows and all the available channels was computed.

2.2.8 Temporal Lempel–Ziv Complexity Analysis

Lempel–Ziv complexity computes the complexity of data with finite length sequences[90,182,183] and has been shown to be a valuable tool to investigate the neurophysiological changes associated with states of consciousness[73,75,76,79,83,88,175] Because of the limited number of EEG channels,[158] we could not compute the spatial complexity and therefore focused on the temporal complexity in ipsilateral frontal and parietal channels. The EEG signals were detrended using local linear regression with a 10 s window at a 5 s overlap (locdetrend function in Chronux analysis software), and lowpass filtered at 175 Hz via Butterworth filter of order 5 (butter and filtfilt functions in MATLAB signal processing toolbox). The instantaneous amplitude was calculated from the Hilbert transform of the signal, which was then binarized using its mean value as the threshold for each channel.[83] The binary sequence was segmented into nonoverlapped 10 s windows. For each of these 10 s windows, the Lempel–Ziv complexity algorithm searches for the instances of consecutive characters or "words" and counts the number of times a new word is encountered. To assess the degree to which the difference in the complexity across the states is not due to spectral changes, we generated surrogate data through phase randomization while preserving the spectral profiles of the signal[75,83] and normalized the original Lempel–Ziv complexity by the mean of the Lempel–Ziv complexity values from N = 50 surrogate time series. The resultant normalized Lempel–Ziv complexity values reflect complexity beyond the spectral changes, which were then averaged across all the windows as the estimate of the complexity at each studied state.

2.2.9 Spatiotemporal Lempel–Ziv Complexity Analysis

To overcome the limitations of low channel count (five) and to reveal the complexity changes in terms of spatial diversity, we implanted a new cohort of rats (n = 7) in the current study for high-density EEG recordings. The spatial distribution of electrodes (thirty) covering the entire cortex allowed us to quantify spatiotemporal complexity, and in addition served as an important control group to ascertain the validity of the temporal complexity analysis conducted on five-channel EEG data. The EEG data in 3 of 7 rats in the high-density cohort were

not useable because of excessive artifacts and noise levels. After excluding these rats and any bad channels, the remaining EEG signals (number of channels: 25–29) were detrended, lowpass filtered at 175 Hz, and divided into nonoverlapped 2 s windows after removing the common signal across channels. For each window, the instantaneous amplitude was estimated by applying the Hilbert transform,[75,83] which was binarized using its mean value as the threshold for each channel. The data were then converted into a binary matrix, in which rows represent channels and columns represent time points. The complexity of the spatiotemporal matrix was assessed by Lempel–Ziv complexity,[73,79] which searches the binary matrix, time point by time point, and counts the number of different spatial patterns across different time points. We then normalized the spatiotemporal complexity by the mean of those from the surrogate data through phase randomization, to examine whether the difference in the spatiotemporal complexity across the states is due to spectral changes.

2.2.10 Statistical Analyses

Statistical analyses were conducted in consultation with the Consulting for Statistics, Computing and Analytics Research unit at the University of Michigan (Ann Arbor, Michigan). The initial study[158] from which the EEG data were used in the current study was designed to have 80% power at α of 0.05. All statistical comparisons were conducted in a within-group design using the programming and statistical language R (version 3.6.0).[184] We used a linear mixed model with random intercept for each rat. This accounts for the correlations among observations of the same rat and allows unified reporting of all pairwise state comparisons. *Post hoc* pairwise tests were single-step corrected for multiple comparisons (Package *multicomp*). Models were fit with restricted maximum likelihood. p values of <0.05 were considered statistically significant. For clarity and readability, we have provided the p values in Section 2.3, whereas the mean, SD, F statistics, and effect sizes for all datasets and comparisons (except the acetylcholine dataset) have been provided in tabular format, as likewise referenced in Sections 2.3.1-2.3.5. The acetylcholine dataset has relatively fewer comparisons because of which we have reported the associated statistical values in the text in Sections 2.3.1 – 2.3.5.

2.3 Results

2.3.1 Corticocortical Gamma Coherence Does Not Correlate with Level of Consciousness

2.3.1.1 Carbachol Delivery into Prefrontal and Parietal Cortices

Compared with the baseline wake state, sevoflurane anesthesia was characterized by a significant reduction ($p \leq 0.001$) in the corticocortical coherence across the gamma bandwidth in both the prefrontal and parietal cortical groups (Figures 2.1A, 2.1C, and 2.1E; Table 2.1). Carbachol delivery into PFC of sevoflurane-anesthetized rats was shown to restore wakefulness despite the continuous presence of sevoflurane anesthesia.[158] However, analysis of the EEG from the same epoch showed that, despite the restoration of wakefulness, the corticocortical gamma coherence (high, medium, low) was not statistically different from that observed during sevoflurane anesthesia ($p \geq 0.74$), and remained significantly reduced ($p \leq 0.0017$) compared with the baseline wake state (Figures 2.1A, 2.1C, and 2.1E; Table 2.1). Wakefulness was determined based on clear attempts at righting or recovery of the righting reflex. All rats in the prefrontal carbachol group showed such behavioral responses and 4 of 11 rats regained complete mobility. Detailed descriptions of behavioral and physiological changes, as well as a representative movie clip showing completely mobile animal after carbachol delivery, are provided in our previous publication.[158] As opposed to the effect of carbachol in PFC, the reverse dialysis delivery of carbachol into parietal cortex of sevoflurane-anesthetized rat was ineffective in restoring wakefulness[158] and analysis of the EEG during the same epoch showed that coherence across the gamma bandwidth remained significantly low ($p < 0.001$) compared with the baseline wake state (Figures 2.1A, 2.1C, and 2.1E; Table 2.1); there was no significant difference in coherence in any of the gamma bands between the sevoflurane anesthesia epoch and the carbachol delivery epoch ($p \geq 0.88$). The post-sevoflurane recovery wake state in the prefrontal and parietal groups was characterized by increase in coherence in high gamma ($p \leq 0.001$ compared with sevoflurane, $p < 0.001$ compared with carbachol epochs) and medium gamma ($p < 0.001$ compared with sevoflurane, $p < 0.001$ compared with carbachol epochs) bands, which returned to the baseline wake levels ($p \geq 0.12$) (Figures 2.1A and 2.1C; Table 2.1). The low gamma coherence during post-sevoflurane recovery wake state in both prefrontal and parietal groups remained significantly below ($p < 0.001$) than that observed during the baseline wake state (Figure 2.1E; Table 2.1), even though there was a significant increase in the PFC

group compared with both sevoflurane ($p < 0.001$) and carbachol delivery ($p < 0.001$) epochs (Figure 2.1E; Table 2.1).

2.3.1.2 NA Delivery into Prefrontal and Parietal Cortices

Sevoflurane anesthesia produced a significant reduction ($p < 0.001$) in the corticocortical coherence across the gamma bandwidth (Figures 2.1B, 2.1D, and 2.1F; Table 2.2). Reverse dialysis delivery of NA into either prefrontal or parietal cortex during sevoflurane anesthesia was not observed to produce any signs of wakefulness.[158] During the same epoch (NA delivery), the corticocortical coherence in high gamma ($p < 0.001$) and medium gamma ($p < 0.001$) bands in both prefrontal and parietal groups remained significantly reduced compared with the baseline wake state (Figures 2.1B and 2.1D; Table 2.2), even though there was a significant increase ($p = 0.021$ compared with sevoflurane) in medium gamma coherence in the parietal cortex group. The post-sevoflurane recovery wake state in both prefrontal and parietal groups was also characterized by a significant increase in high and medium gamma coherence ($p < 0.001$) compared with both sevoflurane and NA epochs (Figures 2.1B and 2.1D; Table 2.2). Although the increase in high gamma coherence during post-sevoflurane recovery period in the prefrontal group reached the baseline levels and was not statistically different from the wake state ($p = 0.14$), the high gamma coherence in parietal group remained significantly lower than the baseline levels ($p = 0.0036$). Similarly, the medium gamma coherence during the post-sevoflurane recovery period, in both prefrontal and parietal groups, remained significantly lower ($p < 0.001$) than the baseline wake levels. The low gamma coherence during post-sevoflurane recovery wake state in the prefrontal group increased compared with sevoflurane ($p < 0.001$) and NA delivery ($p < 0.001$) epochs but still remained significantly low ($p < 0.001$) compared with baseline wake state (Figure 2.1F; Table 2.2). In the parietal group, the low gamma coherence during the post-sevoflurane epoch remained significantly low ($p < 0.001$) compared with the baseline wake levels and was not significantly different from either sevoflurane ($p = 0.11$) or NA ($p = 0.17$) epochs (Figure 2.1F; Table 2.2).

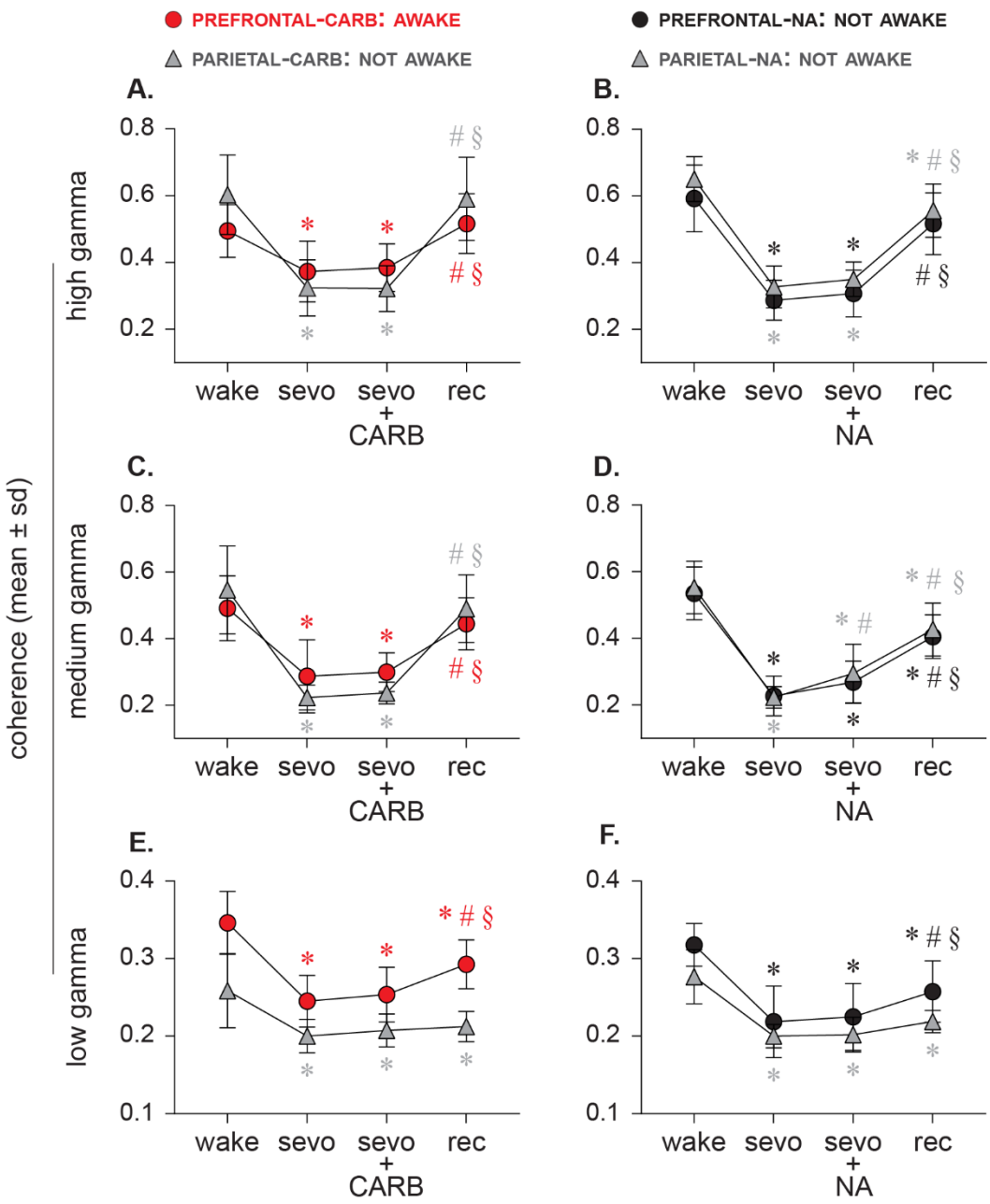

Figure 2.1 Corticocortical coherence does not correlate with level of consciousness.
(A–F) Sevoflurane anesthesia (sevo) significantly reduced corticocortical coherence in high (125–155 Hz), medium (85–125 Hz), and low (25–55 Hz) gamma range. Cholinergic stimulation of PFC through reverse dialysis delivery of 5 mM carbachol (CARB) was reported to induce wakefulness in the presence of sevoflurane anesthesia[158] but failed to restore gamma coherence (high, medium, low) to baseline wake levels (A,C,E). Similar delivery of CARB into parietal cortex or 20mM NA into prefrontal and parietal cortices during sevoflurane anesthesia did not restore wakefulness[158], and none of these interventions restored disrupted gamma coherence (A–F). The gamma coherence during the post-sevoflurane recovery wake epoch (rec) showed a trend toward return to baseline wake levels (A–F) but remained significantly low, except in the high and medium gamma bands for prefrontal- and parietal cortex-CARB (A) and prefrontal-NA (B) groups. A linear mixed model with random intercept for each rat was used for the statistical comparisons, and the post hoc pairwise tests were single-step corrected for multiple comparisons. The statistical comparisons are shown at $p < 0.05$. The mean, SD, exact p values, F statistics, and the effect sizes for each statistical comparison are provided in Tables 2.1 and 2.2. The significance symbols are color-coded to match the line-symbol plots. *Significant compared with baseline wake state. #Significant compared with sevo. §Significant compared with CARB or NA during sevo.

PREFRONTAL CORTEX – CARBACHOL												
	Low gamma				Medium gamma				High gamma			
	Wake	Sevo	CARB	Rec	Wake	Sevo	CARB	Rec	Wake	Sevo	CARB	Rec
Wake	**0.35 (0.041)**	-0.10 (0.027)	-0.093 (0.032)	-0.054 (0.034)	**0.49 (0.097)**	-0.20 (0.12)	-0.19 (0.093)	-0.047 (0.10)	**0.49 (0.079)**	-0.12 (0.11)	-0.11 (0.085)	-0.022 (0.11)
Sevo	p<0.001	**0.25 (0.033)**	0.0084 (0.019)	0.048 (0.019)	p<0.001	**0.29 (0.11)**	0.012 (0.087)	0.16 (0.096)	p<0.001	**0.37 (0.091)**	0.012 (0.11)	0.14 (0.11)
CARB	p<0.001	p=0.74	**0.25 (0.035)**	0.039 (0.021)	p<0.001	p=0.98	**0.30 (0.058)**	0.15 (0.036)	p=0.0017	p=0.98	**0.38 (0.071)**	0.13 (0.038)
Rec	p<0.001	p<0.001	p<0.001	**0.29 (0.032)**	p=0.39	p<0.001	p<0.001	**0.45 (0.078)**	p=0.89	p<0.001	p<0.001	**0.52 (0.090)**
	F(3,27)=63; p<0.001				**F(3,27)=25; p<0.001**				**F(3,27)=12; p<0.001**			
PARIETAL CORTEX – CARBACHOL												
	Low gamma				Medium gamma				High gamma			
	Wake	Sevo	CARB	Rec	Wake	Sevo	CARB	Rec	Wake	Sevo	CARB	Rec
Wake	**0.26 (0.048)**	-0.059 (0.038)	-0.051 (0.042)	-0.046 (0.046)	**0.55 (0.13)**	-0.32 (0.11)	-0.31 (0.11)	-0.056 (0.078)	**0.60 (0.12)**	-0.28 (0.087)	-0.28 (0.10)	-0.013 (0.10)
Sevo	p<0.001	**0.20 (0.021)**	0.0072 (0.021)	0.012 (0.013)	p<0.001	**0.22 (0.037)**	0.014 (0.028)	0.27 (0.075)	p<0.001	**0.32 (0.084)**	-0.0018 (0.061)	0.27 (0.13)
CARB	p<0.001	p=0.88	**0.21 (0.021)**	0.0051 (0.018)	p<0.001	p=0.95	**0.24 (0.033)**	0.25 (0.079)	p<0.001	p=1	**0.32 (0.069)**	0.27 (0.11)
Rec	p<0.001	p=0.59	p=0.96	**0.21 (0.019)**	p=0.12	p<0.001	p<0.001	**0.49 (0.10)**	p=0.98	p<0.001	p<0.001	**0.59 (0.13)**
	F(3,30)=15; p<0.001				**F(3,30)=88; p<0.001**				**F(3,30)=54; p<0.001**			

Table 2.1 Corticocortical coherence before, during, and after sevoflurane administration and carbachol delivery into prefrontal and parietal cortices.
Mean(±sd) for each state is shown in bold along the diagonal of each section. The cells above the mean(±sd) values show the effect sizes as the difference of the means(±sd). Sevo: sevoflurane administration, CARB: carbachol delivered during sevo, Rec: post-sevoflurane recovery wake.

PREFRONTAL CORTEX – NORADRENALINE												
	Low gamma				Medium gamma				High gamma			
	Wake	Sevo	NA	Rec	Wake	Sevo	NA	Rec	Wake	Sevo	NA	Rec
Wake	**0.32 (0.028)**	-0.099 (0.023)	-0.093 (0.023)	-0.060 (0.024)	**0.54 (0.079)**	-0.31 (0.053)	-0.27 (0.080)	-0.13 (0.074)	**0.59 (0.10)**	-0.31 (0.12)	-0.29 (0.13)	-0.076 (0.11)
Sevo	p<0.001	**0.22 (0.046)**	0.0063 (0.014)	0.039 (0.029)	p<0.001	**0.23 (0.059)**	0.041 (0.036)	0.18 (0.061)	p<0.001	**0.29 (0.060)**	0.020 (0.035)	0.23 (0.096)
NA	p<0.001	p=0.87	**0.23 (0.043)**	0.033 (0.025)	p<0.001	p<0.26	**0.27 (0.063)**	0.14 (0.068)	p<0.001	p=0.94	**0.31 (0.070)**	0.21 (0.089)
Rec	p<0.001	p<0.001	p<0.001	**0.26 (0.040)**	p<0.001	p<0.001	p<0.001	**0.41 (0.066)**	p=0.14	p<0.001	p<0.001	**0.52 (0.093)**
	F(3,21)=61; p<0.001				**F(3,21)=78; p<0.001**				**F(3,21)=36; p<0.001**			
PARIETAL CORTEX – NORADRENALINE												
	Low gamma				Medium gamma				High gamma			
	Wake	Sevo	NA	Rec	Wake	Sevo	NA	Rec	Wake	Sevo	NA	Rec
Wake	**0.28 (0.035)**	-0.077 (0.032)	-0.075 (0.036)	-0.058 (0.029)	**0.55 (0.079)**	-0.33 (0.068)	-0.26 (0.082)	-0.13 (0.11)	**0.65 (0.067)**	-0.32 (0.068)	-0.30 (0.10)	-0.095 (0.12)
Sevo	p<0.001	**0.20 (0.015)**	0.0019 (0.024)	0.019 (0.018)	p<0.001	**0.22 (0.033)**	0.072 0.083	0.21 (0.083)	p<0.001	**0.33 (0.062)**	0.023 (0.064)	0.23 (0.11)
NA	p<0.001	p=1	**0.20 (0.22)**	0.017 (0.021)	p<0.001	p=0.021	**0.29 (0.088)**	0.13 (0.065)	p<0.001	p=0.84	**0.35 (0.052)**	0.21 (0.079)
Rec	p<0.001	p=0.11	p=0.17	**0.22 (0.014)**	p<0.001	p<0.001	p<0.001	**0.43 (0.079)**	p=0.0036	p<0.001	p<0.001	**0.56 (0.080)**
	F(3,30)=38; p<0.001				**F(3,30)=69; p<0.001**				**F(3,30)=65; p<0.001**			

Table 2.2 Corticocortical coherence before, during, and after sevoflurane administration and noradrenaline delivery into prefrontal and parietal cortices.
Mean(±sd) for each state is shown in bold along the diagonal of each section. The cells above the mean(±sd) values show the effect sizes as the difference of the means(±sd). Sevo: sevoflurane administration, NA: noradrenaline delivered during sevo, Rec: post-sevoflurane recovery wake

2.3.2 Directed Cortical Gamma Connectivity Does Not Correlate with Level of Consciousness

2.3.2.1 Carbachol Delivery into Prefrontal and Parietal Cortices

Compared with the baseline wake state, sevoflurane anesthesia was characterized by a significant suppression of bidirectional (frontal-to-parietal and parietal-to frontal) connectivity in the high and medium gamma bands ($p \leq 0.020$) in both prefrontal and parietal groups (Figures 2.2A, 2.2C, 2.3A, and 2.3C; Tables 2.3 and 2.4). The delivery of carbachol into prefrontal, but not parietal cortex, was earlier shown to restore wakefulness in the presence of sevoflurane anesthesia.[158] However, bidirectional frontal-parietal gamma connectivity was not restored after delivery of carbachol into either PFC (restored wakefulness) or parietal cortex (no signs of wakefulness). High and medium gamma connectivity remained significantly below the baseline wake levels (high gamma: $p < 0.0074$; medium gamma: $p < 0.001$) and was not significantly different from that observed during sevoflurane anesthesia ($p \geq 0.070$) (Figures 2.2A, 2.2C, 2.3A, and 2.3C; Tables 2.3 and 2.4). In both the prefrontal and parietal groups, the post-sevoflurane recovery wake state was characterized by a significant increase in high gamma and medium gamma bidirectional frontal-parietal connectivity ($p < 0.001$ compared with both sevoflurane and carbachol epochs) (Figures 2.2A, 2.2C, 2.3A, and 2.3C; Tables 2.3 and 2.4); the connectivity levels in both the groups returned to baseline wake levels ($p \geq 0.1$). The bidirectional frontal-parietal connectivity in low gamma bandwidth showed widely variable effects (Figures 2.2E and 2.3E; Tables 2.3 and 2.4).

2.3.2.2 NA Delivery into Prefrontal and Parietal Cortices

Sevoflurane anesthesia was characterized by a significant suppression of bidirectional (frontal-to-parietal and parietal-to-frontal) connectivity in the high and medium gamma bands ($p < 0.001$) in both prefrontal and parietal groups (Figures 2.2B, 2.2D, 2.3B, and 2.3D; Tables 2.5 and 2.6). NA delivery into the prefrontal or parietal cortex of sevoflurane-anesthetized rats did not produce any signs of wakefulness,[158] and the analysis of the concomitant EEG showed no significant change in the high gamma or medium gamma bidirectional frontal-parietal

connectivity ($p \geq 0.85$ compared with sevoflurane anesthesia), which remained significantly below the baseline wake levels ($p < 0.001$) (Figures 2.2B, 2.2D, 2.3B, and 2.3D; Tables 2.5 and 2.6). The post-sevoflurane recovery wake epoch in both prefrontal and parietal groups was characterized by a significant increase in bidirectional frontal-parietal connectivity in both high gamma ($p < 0.001$ compared with sevoflurane anesthesia and NA epochs) and medium gamma ($p \leq 0.029$ compared with sevoflurane anesthesia, $p \leq 0.0094$ compared with NA) bands (Figures 2.2B, 2.2D, 2.3B, and 2.3D; Tables 2.5 and 2.6); the high and medium gamma bidirectional connectivity in the prefrontal group returned to baseline wake levels ($p \geq 0.077$) but in the parietal cortex group it remained significantly below ($p \leq 0.019$) the baseline wake levels (Figures 2.2B, 2.2D, 2.3B, and 2.3D; Tables 2.5 and 2.6). The bidirectional frontal-parietal connectivity in low gamma bandwidth showed widely variable effects (Figures 2.2F and 2.3F; Tables 2.5 and 2.6).

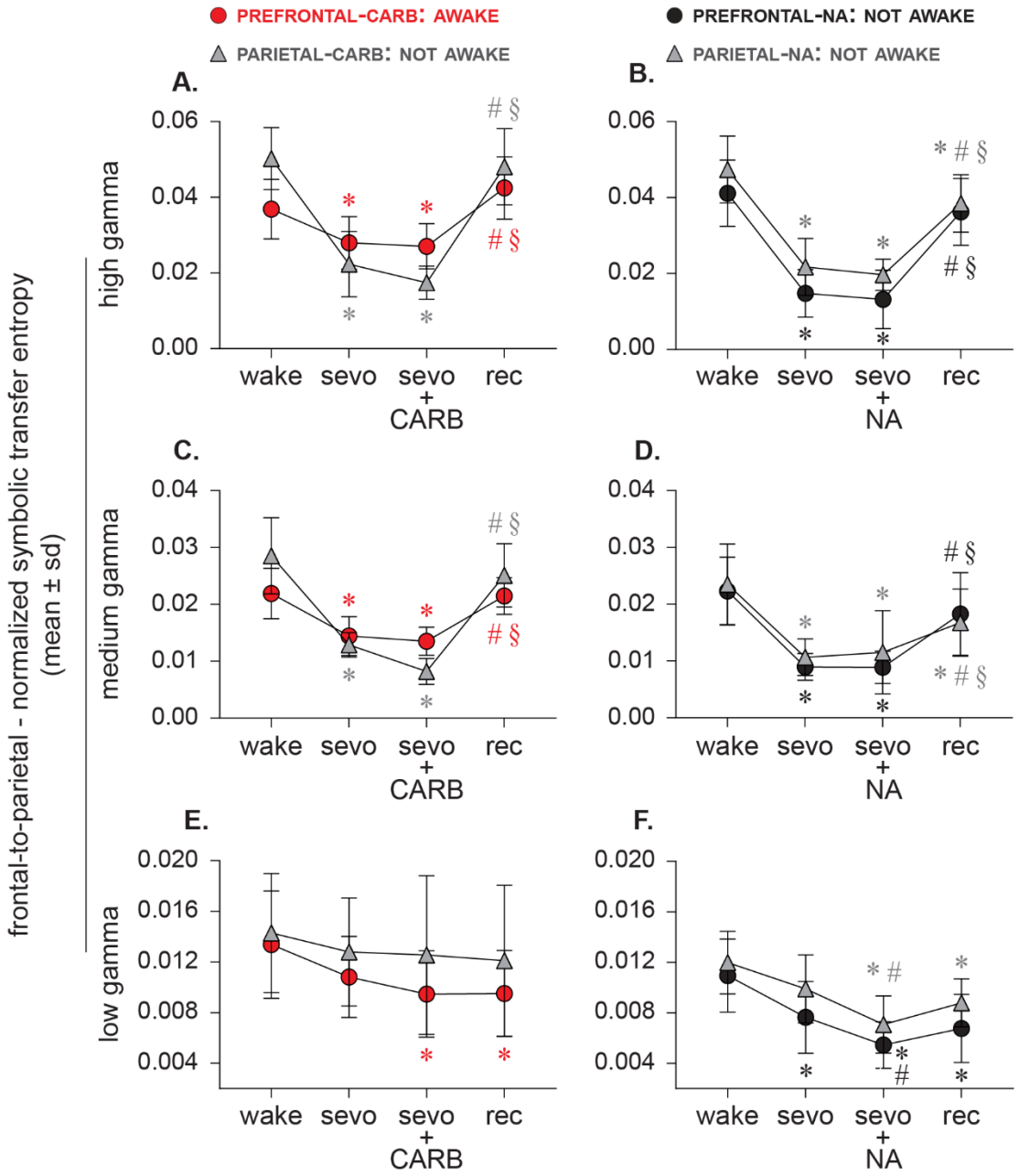

Figure 2.2 Frontal-to-parietal directed gamma connectivity does not correlate with level of consciousness.
(A–D) Frontal-to parietal connectivity in the high (125–155 Hz) and medium (85–125 Hz) gamma bands was significantly reduced during sevoflurane anesthesia (sevo). Neither the restoration of wakefulness through 5 mM carbachol (CARB) delivery to PFC nor the absence of wakefulness after CARB delivery to parietal cortex or 20mM NA delivery to prefrontal and parietal cortices, as reported previously[158], had any significant effect on the high and medium gamma frontal-to-parietal connectivity, which remained disrupted and was not significantly different from that observed during sevoflurane anesthesia alone (A–D). The frontal-to parietal connectivity during the post-sevoflurane recovery wake epoch (rec) returned to baseline wake levels (wake) for high and medium gamma bands for all conditions, except in the parietal cortex-NA group (B,D), where it remained significantly lower compared with wake. The connectivity changes in low gamma bandwidth were highly variable between groups (E,F). A linear mixed model with random intercept for each rat was used for the statistical comparisons, and the post hoc pairwise tests were single-step corrected for multiple comparisons. The statistical comparisons are shown at $p < 0.05$. The mean, SD, exact p values, F statistics, and the effect sizes for each statistical comparison are provided in Tables 2.3 and 2.5. The significance symbols are color-coded to match the line-symbol plots. *Significant compared with wake. #Significant compared with sevo. §Significant compared with CARB or NA during sevo.

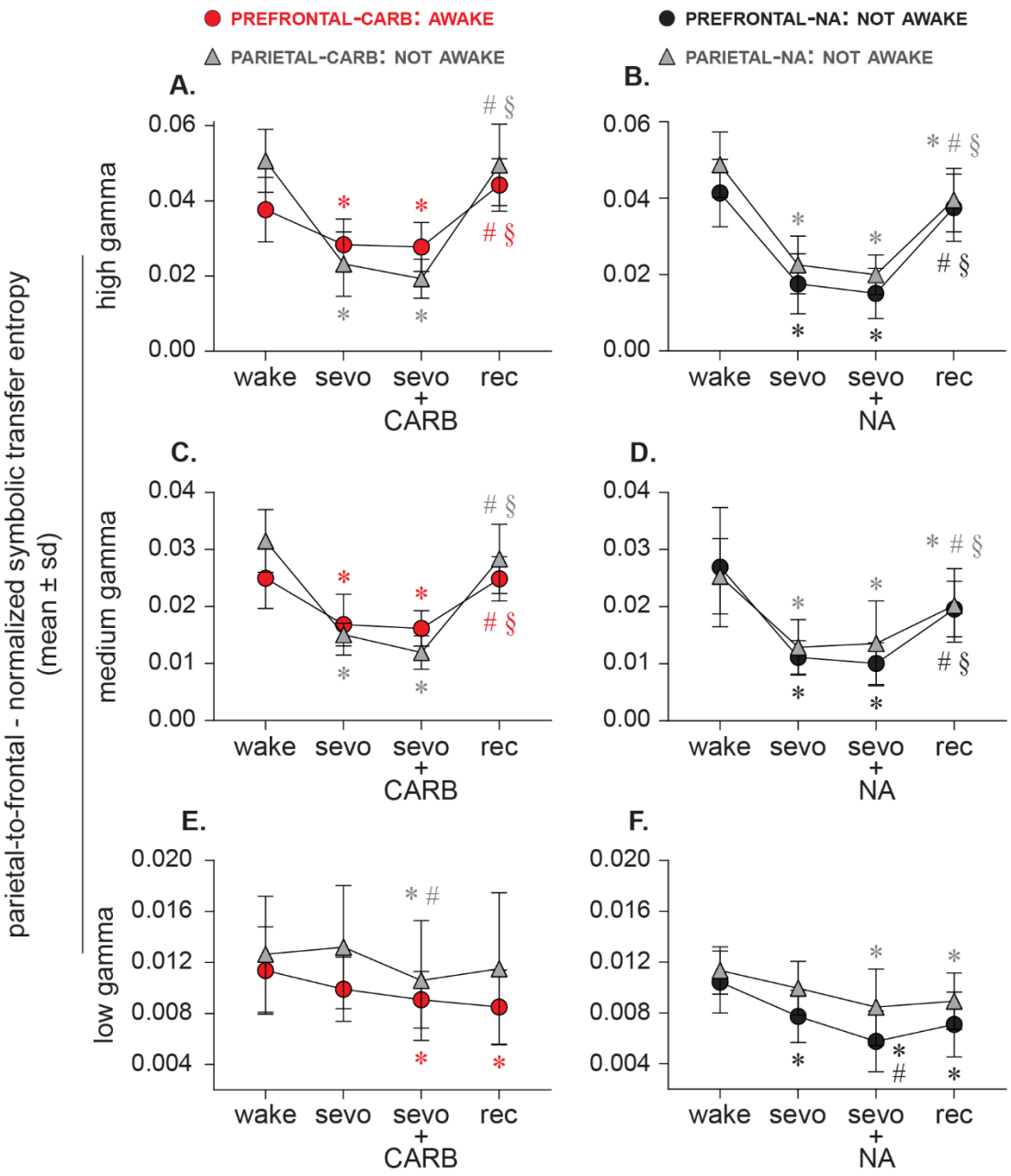

Figure 2.3 Parietal-to-frontal directed gamma connectivity does not correlate with level of consciousness.
(A–D) Parietal-to frontal connectivity in the high (125–155 Hz) and medium (85–125 Hz) gamma bands was significantly reduced during sevoflurane anesthesia (sevo). Neither the restoration of wakefulness through 5 mM carbachol (CARB) delivery to PFC nor the absence of wakefulness after CARB into parietal cortex or 20mM NA delivery to prefrontal and parietal cortices, as reported previously[158], had any significant effect on the high and medium gamma parietal-to-frontal connectivity, which remained disrupted and was not significantly different from that observed during sevoflurane anesthesia alone (A–D). The parietal-to-frontal connectivity during the post-sevoflurane recovery wake epoch (rec) returned to baseline wake (wake) levels for high and medium gamma bands for all conditions, except in the parietal cortex-NA group (A) where it remained significantly lower compared with wake. The connectivity changes in low gamma bandwidth were highly variable between groups (E,F). A linear mixed model with random intercept for each rat was used for the statistical comparisons, and the post hoc pairwise tests were single-step corrected for multiple comparisons. The statistical comparisons are shown at $p < 0.05$. The mean, SD, exact p values, F statistics, and the effect sizes for each statistical comparison are provided in Tables 2.4 and 2.6. The significance symbols are color-coded to match the line-symbol plots. *Significant compared with wake. #Significant compared with sevo. §Significant compared with CARB or NA during sevo.

PREFRONTAL CORTEX – CARBACHOL												
	Low gamma				Medium gamma				High gamma			
	Wake	Sevo	CARB	Rec	Wake	Sevo	CARB	Rec	Wake	Sevo	CARB	Rec
Wake	**0.013 (0.0042)**	-0.0026 (0.0030)	-0.0039 (0.0040)	-0.0039 (0.0031)	**0.022 (0.0045)**	-0.0075 (0.0058)	-0.0084 (0.0054)	-44e-5 (0.0044)	**0.037 (0.0079)**	-0.0089 (0.0082)	-0.010 (0.010)	0.0056 (0.010)
Sevo	p=0.044	**0.011 (0.0032)**	-0.0014 (0.0020)	-0.0013 (0.0026)	p<0.001	**0.014 (0.0034)**	-93e-5 (0.0041)	0.0071 (0.0050)	p=0.020	**0.028 (0.0069)**	-93e-5 (0.011)	0.015 (0.012)
CARB	p<0.001	p=0.51	**0.0095 (0.0034)**	38e-6 (0.0035)	p<0.001	p=0.92	**0.014 (0.0025)**	0.0080 (0.0023)	p=0.0074	p=1	**0.027 (0.0060)**	0.015 (0.0067)
Rec	p<0.001	p=0.54	p=1	**0.010 (0.0034)**	p=1	p<0.001	p<0.001	**0.022 (0.0032)**	p=0.27	p<0.001	p<0.001	**0.043 (0.0082)**
	F(3,27)=7.0; p=0.0012				**F(3,27)=19; p<0.001**				**F(3,27)=12; p<0.001**			
PARIETAL CORTEX – CARBACHOL												
	Low gamma				Medium gamma				High gamma			
	Wake	Sevo	CARB	Rec	Wake	Sevo	CARB	Rec	Wake	Sevo	CARB	Rec
Wake	**0.014 (0.0047)**	-0.0015 (0.0028)	-0.0017 (0.0041)	-0.0022 (0.0032)	**0.029 (0.0067)**	-0.016 (0.0069)	-0.020 (0.0081)	-0.0034 (0.0075)	**0.050 (0.0082)**	-0.028 (0.010)	-0.033 (0.0095)	-0.0022 (0.011)
Sevo	p=0.41	**0.013 (0.0043)**	-24e-5 (0.0034)	-69e-5 (0.0023)	p<0.001	**0.013 (0.0022)**	-0.0047 (0.0027)	0.012 (0.0060)	p<0.001	**0.022 (0.0086)**	-0.0049 0.0065	0.026 (0.014)
CARB	p=0.28	p=1	**0.013 (0.0063)**	-45e-5 (0.0032)	p<0.001	p=0.070	**0.0082 (0.0023)**	0.017 (0.0056)	p<0.001	p=0.43	**0.017 (0.0044)**	0.031 (0.011)
Rec	p=0.11	p=0.89	p=0.97	**0.012 (0.0060)**	p=0.28	p<0.001	p<0.001	**0.025 (0.0056)**	p=0.91	p<0.001	p<0.001	**0.048 (0.010)**
	F(3,30)=1.9; p=0.15				**F(3,30)=51; p<0.001**				**F(3,30)=56; p<0.001**			

Table 2.3 Frontal-to-Parietal connectivity before, during, and after sevoflurane administration and carbachol delivery into prefrontal and parietal cortices.
Mean(±sd) for each state is shown in bold along the diagonal of each section. The cells above the mean(±sd) values show the effect sizes as the difference of the means(±sd). Sevo: sevoflurane administration, CARB: carbachol delivered during sevo, Rec: post-sevoflurane recovery wake.

PREFRONTAL CORTEX – CARBACHOL												
	Low gamma				Medium gamma				High gamma			
	Wake	Sevo	CARB	Rec	Wake	Sevo	CARB	Rec	Wake	Sevo	CARB	Rec
Wake	**0.011 (0.0034)**	-0.0015 (0.023)	-0.0023 (0.0029)	-0.0029 (0.0019)	**0.025 (0.0053)**	-0.0081 (0.0068)	-0.0088 (0.0058)	-11e-5 (0.0054)	**0.038 (0.0086)**	-0.0093 (0.0087)	-0.0099 (0.0090)	0.0065 (0.0091)
Sevo	p=0.18	**0.0099 (0.0025)**	-83e-5 (0.0018)	-0.0014 (0.0022)	p<0.001	**0.017 (0.0053)**	-66e-5 (0.0054)	0.0080 (0.0064)	p=0.0077	**0.028 (0.0068)**	-58e-5 (0.011)	0.016 (0.011)
CARB	p=0.0077	p=0.66	**0.0091 (0.0022)**	-58e-5 (0.0025)	p<0.001	p=0.98	**0.016 (0.0031)**	0.0087 (0.0020)	p=0.0038	p=1	**0.028 (0.0065)**	0.017 (0.0046)
Rec	p<0.001	p=0.21	p=0.85	**0.0085 (0.0029)**	p=1	p<0.001	p<0.001	**0.025 (0.0039)**	p=0.11	p<0.001	p<0.001	**0.044 (0.0070)**
	F(3,27)=6.0; p=0.0029				**F(3,27)=16; p<0.001**				**F(3,27)=15; p<0.001**			
PARIETAL CORTEX – CARBACHOL												
	Low gamma				Medium gamma				High gamma			
	Wake	Sevo	CARB	Rec	Wake	Sevo	CARB	Rec	Wake	Sevo	CARB	Rec
Wake	**0.013 (0.0045)**	55e-5 (0.0016)	-0.0021 (0.0025)	-0.0011 (0.0030)	**0.031 (0.0052)**	-0.016 (0.0041)	-0.019 (0.0064)	-0.0030 (0.0060)	**0.051 (0.0084)**	-0.028 (0.011)	-0.031 (0.011)	-0.0011 (0.012)
Sevo	p=0.88	**0.013 (0.0048)**	-0.0026 (0.0024)	-0.0017 (0.0025)	p<0.001	**0.015 (0.0020)**	-0.0030 (0.0035)	0.013 (0.0053)	p<0.001	**0.023 (0.0086)**	-0.0039 (0.0071)	0.026 (0.016)
CARB	p=0.031	p=0.0028	**0.011 (0.0047)**	92e-5 (0.0028)	p<0.001	p=0.26	**0.012 (0.0028)**	0.016 (0.0060)	p<0.001	p=0.71	**0.019 (0.0052)**	0.030 (0.013)
Rec	p=0.43	p=0.11	p=0.61	**0.012 (0.0060)**	p=0.23	p<0.001	p<0.001	**0.028 (0.0058)**	p=1	p<0.001	p<0.001	**0.050 (0.011)**
	F(3,30)=4.9; p=0.0072				**F(3,30)=71; p<0.001**				**F(3,30)=43; p<0.001**			

Table 2.4 Parietal-to-Frontal connectivity before, during, and after sevoflurane administration, and carbachol delivery into prefrontal and parietal cortices.
Mean(±sd) for each state is shown in bold along the diagonal of each section. The cells above the means(±sd) values show the effect sizes as the difference of the means(±sd). Sevo: sevoflurane administration, CARB: carbachol delivered during sevo, Rec: post-sevoflurane recovery wake.

PREFRONTAL CORTEX – NORADRENALINE												
	Low gamma				Medium gamma				High gamma			
	Wake	**Sevo**	**NA**	**Rec**	**Wake**	**Sevo**	**NA**	**Rec**	**Wake**	**Sevo**	**NA**	**Rec**
Wake	**0.011 (0.0029)**	-0.0033 (0.0014)	-0.0055 (0.0019)	-0.0042 (0.0014)	**0.022 (0.0060)**	-0.013 (0.0062)	-0.013 (0.0081)	-0.0040 (0.0087)	**0.041 (0.0087)**	-0.026 (0.014)	-0.028 (0.014)	-0.0049 (0.011)
Sevo	p<0.001	**0.0076 (0.0028)**	-0.0022 (0.0013)	-87e-5 (0.0016)	p<0.001	**0.0090 (0.0024)**	-83e-6 (0.0024)	0.0093 (0.0075)	p<0.001	**0.015 (0.0063)**	-0.0016 (0.0038)	0.021 (0.0084)
NA	p<0.001	p<0.001	**0.0055 (0.0018)**	0.0013 (0.0014)	p<0.001	p=1	**0.0089 (0.0028)**	0.0094 (0.0082)	p<0.001	p=0.97	**0.013 (0.0077)**	0.023 (0.0074)
Rec	p<0.001	p=0.36	p=0.066	**0.0068 (0.0027)**	p=0.38	p=0.0012	p=0.0010	**0.018 (0.0073)**	p=0.54	p<0.001	p<0.001	**0.036 (0.0088)**
	F(3,21)=38; p<0.001				**F(3,28)=14; p<0.001**				**F(3,21)=31; p<0.001**			
PARIETAL CORTEX – NORADRENALINE												
	Low gamma				**Medium gamma**				**High gamma**			
	Wake	**Sevo**	**NA**	**Rec**	**Wake**	**Sevo**	**NA**	**Rec**	**Wake**	**Sevo**	**NA**	**Rec**
Wake	**0.012 (0.0025)**	-0.0021 (0.0033)	-0.0049 (0.0029)	-0.0032 (0.0022)	**0.024 (0.0071)**	-0.013 (0.0058)	-0.012 (0.0060)	-0.0068 (0.0058)	**0.047 (0.0088)**	-0.026 (0.011)	-0.028 (0.010)	-0.0089 (0.013)
Sevo	p=0.058	**0.0099 (0.0027)**	-0.0028 (0.0034)	-0.0011 (0.0029)	p<0.001	**0.011 (0.0032)**	88e-5 (0.0062)	0.0061 (0.0052)	p<0.001	**0.022 (0.0075)**	-0.0021 (0.0059)	0.017 (0.011)
NA	p<0.001	p=0.0035	0.0071 (0.0023)	0.0017 (0.0012)	p<0.001	p=0.96	**0.012 (0.0073)**	0.0052 (0.0040)	p<0.001	p=0.90	**0.020 (0.0041)**	0.019 (0.0070)
Rec	p<0.001	p=0.54	p=0.16	**0.0088 (0.0019)**	p<0.001	p=0.0014	p=0.0091	**0.017 (0.0059)**	p=0.016	p<0.001	p<0.001	**0.039 (0.0076)**
	F(3,30)=12; p<0.001				**F(3,30)=25; p<0.001**				**F(3,30)=39; p<0.001**			

Table 2.5 Frontal-to-Parietal connectivity before, during, and after sevoflurane administration, and noradrenaline delivery into prefrontal and parietal cortices.
Mean(±sd) for each state is shown in bold along the diagonal of each section. The cells above the mean(±sd) values show the effect sizes as the difference of the means(±sd). Sevo: sevoflurane administration, NA: noradrenaline delivered during sevo, Rec: post-sevoflurane recovery wake.

PREFRONTAL CORTEX – NORADRENALINE												
	Low gamma				Medium gamma				High gamma			
	Wake	**Sevo**	**NA**	**Rec**	**Wake**	**Sevo**	**NA**	**Rec**	**Wake**	**Sevo**	**NA**	**Rec**
Wake	**0.010 (0.0024)**	-0.0027 (0.0020)	-0.0047 (0.0026)	-0.0033 (0.0019)	**0.027 (0.010)**	-0.016 (0.010)	-0.017 (0.012)	-0.0073 (0.011)	**0.041 (0.0088)**	-0.024 (0.012)	-0.026 (0.013)	-0.0038 (0.011)
Sevo	p<0.001	**0.0077 (0.0021)**	-0.0020 (0.0011)	-63e-5 (0.0017)	p<0.001	**0.011 (0.0029)**	-0.0011 (0.0022)	0.0085 (0.0055)	p<0.001	**0.018 (0.0078)**	-0.0025 (0.0054)	0.020 (0.011)
NA	p<0.001	p=0.018	**0.0058 (0.0024)**	0.0013 (0.0019)	p<0.001	p=0.99	**0.010 (0.0036)**	0.0096 (0.0063)	p<0.001	p=0.90	**0.015 (0.0066)**	0.022 (0.0082)
Rec	p<0.001	p=0.79	p=0.19	**0.0071 (0.0026)**	p=0.077	p=0.029	p=0.0094	**0.020 (0.0049)**	p=0.72	p<0.001	p<0.001	**0.038 (0.0088)**
	F(3,21)=17; p<0.001				**F(3,21)=13; p<0.001**				**F(3,21)=28; p<0.001**			
PARIETAL CORTEX – NORADRENALINE												
	Low gamma				Medium gamma				High gamma			
	Wake	**Sevo**	**NA**	**Rec**	**Wake**	**Sevo**	**NA**	**Rec**	**Wake**	**Sevo**	**NA**	**Rec**
Wake	**0.011 (0.0019)**	-0.0014 (0.0024)	-0.0029 (0.0039)	-0.0024 (0.0020)	**0.025 (0.0066)**	-0.012 (0.0047)	-0.012 (0.0057)	-0.0051 (0.0059)	**0.049 (0.0086)**	-0.026 (0.0095)	-0.029 (0.012)	-0.0092 (0.014)
Sevo	p=0.39	**0.0099 (0.0021)**	-0.0015 (0.0031)	-0.0010 (0.0026)	p<0.001	**0.013 (0.0049)**	69e-5 (0.0062)	0.0074 (0.0054)	p<0.001	**0.023 (0.0076)**	-0.0026 (0.0070)	0.017 (0.011)
NA	p=0.0060	p=0.33	**0.0085 (0.0030)**	48e-5 (0.0032)	p<0.001	p=0.97	**0.014 (0.0074)**	0.0067 (0.0032)	p<0.001	p=0.85	**0.020 (0.0052)**	0.020 (0.0079)
Rec	p=0.032	p=0.66	p=0.95	**0.0089 (0.0022)**	p=0.0071	p<0.001	p<0.001	**0.020 (0.0064)**	p=0.019	p<0.001	p<0.001	**0.040 (0.0083)**
	F(3,30)=4.2; p=0.014				**F(3,30)=28; p<0.001**				**F(3,30)=38; p<0.001**			

Table 2.6 Parietal-to-Frontal connectivity before, during, and after sevoflurane administration, and noradrenaline delivery into prefrontal and parietal cortices.
Mean(±sd) for each state is shown in bold along the diagonal of each section. The cells above the mean(±sd) values show the effect sizes as the difference of the means(±sd). Sevo: sevoflurane administration, NA: noradrenaline delivered during sevo, Rec: post-sevoflurane recovery wake.

2.3.3 Spectral Power in Slow Oscillations Does Not Correlate with Level of Consciousness

2.3.3.1 Carbachol Delivery into Prefrontal and Parietal Cortices

As expected, compared with the baseline wake state, sevoflurane anesthesia was associated with a significant increase ($p \leq 0.02$) in spectral power in slow oscillations (Figure 2.4A; Table 2.7). In our previous report,[158] we showed that the delivery of carbachol into PFC of sevoflurane-anesthetized rats could restore wakefulness and produce EEG activation, while carbachol into parietal cortex produced only EEG activation.[158] Analysis of the carbachol epoch showed that regardless of the presence
(stimulation of PFC) or absence (stimulation of parietal cortex) of wakefulness, the EEG activation was accompanied by a significant decrease in slow oscillations power compared with the sevoflurane epoch ($p \leq 0.001$ for carbachol in the PFC, $p < 0.001$ for carbachol in the parietal cortex) (Figure 2.4A; Table 2.7). The post-sevoflurane recovery wake period in both the prefrontal and parietal groups was also characterized by decrease in the spectral power in slow oscillations that was significantly lower than that observed during sevoflurane anesthesia ($p = 0.0018$ for carbachol in the PFC, $p < 0.001$ for carbachol in the parietal cortex). For both the prefrontal and parietal cortical groups, there was no significant difference ($p \geq 0.23$) in the spectral power between baseline wake state, carbachol-induced EEG activation, and the post-sevoflurane recovery wake period (Figure 2.4A; Table 2.7).

2.3.3.2 NA Delivery into Prefrontal and Parietal Cortices

Sevoflurane anesthesia produced a significant increase ($p \leq 0.0051$) in the spectral power in slow oscillations in both the prefrontal and parietal cortical groups (Figure 2.4B; Table 2.7). NA in prefrontal or parietal cortex did not restore wakefulness during ongoing sevoflurane administration, but it was shown to produce EEG activation.[158] These findings are consistent with a previous study that demonstrated EEG activation without behavioral arousal in propofol-anesthetized rats after systemic treatment with a noradrenergic reuptake blocker.[185] The NA epoch, characterized by EEG activation, was also marked by a significant decrease in the spectral power in slow oscillations in both the prefrontal and parietal groups ($p < 0.001$ compared with sevoflurane anesthesia) (Figure 2.4B; Table 2.7). The power in

slow oscillations in the post-sevoflurane recovery wake period in both prefrontal and parietal groups was significantly reduced ($p < 0.001$) compared with sevoflurane anesthesia epoch (Figure 2.4B; Table 2.7). For both the prefrontal and parietal cortical groups, there was no significant difference ($p \geq 0.56$) in the spectral power between the post-sevoflurane recovery wake period, the NA-induced EEG activation, and the baseline wake state (Figure 2.4B; Table 2.7).

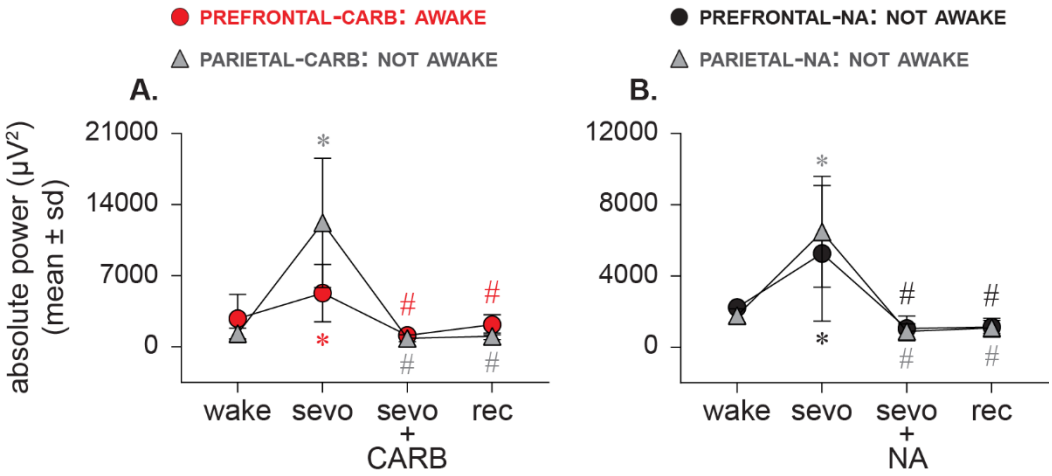

Figure 2.4 Spectral power of slow oscillations does not correlate with level of consciousness.
(A, B) Spectral power of slow oscillations (0.5–1 Hz) showed a significant increase during sevoflurane anesthesia (sevo). The restoration of wakefulness through 5 mM carbachol (CARB) delivery to PFC as well as the absence of wakefulness after CARB delivery to parietal cortex or 20 mM NA delivery to prefrontal and parietal cortices were reported to be accompanied with EEG activation[158], which produced a significant decrease (compared with sevo) in spectral power regardless of the presence or absence of wakefulness (A, B). The spectral power during post-sevoflurane recovery wake (rec) epoch remained significantly lower than sevo and was not significantly different from CARB or NA or the baseline wake state (wake) (A, B). A linear mixed model with random intercept for each rat was used for the statistical comparisons, and the post hoc pairwise tests were single-step corrected for multiple comparisons. The statistical comparisons are shown at $p < 0.05$. The mean, SD, exact p values, F statistics, and the effect sizes for each statistical comparison are provided in Table 2.7. The significance symbols are color-coded to match the line-symbol plots. *Significant compared with wake. #Significant compared with sevo.

PREFRONTAL CORTEX - CARBACHOL					PREFRONTAL CORTEX - NORADRENALINE				
	Wake	**Sevo**	**CARB**	**Rec**		**Wake**	**Sevo**	**NA**	**Rec**
Wake	**2785 (2376)**	2506 (4309)	-1654 (2476)	-608 (2557)	**Wake**	**2225 (419)**	3040 (3746)	-1171 (637)	-1087 (470)
Sevo	p=0.021	**5291 (2824)**	-4160 (3074)	-3113 (3576)	**Sevo**	p=0.0051	**5265 (3811)**	-4211 (3549)	-4127 (3519)
CARB	p=0.23	p<0.001	**1131 (722)**	1047 (1285)	**NA**	p=0.58	p<0.001	**1054 (692)**	84 (695)
Rec	p=0.90	p=0.0018	p=0.62	**2178 (986)**	**Rec**	p=0.63	p<0.001	p=1	**1138 (371)**
	F(3,32)=8.3; p<0.001					**F(3,3)=9.3; p=0.069**			
PARIETAL CORTEX - CARBACHOL					**PARIETAL CORTEX - NORADRENALINE**				
	Wake	**Sevo**	**CARB**	**Rec**		**Wake**	**Sevo**	**NA**	**Rec**
Wake	**1303 (533)**	10900 (6044)	-458 (585)	-264 (393)	**Wake**	**1772 (381)**	4708 (3273)	-890 (604)	-684 (769)
Sevo	p<0.001	**12203 (6362)**	-11358 6232)	-11163 (6251)	**Sevo**	p<0.001	**6480 (3110)**	-5597 (3131)	-5392 (3134)
CARB	p=0.99	p<0.001	**845 (337)**	194 (493)	**NA**	p=0.56	p<0.001	**883 (419)**	205 (773)
Rec	p=1	p<0.001	p=1	**1040 (328)**	**Rec**	p=0.75	p<0.001	p=0.99	**1088 (530)**
	F(3,72)=36; p<0.001					**F(3,44)=30; p<0.001**			

Table 2.7 Absolute power of slow oscillations before, during, and after sevoflurane administration, and carbachol and noradrenaline delivery into prefrontal and parietal cortices.
Mean(±sd) for each state is shown in bold along the diagonal of each section. The cells above the mean(±sd) values show the effect sizes as the difference of the means(±sd). Sevo: sevoflurane administration, CARB: carbachol delivered during sevo, NA: noradrenaline delivered during sevo Rec: post-sevoflurane recovery wake.

2.3.4 Electroencephalographic Temporal Lempel-Ziv Complexity Does Not Correlate with Level of Consciousness

2.3.4.1 Carbachol Delivery into Prefrontal and Parietal Cortices

The temporal complexity was measured over the frontal and parietal areas. As compared with the baseline wake state, sevoflurane anesthesia was characterized by a significant reduction ($p < 0.001$) in the temporal complexity (Figures 2.5A and 2.5C; Table 2.8). Carbachol delivery into PFC (restoration of wakefulness) or parietal cortex (no behavioral arousal) during sevoflurane anesthesia produced EEG activation, which was characterized by increase in temporal complexity ($p < 0.001$ compared with sevoflurane anesthesia) (Figures 2.5A and 2.5C; Table 2.8). In both the prefrontal and parietal groups, the post-sevoflurane recovery wake period was characterized by high temporal complexity in frontal (Figure 2.5A; Table 2.8) and parietal areas (Figure 2.5C; Table 2.8) ($p < 0.001$ compared with sevoflurane anesthesia), which was not significantly different ($p \geq 0.28$) from that observed during the baseline wake state and the carbachol delivery epoch (Figures 2.5A and 2.5C; Table 2.8).

2.3.4.2 NA Delivery into Prefrontal and Parietal Cortices

Compared with the baseline wake state, the temporal complexity was significantly reduced during sevoflurane anesthesia ($p < 0.001$) (Figures 2.5B and 2.5D; Table 2.9). NA delivery into PFC or parietal cortex of sevoflurane anesthetized rats did not produce any signs of wakefulness, but it did produce EEG activation.[158] Analysis of the NA epoch in both the prefrontal and parietal cortical groups showed a significant increase in the temporal complexity over the frontal ($p < 0.001$) (Figure 2.5B; Table 2.9) and parietal ($p < 0.001$) (Figure 2.5D; Table 2.9) areas, compared with sevoflurane anesthesia; despite the increase, the temporal complexity in the frontal area (Figure 2.5B; Table 2.9) remained significantly lower than that observed during the baseline wake levels ($p < 0.001$), whereas for the parietal area (Figure 2.5D; Table 2.9) it was comparable with baseline wake state ($p = 0.12$). The temporal complexity in the frontal and parietal areas during the post-sevoflurane recovery wake period remained significantly high compared with sevoflurane anesthesia ($p < 0.001$) (Figures 2.5B and 2.5D; Table 2.9) but was not significantly different from that observed during baseline wake state ($p \geq 0.2$) and the NA delivery epoch ($p \geq 0.089$) (Figures 2.5B and 2.5D; Table 2.9).

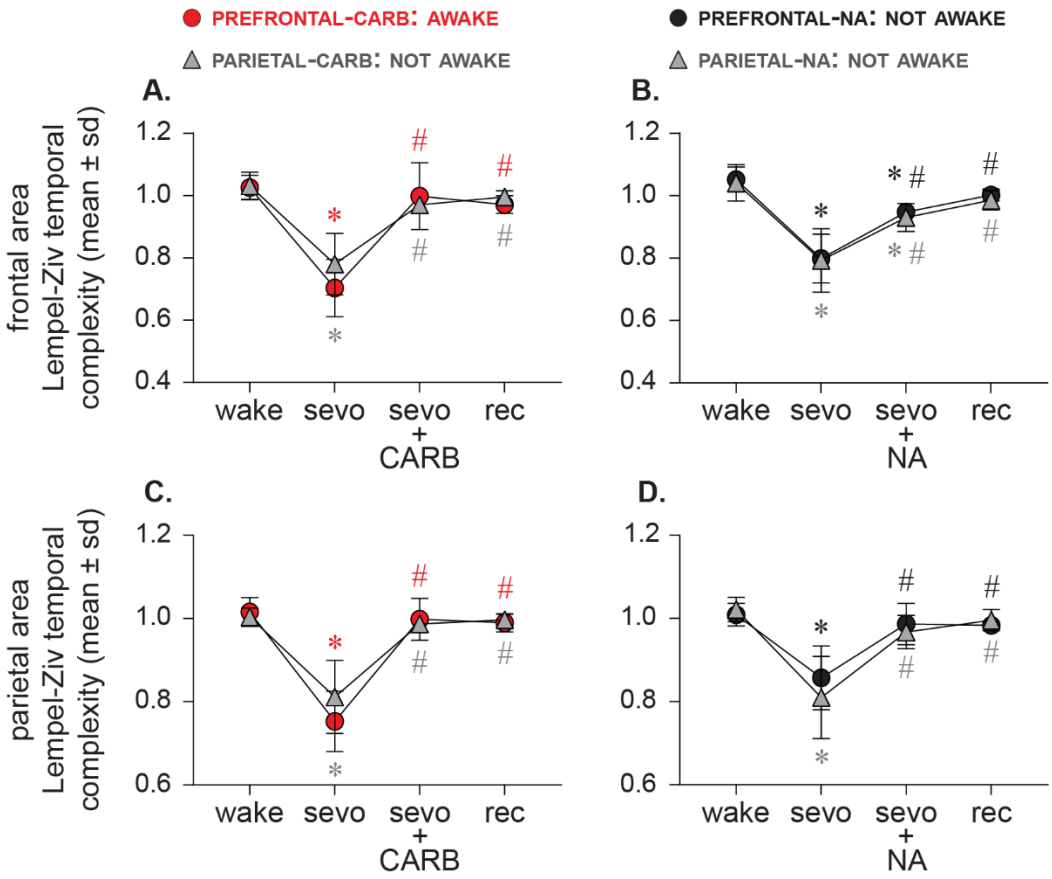

Figure 2.5 Electroencephalographic temporal Lempel–Ziv complexity does not correlate with level of consciousness. Sevoflurane anesthesia (sevo) was characterized by a significant reduction in Lempel–Ziv complexity in frontal (A,B) and parietal areas (C,D). The restoration of wakefulness through 5mM carbachol (CARB) delivery to PFC as well as the absence of wakefulness after CARB delivery to parietal cortex or 20mMNAdelivery to prefrontal and parietal cortices was reported to be accompanied by EEG activation[158], which reversed the sevoflurane-induced decrease in complexity. The increase was significant (compared with sevo) for all groups and was not different from baseline wake state (wake), except for prefrontal- and parietal cortex-NA groups (B–D), where it remained significantly lower compared with wake. The complexity during post-sevoflurane recovery wake (rec) epoch remained significantly higher than sevo and was not significantly different from CARB or NA epochs or wake (A–D). The plotted values for complexity were obtained after normalizing raw temporal complexity data with phase-randomized surrogate time series and show complexity changes beyond that explained by only spectral changes. A linear mixed model with random intercept for each rat was used for the statistical comparisons, and the post hoc pairwise tests were single-step corrected for multiple comparisons. The statistical comparisons are shown at $p<0.05$. The mean, SD, exact p values, F statistics, and the effect sizes for each statistical comparison are provided in Tables 2.8 and 2.9. The significance symbols are color-coded to match the line-symbol plots. *Significant compared with baseline wake state. #Significant compared with sevo.

		PREFRONTAL CORTEX - CARBACHOL				PARIETAL CORTEX – CARBACHOL			
		Wake	**Sevo**	**CARB**	**Rec**	**Wake**	**Sevo**	**CARB**	**Rec**
FRONTAL AREA	**Wake**	**1.0 (0.039)**	-0.32 (0.086)	-0.028 (0.11)	-0.055 (0.049)	**1.0 (0.043)**	-0.25 (0.092)	-0.062 (0.046)	-0.036 (0.037)
	Sevo	p<0.001	**0.70 (0.092)**	0.29 (0.10)	0.27 (0.11)	p<0.001	**0.78 (0.099)**	0.19 (0.11)	0.22 0.10
	CARB	p=0.80	p<0.001	**1.0 (0.11)**	-0.027 (0.11)	p=0.039	p<0.001	**0.97 (0.024)**	0.026 (0.027)
	Rec	p=0.28	p<0.001	p=0.81	**0.97 (0.028)**	p=0.41	p<0.001	p=0.69	**1.0 (0.020)**
		F(3,27)=48; p<0.001				**F(3,30)=48; p<0.001**			
		Wake	**Sevo**	**CARB**	**Rec**	**Wake**	**Sevo**	**CARB**	**Rec**
PARIETAL AREA	**Wake**	**1.0 (0.035)**	-0.26 (0.078)	-0.017 (0.060)	-0.026 (0.042)	**1.0 (0.021)**	-0.19 (0.077)	-0.017 (0.030)	-0.0073 (0.026)
	Sevo	p<0.001	**0.75 (0.073)**	0.25 (0.084)	0.24 (0.080)	p<0.001	**0.81 (0.089)**	0.18 (0.095)	0.19 (0.089)
	CARB	p=0.85	p<0.001	**1.0 (0.050)**	-0.0084 (0.057)	p=0.81	p<0.001	**0.99 (0.019)**	0.0098 (0.016)
	Rec	p=0.63	p<0.001	p=0.98	**0.99 (0.022)**	p=0.98	p<0.001	p=0.96	**1.0 (0.014)**
		F(3,27)=66; p<0.001				**F(3,30)=46; p<0.001**			

Table 2.8 Temporal Lempel-Ziv complexity (normalized) in frontal and parietal areas before, during, and after sevoflurane administration and carbachol delivery into prefrontal and parietal cortices
Mean(±sd) for each state is shown in bold along the diagonal of each section. The cells above the mean(±sd) values show the effect sizes as the difference of the means(±sd). Sevo: sevoflurane administration, CARB: carbachol delivered during sevo, Rec: post-sevoflurane recovery wake.

		PREFRONTAL CORTEX - NORADRENALINE				PARIETAL CORTEX - NORADRENALINE			
		Wake	**Sevo**	**NA**	**Rec**	**Wake**	**Sevo**	**NA**	**Rec**
FRONTAL AREA	**Wake**	**1.1 (0.040)**	-0.25 (0.077)	-0.10 (0.058)	-0.049 (0.036)	**1.0 (0.058)**	-0.25 (0.13)	-0.11 (0.080)	-0.056 (0.070)
	Sevo	p<0.001	**0.80 (0.078)**	0.14 (0.099)	0.20 (0.078)	p<0.001	**0.79 (0.10)**	0.14 (0.097)	0.19 (0.12)
	NA	p<0.001	p<0.001	**0.95 (0.026)**	0.055 (0.038)	p<0.001	p<0.001	**0.93 (0.045)**	0.055 (0.069)
	Rec	p=0.15	p<0.001	p=0.089	**1.0 (0.019)**	p=0.18	p<0.001	p=0.19	**0.99 (0.031)**
		F(3,28)=44; p<0.001				**F(3,40)=30; p<0.001**			
		Wake	**Sevo**	**NA**	**Rec**	**Wake**	**Sevo**	**NA**	**Rec**
PARIETAL AREA	**Wake**	**1.0 (0.027)**	-0.15 (0.087)	-0.022 (0.066)	-0.026 (0.033)	**1.0 (0.030)**	-0.21 (0.11)	-0.054 (0.051)	-0.025 (0.047)
	Sevo	p<0.001	**0.86 (0.077)**	0.13 (0.068)	0.13 (0.072)	p<0.001	**0.81 (0.099)**	0.16 (0.089)	0.19 (0.11)
	NA	p=0.76	p<0.001	**0.99 (0.050)**	-0.0035 (0.042)	p=0.12	p<0.001	**0.97 (0.040)**	0.029 (0.052)
	Rec	p=0.67	p<0.001	p=1	**0.98 (0.011)**	p=0.72	p<0.001	p=0.64	**1.0 (0.026)**
		F(3,21)=19; p<0.001				**F(3,40)=31; p<0.001**			

Table 2.9 Temporal Lempel-Ziv complexity (normalized) in frontal and parietal areas before, during, and after sevoflurane administration and noradrenaline delivery into prefrontal and parietal cortices.
Mean(±sd) for each state is shown in bold along the diagonal of each section. The cells above the mean(±sd) values show the effect sizes as the difference of the means(±sd). Sevo: sevoflurane administration, NA: noradrenaline delivered during sevo, Rec: post-sevoflurane recovery wake.

2.3.5 Electroencephalographic Spatiotemporal Lempel-Ziv Complexity Does Not Correlate with Level of Consciousness

Compared with the baseline wake state, there was a significant decrease ($p < 0.001$) in spatiotemporal complexity during sevoflurane anesthesia (Table 2.10). Reverse dialysis delivery of 5 mM carbachol into PFC of these high-density cohort rats (under constant sevoflurane anesthesia) restored wakefulness (defined by attempts or recovery of righting), produced EEG activation, and caused a significant increase in the spatiotemporal complexity ($p < 0.001$) compared with sevoflurane anesthesia; there was no significant difference compared with the baseline wake state ($p = 0.58$) (Table 2.10). The spatiotemporal complexity during the post-sevoflurane recovery wake epoch was significantly higher compared with sevoflurane anesthesia ($p < 0.001$) but was not significantly different from either baseline wake state ($p = 0.95$) or carbachol delivery epoch ($p = 0.27$) (Table 2.10). These changes in spatiotemporal complexity (Table 2.10) mirrored the changes in temporal complexity over frontal and parietal areas, as described earlier (Figure 3.5A–D). Of note, we also measured changes in local acetylcholine levels before, during, and after sevoflurane anesthesia, as well as carbachol delivery to PFC in these rats. Statistical comparison using linear mixed model showed a significant effect on the acetylcholine levels across conditions ($F_{(3,9)} = 8.2$, $p = 0.006$). Compared with the baseline wake state, sevoflurane anesthesia was characterized by an 84% decrease in acetylcholine levels [mean ± SD (CI): 0.078 ± 0.043 (0.036–0.12) for sevoflurane vs 0.49 ± 0.35 (0.15– 0.84) for wake state, $p = 0.58$], which is comparable with that reported in our previous publication[158]. Carbachol delivery to PFC during sevoflurane anesthesia produced a highly significant increase in the local acetylcholine levels [mean ± SD (CI): 1.57 ± 0.92 (0.66 –2.47), $p < 0.001$ compared with sevoflurane anesthesia], which remained significantly elevated during post-sevoflurane recovery period [mean ± SD (CI): 1.13 ± 0.87 (0.29 –1.99), $p = 0.007$ compared with sevoflurane]. Overall, these changes in prefrontal acetylcholine levels after sevoflurane administration and carbachol delivery, both in the direction of change and magnitude, are consistent with the data reported in our previous study.[158]

PREFRONTAL – CARBACHOL				
	Wake	**Sevo**	**CARB**	**Rec**
Wake	**0.92 (0.018)**	-0.16 (0.024)	-0.017 (0.020)	0.0072 (0.014)
Sevo	p<0.001	**0.76 (0.033)**	0.14 (0.042)	0.17 (0.019)
CARB	p=0.58	p<0.001	**0.90 (0.031)**	0.024 (0.033)
Rec	p=0.95	p<0.001	p=0.27	**0.92 (0.022)**
	F(3,9)=69; p<0.001			

Table 2.10 Spatiotemporal Lempel-Ziv complexity (normalized) before, during, and after sevoflurane administration and carbachol delivery into prefrontal cortex
Mean(±sd) for each state is shown in bold along the diagonal of each section. The cells above the mean(±sd) values show the effect sizes as the difference of the means(±sd). Sevo: sevoflurane administration, CARB: carbachol delivered during sevo, Rec: post-sevoflurane recovery wake.

2.4 Discussion

The divergent effects of cholinergic stimulation on the prefrontal and parietal cortices enabled the discovery that the level of consciousness can be dissociated from EEG measures of cortical functional connectivity and cortical dynamics. A number of major theories of consciousness are grounded in the requirement for functional, directed, or effective connectivity across the cortex in the conscious state.[64,101,160,186] Indeed, these theories have made successful predictions regarding the reduction in connectivity strength or repertoire empirically observed during sleep, general anesthesia induced by distinct drugs, and pathological states of unconsciousness.[69,73,110,112,113,124,161,163,165–171,187–194] However, it has been unclear whether the reduction of functional or cortical connectivity played a causal role in the state transition, was associated more closely with loss of higher cognition rather than consciousness per se, or was an epiphenomenon. By dissociating level of consciousness from large-scale cortical connectivity, our findings prompt a reevaluation of the role of these connectivity measures in distinguishing states of consciousness and unconsciousness. Similarly, strategies for clinical monitoring of consciousness based on connectivity patterns[112,113,165,188,192] should be reconsidered. Importantly, our findings apply only to the level of consciousness, which can be defined by objective observations, such as wakeful behavior. It is possible that disruptions of large-scale cortical connectivity critically impair the phenomenological contents of consciousness, conscious access, or cognitive processing.[195] Furthermore, because of our experimental design requiring a

closed, air-tight chamber for continuous sevoflurane exposure, we could not test whether the absence of behavioral arousal or wake state after pharmacological manipulation of the cortex constitutes a truly unresponsive condition. Our inferences are based on the observations of spontaneous behaviors and speak only to the spontaneous changes in level of arousal. Our recent studies in human volunteers[196] and surgical patients[197] reported dynamic changes in connectivity patterns under deep anesthesia, but these connectivity patterns were not sufficient to reliably distinguish the changes in the level of consciousness. Although supportive of our results in the current study, it is important to note that these recent studies in humans were restricted to bandwidths below low gamma frequency and entailed long periods of a stable and deep anesthetic plane. A previous study in rats demonstrated that the emergence from isoflurane anesthesia was characterized by multistep discreet fluctuations in spectral power as opposed to a discrete binary process or continuous path to recovery.[198] Similar studies in rats with long duration of anesthetics can further clarify whether the connectivity patterns, in particular in gamma frequency, also demonstrate a dynamic evolution.

In both clinical and preclinical settings, the presence of increased spectral power of slow oscillations (0.5–1 Hz) is considered a signature of unconsciousness,[171–174,199] whereas the appearance of a low-amplitude fast EEG, along with the dissipation of slow oscillations, correlates with the return of consciousness. In the current study, we did indeed observe the appearance of high-amplitude slow EEG and increase in spectral power of slow oscillations during sevoflurane anesthesia. However, the increased spectral power of slow oscillations was dissipated not only in association with restoration of wakefulness and accompanying EEG activation, an expected finding, but also in the cohorts that showed only EEG activation without any signs of wakefulness. These findings demonstrate that dissipation of slow oscillations correlates with an activated EEG rather than behavioral arousal, per se. Furthermore, the known occurrence of low-amplitude fast EEG, a pattern typically associated with wakefulness, during rapid eye movement sleep,[200] the occurrence of high-amplitude slow-wave EEG during wakefulness in patients with Angelman syndrome[201], and the experimental induction of high-amplitude slow-wave EEG in freely moving rats through systemic atropine administration[202] all show various instances of dissociation between EEG patterns and level of consciousness. Similar reports from human subjects under general anesthesia further support these findings across species and states of unconsciousness. For instance, using the isolated forearm technique,

Gaskell et al.[203] demonstrated that the presence of frontal α-δ pattern in the EEG, typically considered to be a marker of anesthetic-induced unconsciousness, cannot reliably discriminate between behavioral responsiveness and unresponsiveness in certain patients under anesthesia, a conclusion that was supported by another patient report.[204] Conversely, ketamine is known to produce fast EEG signatures that, unlike other commonly used general anesthetics, such as propofol or sevoflurane, are not reliably tracked by anesthesia monitors.[205] Our data are consistent with these past findings by demonstrating that slow oscillations can be dissociated from level of consciousness.

Electroencephalographic complexity has been demonstrated to be high during wakefulness as well as in states with high phenomenological contents, such as rapid eye movement sleep[76,88] and the psychedelic experience.[79,83,206] On the other hand, complexity has been reported to be low during the states with reduced level of arousal, such as non-rapid eye movement sleep[73,76,88] and anesthesia.[69,73,85,175] Based on these earlier reports, we expected that EEG complexity would increase after restoration of wakefulness, as achieved by prefrontal cholinergic stimulation, while remaining at a reduced level in the cohorts that failed to demonstrate restoration of wakefulness. Contrary to our expectation, temporal complexity, as measured through Lempel–Ziv algorithm, increased regardless of the presence or absence of wakefulness and instead correlated with EEG activation. In our earlier study,[158] we showed that the restoration of wakefulness following carbachol-mediated cholinergic stimulation of PFC was accompanied by an approximately fivefold increase in local acetylcholine levels. More limited increases in local acetylcholine levels were also observed after NA delivery to PFC as well as carbachol or NA delivery to parietal cortex. In the current study, the changes in spatiotemporal Lempel–Ziv complexity also showed a positive relationship with prefrontal cholinergic tone and EEG activation, which aligns with the changes observed in temporal Lempel–Ziv complexity. Furthermore, the increase in complexity has been reported in states, such as rapid eye movement sleep and ketamine, which are characterized by increased cholinergic tone and EEG activation.[69,83,88,98,207] Therefore, it is possible that underlying changes in cholinergic tone are more closely associated with the complexity changes rather than behavioral arousal.

Interestingly, despite the increase in cortical acetylcholine levels or the behavioral phenotype following carbachol or NA delivery into prefrontal and parietal cortices,[158] the functional connectivity, as measured in the current study, did not show a significant change.

Therefore, functional connectivity is doubly dissociated from both behavior and cortical cholinergic one. Furthermore, our results are consistent with the effect of anesthetics on local neuronal networks. A dissociation between cortical neuronal interactions and spontaneous behavior was demonstrated after stimulation of the ascending arousal system in rats anesthetized with desflurane at comparable effective levels to that used here.[208] Notably, previous studies targeting multiple subcortical pathways with a variety of stimulus modalities (electrical, pharmacological, optogenetic) have demonstrated restoration of wakefulness from unconsciousness induced by different classes of anesthetics,[209–216] suggesting that site of stimulation, rather than stimulus modality or anesthetic agent used for inducing unconsciousness, may play a greater role in modulating behavioral arousal. However, these studies did not investigate changes in connectivity or complexity; therefore, it remains to be seen whether the restoration of wakefulness from anesthesia after subcortical stimulation will produce connectivity and complexity patterns similar to those observed in our study.

Although previous reports of the dissociation between EEG and behavioral states[200–205] are supportive of our results, caution should be applied in the interpretation of these findings because of the reliance of our study on behavioral motor activity for the determination of wakefulness, the inherent limitations of the connectivity and complexity measures used, and the inability to make any inferences related to the content or experiential nature of conscious activity. Furthermore, although we have artificially dissociated levels of consciousness and various cortical measures, it is still possible that they correlate during more typical physiological and pharmacological state transitions or with other techniques of neurophysiology, functional neuroimaging, and analysis.

In conclusion, we conducted a systematic comparison of multiple EEG measures (connectivity, complexity, and spectral power) after cholinergic or noradrenergic stimulation of distinct cortical areas, and demonstrate the dissociation between these cortical measures and level of consciousness.

2.5 Summary and Conclusions

Using EEG data from Pal et al., 2018,[162] we explored the relationship between level of consciousness as assessed by purposeful righting behavior and changes in cortical dynamics – including complexity and frontoparietal connectivity across 3 distinct gamma bandwidths. While

data from Pal et al. 2018 suggests that cholinergic neurotransmission within the PFC is a neurochemical mediator of the level of consciousness, our subsequent Chapter 2 study found that the restoration of behavioral responsiveness in this condition occurred independent of changes in frontoparietal connectivity or cortical cholinergic tone. Frontoparietal connectivity remained suppressed during exposure to sevoflurane across low, medium, and high gamma bandwidths, notwithstanding the presence (PFC carbachol stimulation) or absence (all remaining stimulation conditions) of wakefulness. In contrast, restoration of temporal or spatiotemporal Lempel-Ziv complexity to waking levels was found to be a necessary – but insufficient – dynamic condition for the return of righting reflex. While complexity did not track with the behavioral level of arousal, changes in Lempel-Ziv complexity were found to occur during periods of elevated cortical acetylcholine following stimulation in the original study,[162] as well as spectral signal features such as EEG activation or the presence of slow oscillations. In sum - these findings necessitate further study of the relationship between measures of complexity and cortical cholinergic transmission.

Chapter 3 State-Dependent and Bandwidth-Specific Effects of Ketamine and Propofol on Electroencephalographic Complexity in Rats[217]

3.1 Introduction

Although there is still a debate as to the precise neural correlates of consciousness,[42,43,218] several theories are converging upon the idea that the capacity for conscious experience relates to the diversity of states that the brain is able to generate.[64,66,101,219] Analytical measures that capture the complexity of signals such as electroencephalogram (EEG) have been proposed to serve as a surrogate for the diversity of the brain's repertoire of states and level of consciousness. Relative to states typically associated with phenomenological content, such as wakefulness or rapid eye movement sleep, complexity is suppressed in association with unconsciousness, such as slow-wave sleep,[76,88] coma,[94,220] and the anesthetized state.[69,73,75,78,92,110,159] Conversely, recent MEG/EEG studies have demonstrated elevated signal diversity induced by canonical serotonergic psychedelics and the dissociative NMDA-antagonist ketamine.[80,83,206]

From the perspective of its effects on EEG signal diversity, ketamine diverges from traditional anesthetics at subanesthetic concentrations, as it induces.[79,83] This is in contrast to GABAergic anesthetics such as propofol, which have been shown to degrade sensory integration and attenuate neural signal diversity in a dose-dependent manner.[51,71,221] Furthermore, previous studies have described a remarkably high incidence of subjective reports of dreaming following emergence from ketamine anesthesia that are often described to be vivid, bizarre, and hallucinatory in nature.[69,222] Although dreaming has also been reported in patients receiving GABAergic anesthetic agents such as propofol, the occurrence is reported to be much less common and is often associated with simple phenomenological content more typical of slow-wave sleep [53,223] Previous studies have reported both preserved and attenuated measures of spatiotemporal EEG complexity in humans given doses of ketamine titrated to loss of

Published as: Brito, M. A., Li, D., Mashour, G. A. & Pal, D. State-Dependent and Bandwidth-Specific Effects of Ketamine and Propofol on Electroencephalographic Complexity in Rats. *Front. Syst. Neurosci.* **14**, (2020).

Contributions: M.A.B. and D.L. analyzed the data. M.A.B., D.L., G.A.M. amd D.P. interpreted the data and wrote the manuscript.

responsiveness.[69,79,97] However, these studies have used human scalp EEG filtered to frequencies of 55 Hz or lower and thus could not characterize the dynamics of higher gamma frequencies. Prior studies from our laboratory have shown suppressed cortical connectivity in the higher gamma (85-155 Hz) bandwidth during sleep and anesthetic (ketamine, propofol, sevoflurane) induced unresponsivenes.[98,120] Thus, cortical dynamics in higher gamma bandwidth may be a more reliable indicator of level of consciousness. To determine if ketamine anesthesia is associated with a suppression of signal complexity when higher gamma bandwidth is included in the analysis, we utilized intracranial EEG from our previously published studies in rats to assess temporal EEG complexity in three distinct bandwidths (0.5-175 Hz, 0.5-55 Hz, and 65-175 Hz) in frontal and parietal cortices before, during, and after ketamine anesthesia or, as a GABAergic comparator, propofol anesthesia.

3.2 Methods

Adult male Sprague Dawley rats (n=8 for ketamine, n=8 for propofol; Charles River Laboratories) were used for all experiments. The experiments were approved by the Institutional Animal Care and Use committee and were in compliance with the Guide for the Care and Use of Laboratory Animals. The rats were housed in a temperature-controlled facility with a 12-hour light/12-hour dark cycle (lights ON at 6:00 AM) with free access to food and drinking water. For detailed methods, see the original studies.[98,120]

3.2.1 Surgical procedures

Under surgical isoflurane anesthesia, the rats (n=16) were implanted with stainless steel screw electrodes to record EEG from frontal (Bregma: anterior 3.0 mm, lateral 2.5 mm), parietal (Bregma: posterior 4.0 mm, lateral 2.5 mm), and occipital (Bregma: posterior 8.0 mm, lateral 2.5 mm) cortices. A stainless steel screw electrode over the nasal sinus served as the reference electrode. In a subset of rats (n=8), an indwelling catheter (Micro-Renathane tubing, MRE-040; Braintree Scientific, Braintree, MA, USA) was surgically positioned into the jugular vein to allow for intravenous propofol infusion.

3.2.2 Electroencephalographic data collection before, during, and after ketamine or propofol anesthesia

Monopolar EEG signals – with reference to a screw electrode over nasal sinus – from frontal, parietal, and occipital electrodes were amplified 5000x (Grass Model 15 LT amplifier system, 15A54 Quad Amplifier; Natus Neurology Inc., Middleton, WI, USA), bandpass filtered between 0.1-300 Hz, and digitized at 1kHz using a MP150 data acquisition unit paired with AcqKnowledge software (version 4.1.1; Biopac Systems, Inc., Goleta, CA. USA). The experimental design for ketamine anesthesia experiments is illustrated in Figure 3.1A. Rats were connected to the recording equipment and baseline wake EEG was recorded for 50 minutes. After 50 minutes of baseline data collection, the EEG recording was stopped, and the rats received an intraperitoneal bolus (150 mg/kg) of ketamine hydrochloride. The concentration of ketamine was based on our dose-response experiments, as noted in the original study,[98] and was also informed by a previously published report.[224] After anesthetic induction - as confirmed by the loss of righting reflex (LORR) and the absence of ear, trunk, or whisker movements - EEG data collection was resumed and continued until the completion of recording session. For EEG analysis, 5-minute EEG segments were selected from 1) last 12.5 minutes of baseline wake state, 2) first 5 minutes of ketamine anesthesia, 3) within 12.5 minutes before return of righting reflex - RORR - i.e., pre-RORR, and 4) first 12.5 min after RORR, i.e., post-RORR. In three of these rats, EEG was recorded for an extended period and the last 5 minutes from the recovery period were used for Lempel-Ziv complexity analysis. The experimental design for propofol anesthesia experiments is illustrated in Figure 3.Z for each state analyzed in ketamine and propofol groups.

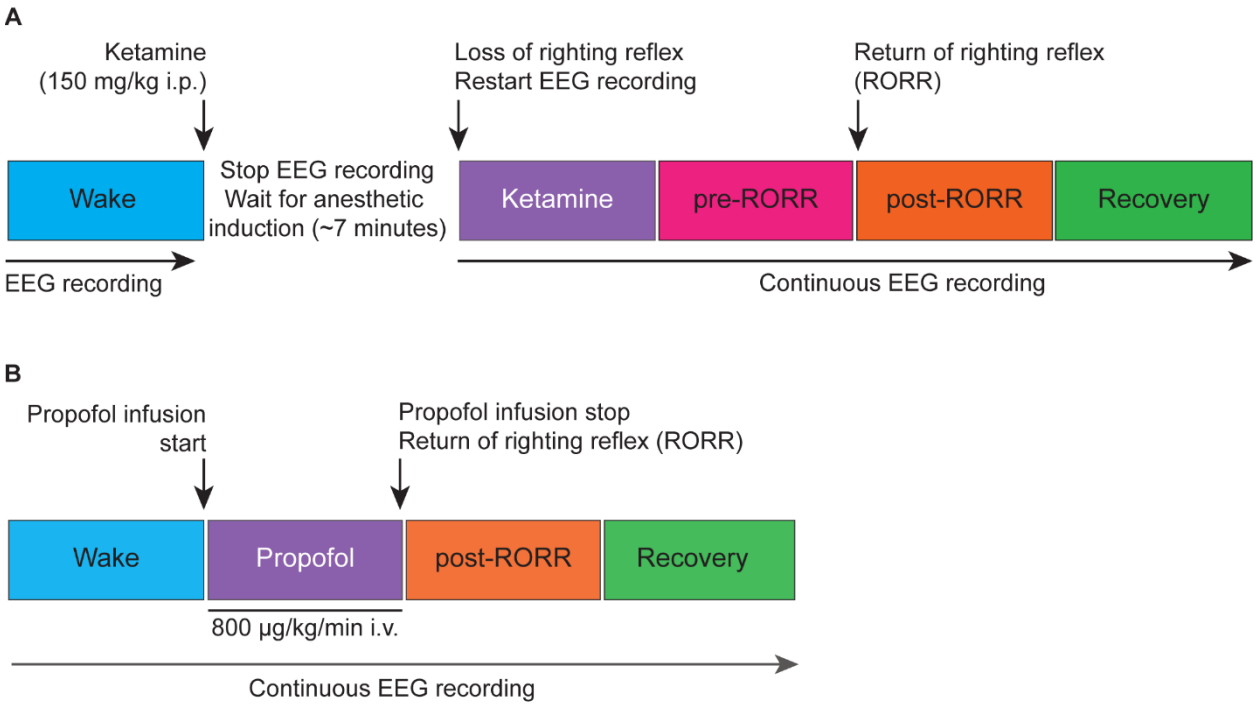

Figure 3.1 Schematic illustrating the experimental design for electroencephalographic recordings before, during, and after ketamine and propofol anesthesia
i.p. – intraperitoneal, i.v. – intravenous.

3.2.3 Lempel-Ziv electroencephalographic complexity analysis

We used Lempel-Ziv complexity (LZc) - a surrogate for neural signal diversity - to analyze EEG complexity before, during, and after ketamine and propofol anesthesia (Lempel and Ziv, 1976). LZc analysis was performed as described in previous studies, including from our laboratory.[75,76,79,83,159] In brief, the frontal and parietal EEG signals were detrended using local linear regression (10-s window with 5-s overlap). EEG data were lowpass filtered at 175 or 55 Hz via a fifth-order butterworth filter. For analysis of higher gamma frequencies, data were bandpass filtered between 65 Hz and 175 Hz. The filtered signal was then segmented into non-overlapping 10-s windows. The instantaneous amplitude was calculated from the Hilbert transform of the signal, which was then binarized using its mean value as the threshold for each channel. LZc searches for the occurrence of consecutive binary characters, or "words," and counts the number of times a new "word" is encountered. The resultant LZc values were averaged across all of the windows as an estimate of the temporal complexity at each state. We normalized the original LZc by the mean of the LZc values from n=50 surrogate time series generated by randomly shuffling the binary sequence, as this leads to maximal value for binary sequences for a fixed length. To examine if the complexity as reflected by the LZc is dissociable

from the spectral content of the signal, we employed an additional control measure that compared the time-shuffled LZc (as described above) with LZc normalized through phase-randomization (obtained from surrogate data in which the power spectrum of the signal is preserved). The resultant normalized LZc measure (denoted LZc_N) reflects changes in complexity beyond the spectral content of the signal. Both LZc and LZc_N are reported in arbitrary units. It is important to note that Lempel-Ziv complexity is a nonlinear measure that does not require linear assumptions about the structure of the signal (i.e., additivity, stationarity) in the same manner as measures such as spectral power. Therefore, it can be used to derive information from a broader signal band without the need to parse the signal into many individual frequency components, as is traditionally done with spectral power. Our choice of two distinct frequency bands was based on the following considerations: complexity analysis in 0.5 to 55 Hz frequency band allowed us to have a direct comparison of our rat data to previously reported human data[69,79,97] and in addition served as a control to validate our methodology against these previous human studies. The complexity analysis in the higher gamma frequency band was motivated by rat studies from our laboratory[98,120] that showed high gamma connectivity (above 65 Hz) as a robust indicator of unconsciousness during anesthetic- and sleep-induced unconsciousness.

3.2.4 Statistical analysis

All statistical analyses were performed using R software (R Core Team, 2016) in consultation with the Consulting for Statistics, Computing, and Analytics Research Core at the University of Michigan, Ann Arbor. A linear mixed model with fixed effects and an alpha of <0.05 was used to compare LZc values at representative epochs before, during, and after ketamine or propofol anesthesia. Tukey's post-hoc test was used to correct for multiple pairwise comparisons across states.

3.3 Results

3.3.1 Ketamine shows state-dependent and bandwidth-specific effects on Lempel-Ziv complexity

LZc analysis was first applied to broadband (0.5-175 Hz) EEG data before, during, and after ketamine anesthesia. As compared to baseline wake state, LZc significantly decreased during ketamine anesthesia in both frontal [$t(7)= -5.432$, $p<0.001$] (Figure 3.2A) and parietal [$t(7)= -3.998$, $p<0.001$] (Figure 2D) areas. During the emergence phase, prior to return of righting reflex (pre-RORR), there was a significant increase in LZc as compared to the baseline wake state [frontal: $t(7)= 9.432$, $p<0.001$, parietal: $t(7)= 10.756$, $p<0.001$] and ketamine anesthesia [frontal: $t(7)= 14.774$, $p<0.001$; parietal: $t(7)= 14.754$, $p<0.001$] (Figure 3.2A, D). The post-RORR phase was characterized by behavior – hyperactivity, hyperlocomotion, running in circles, ataxia – that is typically reported after administration of subanesthetic concentration of ketamine.[225,226] We found the LZc values to be highest during this phase (post-RORR) as compared to wake state [frontal: $t(7)= 14.097$, $p<0.001$; parietal: $t(7)= 18.626$, $p<0.001$], and ketamine anesthesia [frontal: $t(7)= 19.439$, $p<0.001$; parietal: $t(7)= 18.628$, $p<0.001$] (Figure 3.2A, D). The increase in LZc during post-RORR phase was also significantly higher than the LZc in pre-RORR epoch [frontal: $t(7)= 4.665$, $p<0.001$; parietal: $t(7)= 3.872$, $p<0.01$] (Figure 3.2A, D). The recovery wake epoch was characterized by a significant decrease in LZc values as compared to pre-RORR [frontal area: $t(2)= -8.421$, $p<0.001$; parietal: $t(2)= -9.934$, $p<0.001$] and post-RORR [frontal: $t(2)= -11.772$, $p<0.001$; parietal: $t(2)= -12.745$, $p<0.001$], and returned to the baseline wake state (Figure 3.2A, D).

To investigate the effect of ketamine on complexity in higher gamma frequencies, LZc analysis was performed on EEG data filtered between 65-175 Hz. As compared to baseline wake state, LZc was significantly reduced during ketamine anesthesia in the 65-175 Hz bandwidth [frontal: $t(7)= -5.605$, $p<0.001$; parietal: $t(7)= -7.760$, $p<0.001$] (Figure 3.2B, E). No significant differences in LZc were found between wake, pre-RORR, post-RORR, or recovery wake epochs for frontal (Figure 3.2B) or parietal (Figure 3.2E) areas. To compare our data with previously published data from human studies, data were bandpass filtered to 0.5-55 Hz. While the LZc in 0.5-55 Hz band in the ketamine anesthesia epoch was not characterized by any statistical difference as compared to wake state in frontal and parietal areas (Figure 3.2C, F), LZc during pre-RORR as well as post-RORR epochs showed a significant increase as compared to wake state in both frontal [pre-RORR: $t(7)= 7.993$, $p<0.001$; post-RORR: $t(7)= 11.042$, $p<0.001$] (Figure 3.2C) and parietal [pre-RORR: $t(7)= 10.045$, $p<0.001$; post-RORR: $t(7)= 11.859$,

p<0.001] (Figure 3.2F), areas. There was no significant difference in LZc between baseline wake and recovery wake epochs (Figure 3.2C, F).

3.3.2 Changes in EEG complexity during ketamine anesthesia, but not emergence, are independent of spectral changes in the EEG signal

To determine if the changes in complexity were attributable to the change in spectral content of the EEG signal, we normalized LZc from all three frequency bands by n=50 surrogate data in which the phases of the signal are randomly shuffled under the constraints of preserving the spectral profile of the original signal. The resultant phase shuffled normalized LZc (denoted LZc_N), reflects changes in EEG complexity beyond the linear spectral content of the signal. Similar to the ketamine anesthesia-induced decrease in LZc (Figure 3.2A, D), LZc_N during ketamine anesthesia was also found to be significantly reduced in the broadband frequency range (0.5-175 Hz) in both frontal [t(7) = -9.102, p<0.001, compared to baseline wake] (Figure 3.2G) and parietal [t(7)= -9.037, p<0.001, compared to baseline wake] (Figure 3.2J) areas. However, the phase-shuffled normalization of LZc attenuated the increase observed earlier for raw complexity during emergence phase (i.e., pre-RORR and post-RORR as in Figure 3.2A, D), and no significant differences in LZc_N were found between baseline wake state, emergence phase (pre-RORR and post-RORR) and the recovery wake epoch (Figure 3.2G, J). Compared to ketamine anesthesia, there was a significant increase in LZc_N during pre-RORR [frontal: t(7)= 6.599, p<0.001; parietal: t(7)= 7.051, p<0.001], post-RORR [frontal t(7)= 6.493, p<0.001; parietal: t(7)= 7.854, p<0.001], and recovery wake [frontal: t(2)= 4.066, p<0.01; parietal: t(2)= 3.703, p<0.01] (Figure 3.2G, J). The LZc_N in higher gamma frequency range (65-175 Hz) decreased during ketamine anesthesia [frontal: t(7)= -4.748, p<0.001; parietal: t(7)= -5.570, p<0.001] compared to wake, while there was no significant difference in LZc_N between baseline wake, emergence phase, and the recovery wake states (Figure 3.2H, K). Compared to ketamine anesthesia, there was a significant increase in LZc_N during pre-RORR [frontal: t(7)= 6.720, p<0.001; parietal: t(7)= 7.421, p<0.001], post-RORR [frontal: t(7)= 6.791, p<0.001; parietal: t(7)= 7.505, p<0.001], and recovery wake epoch [frontal: t(2)= 4.844, p<0.001; parietal: t(2)= 4.969, p<0.001] (Figure 3.2H, K). In the bandwidth of 0.5-55 Hz, LZc_N was significantly lower than wake during ketamine anesthesia [frontal: t(7)= -4.748, p<0.001; parietal: t(7)= -4.748, p<0.001] (Figure 3.2I, L). Compared to LZc_N during baseline wake state, frontal LZc_N remained

significantly attenuated throughout the remainder of the experiment [pre-RORR: $t(7)= -3.972$, $p<0.01$; post-RORR: $t(7)= -3.835$, $p<0.01$; recovery wake: $t(7)= -4.055$, $p<0.01$] (Figure 3.2I) while parietal LZc was only significantly lower during recovery wake epoch [$t(2)= -3.01$, $p<0.05$] (Figure 3.2L). Compared to ketamine anesthesia, there was a significant increase in LZc_N during pre-RORR [frontal $t(7)= 8.46$, $p<0.001$; parietal: $t(7)= 8.646$, $p<0.001$], post-RORR [frontal $t(7)= 8.596$, $p<0.001$; parietal: $t(7)= 9.921$, $p<0.001$], and recovery wake epoch [frontal: $t(2)= 4.835$, $p<0.001$; parietal: $t(2)= 4.584$, $p<0.001$] (Figure 3.2I, L).

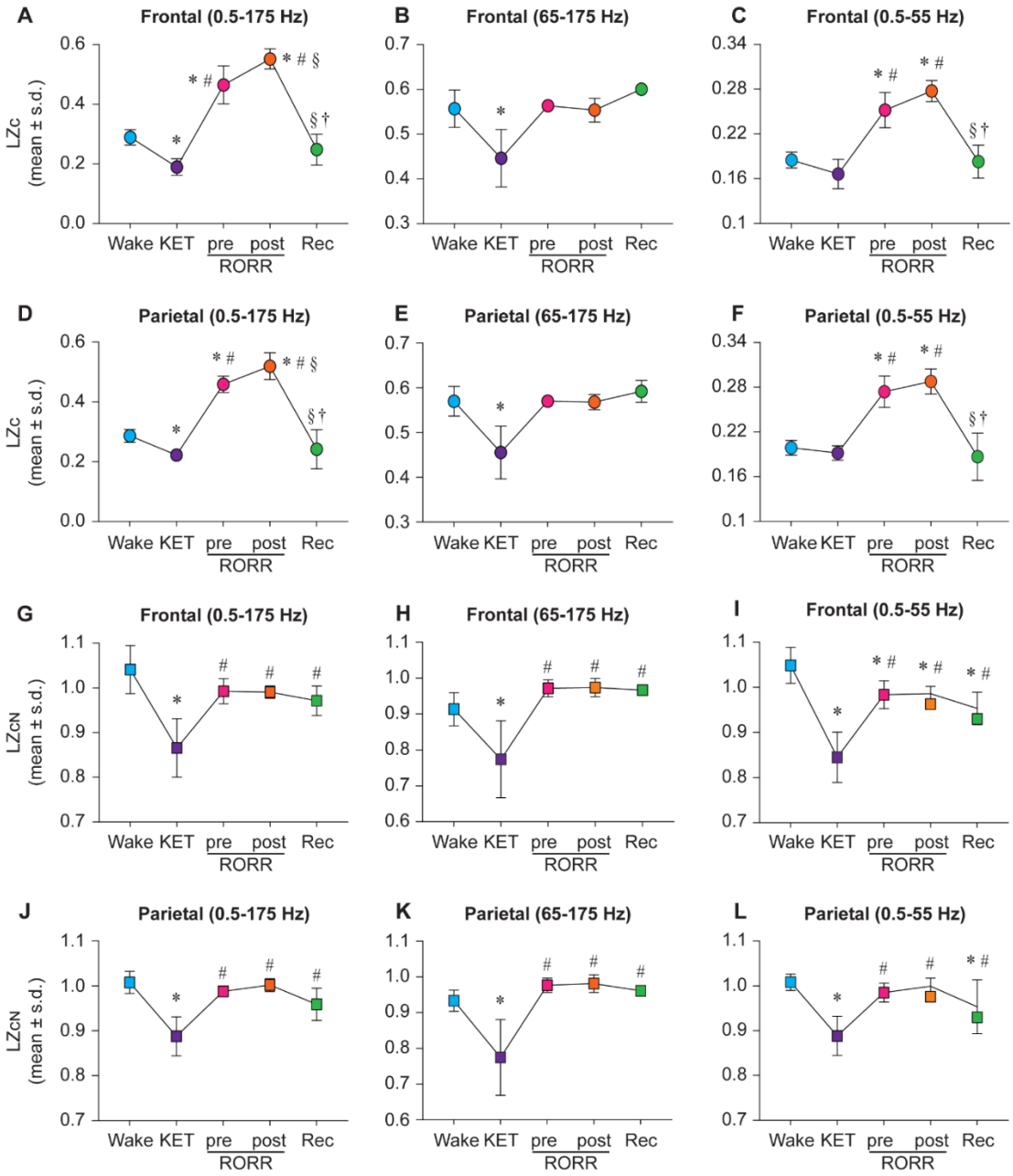

Figure 3.2 State-dependent and bandwidth-specific effects of ketamine on raw and normalized Lempel-Ziv complexity. Ketamine anesthesia suppressed raw LZc in the broadband range in both the frontal and parietal cortices (A, D). LZc in the 0.5-55 Hz range was not significantly different between wake and ketamine anesthesia in either the frontal or the parietal cortex (C, F) while the LZc was significantly decreased in the 65-175 Hz range in both the frontal and parietal (B, E) cortices. In contrast, the LZc during emergence from ketamine anesthesia was significantly increased in broadband (A, D) and 0.5-55 Hz (C, F) range in both frontal and parietal cortices. To assess changes in EEG complexity beyond the spectral content of the signal, we normalized LZc by n=50 phase-shuffled surrogate data. The phase-shuffled complexity (LZc_N) was significantly decreased across all three frequency bands (0.5-175 Hz, 65-175 Hz, 0.5-55 Hz) in frontal and parietal cortices relative to wake during ketamine anesthesia (G-L). Compared to the wake state, LZc_N, at emergence did not significantly differ in frontal or parietal cortices in broadband or 65-175 Hz data (G, H, J, K). In 0.5-55 Hz range, LZc_N remained significantly attenuated relative to wake during pre-RORR, post-RORR, and recovery wake epochs in the frontal channel (I). In the parietal channel, LZc_N was attenuated relative to wake during recovery wake (L). The significance symbols indicate p values at <0.05. The actual p-values are reported in the results section. * significant compared to Wake, # significant compared to ketamine anesthesia (KET), § significant compared to pre-RORR, † significant compared to post-RORR. Tukey's post-hoc test was applied to the data to correct for multiple comparisons. s.d. – standard deviation, Rec – Recovery wake, RORR – return of righting reflex

3.3.3 Propofol shows state-dependent and bandwidth-specific effects on Lempel-Ziv complexity

Propofol anesthesia was marked by a significant reduction in broadband LZc relative to wake state across both frontal [$t(7)= -5.058$, $p<0.001$] (Figure 3.3A) and parietal [$t(7)= -7.264$, $p<0.001$] areas (Figure 3.3D). As compared to baseline wake state, the post-RORR epoch showed a significant increase in LZc values in frontal [$t(7)= 3.111$, $p<0.05$], but not parietal [$t(7)= 2.480$, $p=0.09$] areas (Figure 3.3A, D). Compared to propofol anesthesia, there was a significant increase in LZc during post-RORR [frontal: $t(7)= 8.169$, $p<0.001$; parietal: $t(7)= 9.744$, $p<0.001$] and recovery wake epoch [frontal: $t(7)= 6.692$, $p<0.001$; parietal: $t(7)= 8.824$, $p<0.001$] (Figure 3.3A, D). There was no significant difference in LZc between baseline wake and recovery wake epoch in both frontal and parietal areas (Figure 3.3A, D). LZc analysis in the frequency range of 65-175 Hz showed no significant changes in EEG complexity between any of the states in frontal or parietal areas (Figure 3.3B, E). LZc analysis restricted to 0.5-55 Hz band showed differential effects of propofol on signal diversity that depended on the channel location and state. LZc in the frontal area during propofol anesthesia was not significantly different as compared to LZc during wake state (Figure 3.3C) while parietal LZc showed a significant decrease [$t(7)= -6.55$, $p<0.001$] (Figure 3.3F). As compared to wake state, significant increase in frontal LZc was found in post-RORR [$t(7) = 7.801$, $p<0.001$] and recovery wake epoch [$t(7)= 2.9$, $p<0.05$] (Figure 3.3C). In the parietal channel, signal diversity was also increased compared to wake during post-RORR [$t(7)= 9.776$, $p<0.001$] and recovery epoch [$t(7)= 3.27$, $p<0.05$] (Figure 3.3F). Compared to propofol anesthesia, there was a significant increase in LZc during post-RORR [frontal: $t(7)= 9.553$, $p< 0.001$; parietal: $t(7)= 16.327$, $p<0.001$] and recovery wake epoch [frontal: $t(7)= 4.652$, $p<0.001$; parietal: $t(7)= 9.821$, $p<0001$] (Figure 3.3C, F).

3.3.4 Changes in EEG complexity during propofol anesthesia, but not emergence, are independent of spectral changes in the EEG signal

In order to determine changes in EEG complexity beyond the spectral content of the signal, we normalized propofol LZc data as previously described for ketamine group. LZc_N was found to be suppressed during propofol anesthesia in frontal and parietal channels in the broadband [frontal: $t(7)= -7.583$, $p<0.001$; parietal: $t(7)= -12.915$, $p<0.001$] (Figure 3.3G, J) and

0.5-55 Hz [frontal: t(7)= -10.096, p<0.001, parietal: t(7)= -15.343, p<0.001] bandwidth (Figure 3.3I, L). As compared to propofol anesthesia, post-RORR was characterized by significantly higher LZc_N in broadband [frontal: t(7)= 4.937, p<0.001; parietal: t(7)= 0.764, p<0.001] (Figure 3.3G, J) and 0.5-55 Hz [frontal: t(7)= 8.342, p<0.001, parietal: t(7)= 14.531, p<0.001] range (Figure 3.3I, L). LZc_N was also significantly increased from propofol anesthesia during recovery in broadband [frontal: t(7)= 4.314, p<0.01, parietal: t(7)= 9.561, p<0.001] (Figure 3.3G, J) and 0.5-55 Hz [frontal: t(7)= 7.162, p<0.001; parietal: t(7)= 12.502, p<0.001] range (Figure 3.3I, L). In the broadband range (0.5-175 Hz), LZc_N remained significantly suppressed relative to wake across frontal and parietal channels during post-RORR [frontal: t(7)= -2.915, p<0.05, parietal: t(7)= -3.15, p<0.05] and recovery wake epoch [frontal: t(7)= -3.539, p<0.01; parietal: t(7)= -3.53, p<0.05] (Figure 3.3G, J). As compared to wake state, recovery wake epoch in 0.5-55 Hz range showed suppressed LZc_N in both frontal [t(7)= -2.934, p<0.05] and parietal [t(7)= -2.841, p<0.05] areas (Figure 3.3I, L). There was no significant difference in EEG complexity in 65-175 Hz between any of the states in frontal or parietal areas (Figure 3.3H, K).

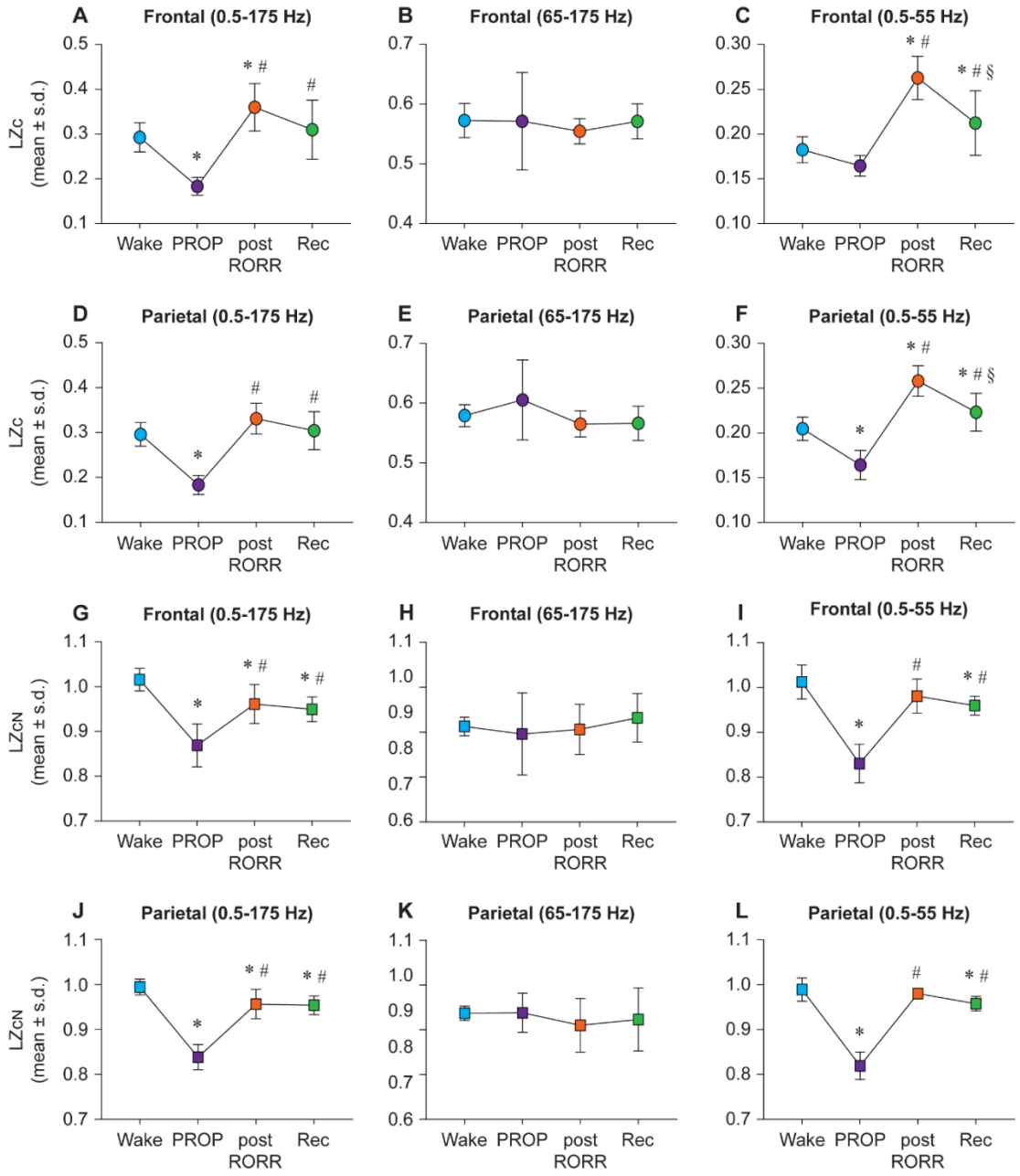

Figure 3.3 Propofol shows distinct state-dependent and bandwidth-specific effects on raw and normalized Lempel-Ziv complexity.

Propofol anesthesia suppressed broadband EEG complexity in both frontal and parietal cortices relative to wake (A, D). Frontal LZc in the 0.5-55 Hz range was not significantly different between wake and propofol anesthesia (C) while parietal LZc was significantly reduced (F). Post-RORR was characterized by a significant increase in LZc in frontal broadband EEG complexity (A). In the 0.5-55 Hz band, significant increases in LZc were seen during post-RORR and recovery wake in frontal and parietal cortices (C, F). Propofol administration did not have significant effect on LZc in the 65-175 Hz range in any of the states (B, E). To assess changes in LZc beyond the spectral content of the signal, we normalized LZc by n=50 phase-shuffled surrogate data (LZc_N). Propofol anesthesia resulted in significant attenuation in LZc_N in frontal and parietal cortices relative to wake in broadband (G, J) and 0.5-55 Hz data (I, L). LZc_N did not significantly differ between any states in the 65-175 Hz range (H, K). There was no difference in LZc_N between wake state and post-RORR in frontal or parietal areas in 0.5-55 Hz range (I, L). The significance symbols indicate p values at <0.05. The actual p-values are reported in the results section. * significantly different from Wake, # significantly from propofol anesthesia (PROP), § significantly different from post-RORR. Tukey's post-hoc test was applied to the data to correct for multiple comparisons. s.d. – standard deviation, Rec – Recovery wake, RORR – return of righting reflex.

3.4 Discussion

There has been a debate as to whether ketamine anesthesia reduces cortical complexity like traditional GABAergic anesthetics. Previous human studies have utilized scalp EEG to characterize the effects of ketamine anesthesia on cortical dynamics and reported both preserved and attenuated levels of EEG complexity during ketamine-induced unresponsiveness.[69,79] However, these studies were based on EEG signals that were low pass-filtered at 55 Hz and lacked cortical dynamics in higher gamma frequencies. Using intracranial EEG data from frontal and parietal cortices of rats receiving ketamine or propofol anesthesia, we demonstrate reduction in broadband (0.5-175 Hz) EEG complexity during ketamine anesthesia that is comparable to that induced by GABAergic anesthetic propofol. Bandwidth-specific analysis restricted to higher gamma frequencies showed that ketamine anesthesia is distinguished from propofol by suppression of EEG complexity in high gamma frequencies in the range of 65-175 Hz, which previous human studies using scalp EEG could not reveal.

To determine if changes in complexity across all states were attributable to processes beyond the spectral content of the signal, we normalized LZc by surrogate data in which the phase information of the EEG was shuffled under the constraints of preserving the original spectral content of the signal. The resultant measure, LZc_N, has been previously used to reflect changes in EEG complexity beyond the spectral profile of the signal.[75,76,80,83,159] Normalized LZc data revealed that reduction in EEG complexity during ketamine and propofol anesthesia was not attributable to changes in spectral content of the EEG signal. However, increases in raw LZc observed during emergence from propofol and ketamine anesthesia were attenuated by normalization across all studied bandwidths, suggesting that changes in complexity during these states can be largely attributed to changes in the spectral contents of the EEG signal. The spectral and connectivity changes in these data have been reported in our previous studies,[98,120,227] which showed a statistically significant increase in high gamma power and coherence during recovery from ketamine and propofol anesthesia. This further confirms that the changes observed in LZc during emergence are likely due to the spectral bias. Of note, the psychedelic state induced by subanesthetic administration of ketamine in humans is associated with increased LZc that has been shown to extend beyond the spectral contents of the signal.[79,83] These data suggest that dynamics characteristic of reaching subanesthetic concentrations during recovery from ketamine

anesthesia might not be equivalent to administration of subanesthetic concentrations of ketamine. This lack of equivalence could relate to the differences between delirium and an organized psychedelic state.

A reduction in neural complexity across brain networks has been suggested to be a common feature of states associated with unconsciousness.[63,93,228–230] Prior human studies have used low-pass filtered EEG (45 Hz and below) to assess the effect of ketamine anesthesia on indices of EEG signal complexity using LZc and a closely related measure known as the perturbational complexity index.[69,97] These studies concluded that ketamine anesthesia failed to reduce neural complexity, attributing this to either a concomitant increase in the entropy of the EEG signal or the presence of a dream-like state of disconnected consciousness. However, a more recent study in humans[79] suggests that ketamine-induced state transitions are characterized by dynamic features of normal waking consciousness, general anesthesia, and altered states of consciousness, depending on the dose administered and the temporal course of ketamine administration. Ketamine-induced unresponsiveness was found to be marked by an alternating delta-gamma burst EEG pattern,[231] creating signatures of both preserved and suppressed EEG complexity.[79] Our data provide evidence that ketamine anesthesia is marked by stable reductions in Lempel-Ziv complexity that are broadly comparable to GABAergic anesthetics. However, these reductions in complexity during anesthesia are masked when higher gamma frequencies above 55 Hz are filtered out from the EEG signal. Furthermore, the lack of controls to account for the influence of the EEG power spectrum on LZc could potentially explain varying results in prior human studies.[69,97]

Our limited channel count restricted us to measurements of single-channel temporal complexity. Although temporal LZc can assess cortical complexity with respect to the diversity of temporal patterns within spontaneous EEG signals, it cannot assess complexity with respect to features such as neural differentiation and functional integration in the same manner as alternative measurements such as the perturbational complexity index. However, measures of temporal complexity have previously been validated in investigations of cortical dynamics as they relate to the level of consciousness during sleep,[88] anesthesia,[75,159] and psychedelic states.[80,83] Furthermore, these measurements are more readily implemented in both human and animal models than measures involving perturbation, as these can be applied to spontaneous neural data and do not require substantial averaging of data over many stimulations. Finally, it is

important to note that the routes of administration for our comparisons of ketamine and propofol differed, as ketamine anesthesia was induced by a single intraperitoneal bolus while propofol anesthesia was administered through a sustained intravenous infusion. Future studies using intravenous infusion of ketamine and GABAergic anesthetics such as propofol or etomidate are warranted for a more direct comparison of their anesthetic actions on EEG complexity in rodents.

In summary, our data demonstrate that ketamine anesthesia is characterized by reduction in broadband (0.5-175 Hz) EEG complexity. As opposed to GABAergic anesthetic propofol, ketamine decreases complexity in the higher gamma bandwidth (65-175 Hz). However, decreased complexity in 0.5-55 Hz range is common to both propofol and ketamine anesthesia. Thus, a reduction in neural complexity may only be a coarse shared phenotype of pharmacologically disparate anesthetics. Future studies will need to focus on the distinct molecular drivers that result in bandwidth-specific reductions of complexity during pharmacologically disparate forms of anesthesia, as well as how these bandwidth-specific reductions in complexity relate to broader mechanisms of anesthetic-induced unconsciousness.

3.5 Summary and Conclusions

In Chapter 3, we utilized EEG data from Pal et al., 2015,[98] and Pal et al., 2016,[120] to characterize the frequency-dependent effects of ketamine and propofol anesthesia on Lempel-Ziv complexity. Temporal EEG complexity was assessed in frontal and parietal cortices in broadband (0.5-175 Hz), high gamma (65-175 Hz), and 0.5-55 Hz bandwidths before, during, and after ketamine or propofol anesthesia. Ketamine and propofol were found to possess differential state-dependent and bandwidth-dependent effects on Lempel-Ziv complexity. During anesthesia, ketamine was distinguished by suppression of complexity in the high gamma bandwidth, while propofol was found to suppress complexity at frequencies 55 Hz or lower. Using a method of Lempel-Ziv complexity normalization based upon phase-shuffling, we confirm comparable changes in Lempel-Ziv complexity at 0.5-175 Hz and 0.5-55 Hz during anesthesia induced by both drugs occurred independent of spectral properties of the EEG. These results warrant caution in the application and interpretation of Lempel-Ziv complexity to assess the level of consciousness, as measures of Lempel-Ziv complexity during anesthesia are not only state-dependent, but frequency-dependent as well.

3.6 Supplementary Information

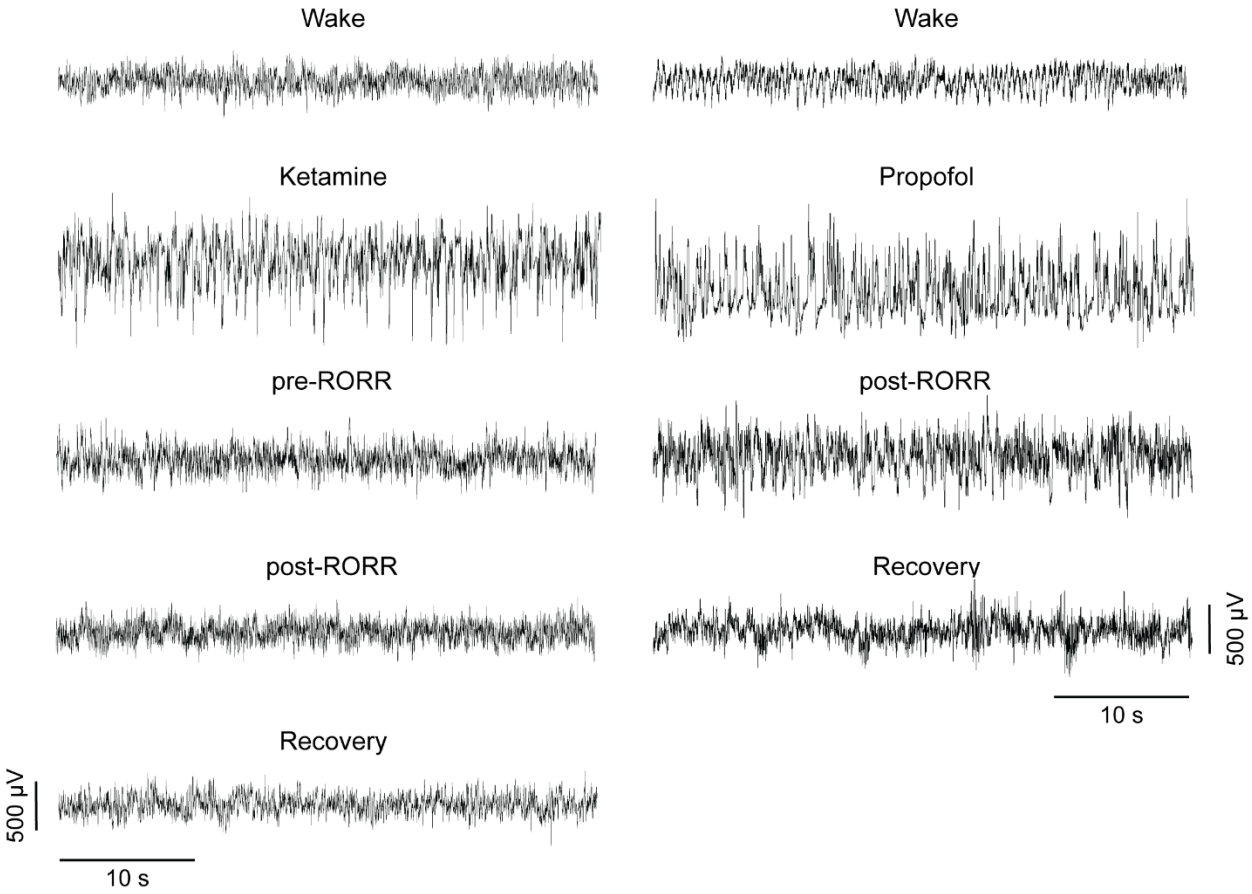

Figure S3.1 Representative electrophysiological traces show frontal-parietal EEG signal before, during, and after ketamine or propofol anesthesia
The left column shows EEG traces from pre-ketamine awake state (Wake), ketamine anesthesia (Ketamine), epoch prior to return of righting reflex (pre-RORR), epoch after the return of righting reflex (post-RORR), and post-ketamine recovery wake state (Recovery). The right column shows the EEG traces from pre-propofol awake state (Wake), propofol anesthesia (Propofol), epoch with the return of righting reflex (post-RORR), and post-propofol recovery wake state (Recovery). RORR – return of righting reflex.

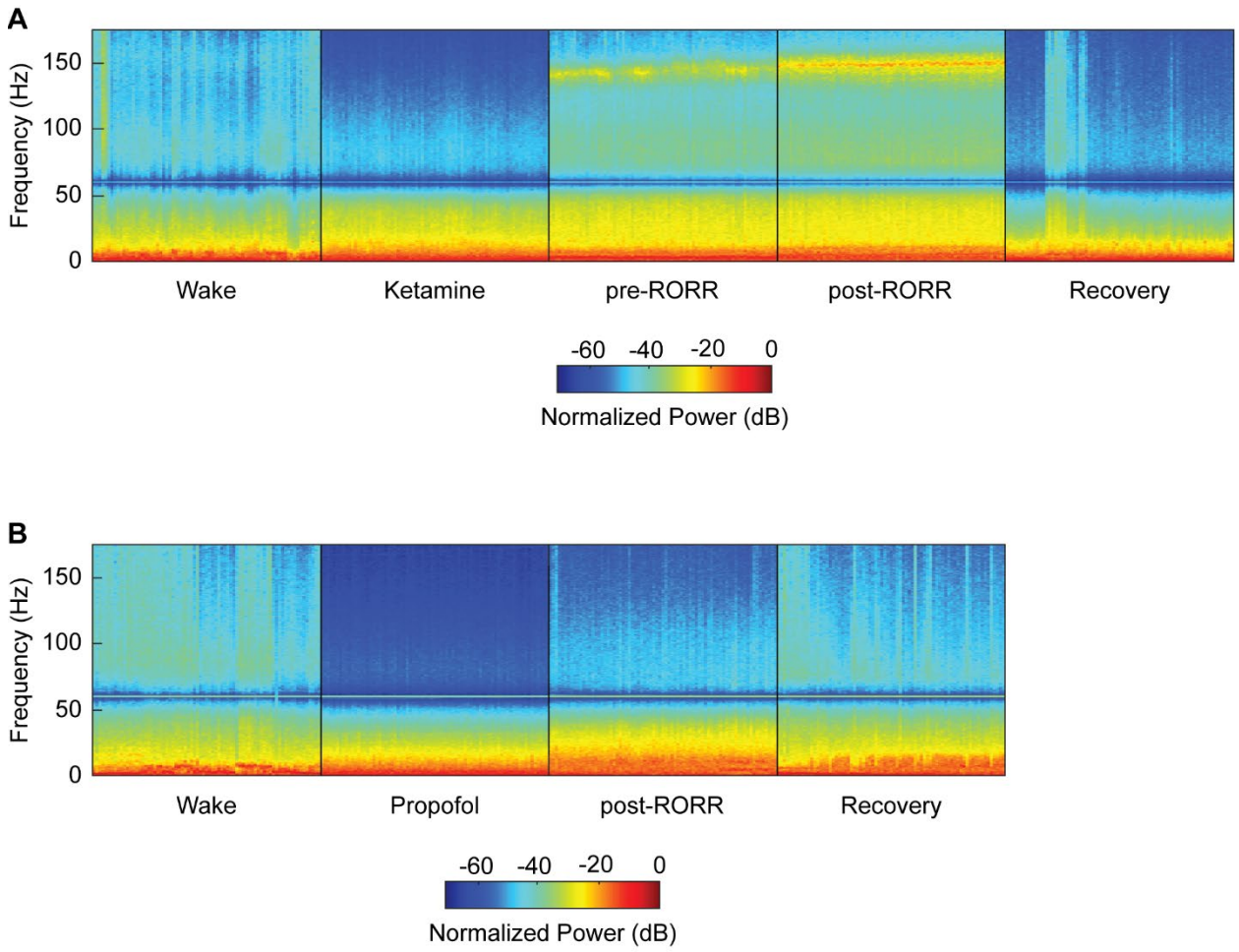

Figure S3.2 Representative spectrograms show normalized power distribution between 0.5 and 175 Hz during the behavioral states analyzed before, during, and after Ketamine (A), and propofol (B) anesthesia.
Each data epoch separated by black vertical lines is 5 minutes in length. Both ketamine (A) and propofol (B) anesthesia epochs show increase in low frequency (<4 Hz) power and decrease in high gamma frequencies (65-175 Hz). The emergence from ketamine (A) anesthesia (pre-RORR and post-RORR) is characterized with the appearance of intense increase in high gamma (65-175 Hz) power, that is not seen during either wake or the recovery epoch. The return of righting reflex after propofol anesthesia (post-RORR) show increased activity in theta (4-10 Hz) and gamma power (65-125 Hz

Chapter 4 Cortical Acetylcholine Levels Correlate with Neurophysiologic Complexity during Subanesthetic Ketamine and Nitrous Oxide Exposure in Rats

4.1 Introduction

Although the precise neural correlates of consciousness are still a matter of active debate,[42,43] there is evidence that cortical neurophysiologic complexity relates to the level of consciousness.[64,66] Neurophysiologic complexity has been shown to be depressed during unconscious states such as slow-wave sleep, coma, and anesthesia.[73,75,76,79,88] Conversely, psychoactive drugs such as classical serotonergic psychedelics or dissociative NMDA-antagonists are known to enhance complexity, with several studies establishing an association between changes in complexity, cortical connectivity, and reports of alterations to conscious contents.[79,80,83,206] While cortical complexity has been characterized across a broad spectrum of brain states, there is limited understanding of the relationship between measures of complexity and underlying neurochemical processes within the cortex.

The cortex receives topographically specific cholinergic projections from the basal forebrain.[232] Cortical acetylcholine levels are high during states associated with high complexity and the presence of phenomenological content, such as wakefulness, rapid eye movement sleep, or after the administration of serotonergic psychedelics or subanesthetic levels of glutamatergic dissociatives.[97,137,138,211,237] Conversely, cortical acetylcholine is suppressed during states of low complexity and reduced conscious content, such as slow-wave sleep or anesthesia.[120,140,142] Despite a biologically plausible relationship that might be inferred from past investigations, there has been no study that has characterized – through concurrent measurements – the relationship between neurophysiologic complexity and cortical acetylcholine. Studies characterizing neurophysiologic complexity have often relied on temporospatial analysis of high-density electroencephalographic recordings in human subjects but have not measured concurrent neurochemical changes. On the other hand, the studies using animal models typically enable neurochemical analysis but have employed sparse electroencephalographic recordings that

prevent the translational application of temporospatial analyses used in human studies. To address this gap, we developed a novel approach to record high-density (30-channel) intracranial electroencephalogram (EEG) in rats while simultaneously measuring acetylcholine levels inprefrontal and parietal cortices. We then leveraged the NMDA-antagonists ketamine and nitrous oxide as pharmacological tools, due to their unique dose-dependent anesthetic and psychedelic properties. Changes in acetylcholine concentration in prefrontal and parietal cortices were compared with Lempel-Ziv complexity[90] before, during, and after administration of subanesthetic ketamine or 50% nitrous oxide. To further characterize cortical dynamics, we computed normalized symbolic transfer entropy, an information theoretic measure to estimate directed connectivity,[113,120,159] within gamma bandwidths between frontal and parietal cortices. We report that changes in cortical acetylcholine levels during subanesthetic ketamine or 50% nitrous oxide exposure correlate with changes in neurophysiologic complexity and high gamma connectivity.

4.2 Methods

4.2.1 Rats

The study was approved by the Institutional Animal Care and Use Committee (University of Michigan, Ann Arbor, Michigan, USA) and was performed in accordance with the Guide for the Care and Use of Laboratory Animals (8th Edition, The National Academies Press, Washington D.C.), as well as ARRIVE guidelines. Adult male and female Sprague-Dawley rats (n = 24, 12 male:12 female, 300-350 g, Charles River Laboratories, MA) were used. The rats were housed in a temperature- and light-controlled facility (12 h light: 12 h dark cycle, lights on at 8:00 am) with *ad libitum* access to food and water.

4.2.2 Surgical Procedures

Rats (n = 24, 12 male, 12 female) were anesthetized with 4–5% isoflurane in 100% oxygen in an anesthesia induction chamber, were re-positioned to breathe through a nose cone (Model 906, David Kopf Instruments, Tujunga, CA), and immobilized in a stereotaxic frame using blunt ear bars (Model 963, David Kopf Instruments, Tujunga, CA). After positioning in the stereotaxic instrument, the isoflurane concentration was titrated to the loss of the pedal and

palpebral reflex. The concentration of isoflurane was monitored throughout the surgery using an anesthetic agent analyzer (Capnomac Ultima, Datex Medical Instrumentation, Tewksbury, MA). Body temperature was maintained at 37 °C using a far-infrared heating pad (RT-0502, Kent Scientific, Torrington, CT) coupled to a rectal probe (Model 7001H, Physitemp Instruments, Clifton, NJ). Subcutaneous buprenorphine (Buprenex, Par Pharmaceutical, Chestnut Ridge, NY; NDC 42023-179-05) was used as a pre- (0.01 mg/kg) and post-surgical (0.03 mg/kg, every 8-12 h for 48 h) analgesic. A pre-surgical subcutaneous dose of carprofen (5 mg/kg) (Zoetis; NADA #141-199) was administered to supplement surgical and post-surgical analgesia achieved via buprenorphine. A single pre-surgical dose of cefazolin (20 mg/kg, subcutaneous) (West-Ward-Pharmaceutical, Eatontown, NJ; NDC 0143-9924-90) was used as a prophylactic antibiotic.

Burr holes (30) were drilled across the skull and stainless-steel screw electrodes (B000FN89DM, Small Parts, Logansport, IN) were implanted in a regularly spaced montage (anterior-posterior coordinates: 4 mm anterior to 10 mm posterior relative to bregma, 8 rows of electrodes; medial-lateral coordinates: 2 mm to 4.5 mm relative to bregma, 4 electrodes in first 7 rows, 2 in the last row **(**Figure 4.1) to allow for the recording of high-density intracranial EEG. A screw electrode was implanted over the nasal sinus to serve as the reference electrode, while another was implanted over the cerebellum as a ground electrode. CMA 11 microdialysis guide cannulae (8309018, Harvard Apparatus, Holliston, MA) were implanted 1.0 mm above the prefrontal prelimbic cortex (Bregma, anterior: 3.24 mm, mediolateral: 0.5 mm, ventral: 3 mm) or 2.0 mm above the somatosensory barrel field region of the parietal cortex (Bregma, posterior 3.48, mediolateral 2.6 mm, ventral 2.5 mm, 40° angle)[1] to allow for simultaneous multi-site measurement of cortical acetylcholine levels. In a subset of rats (n = 12, 6 male, 6 female), an indwelling catheter (MRE-040, Micro-Renathane tubing, Braintree Scientific, Braintree, MA, USA) was surgically positioned into the jugular vein to allow for intravenous infusion of ketamine (Ketalar, Par Pharmaceutical, Chesnut Ridge, NY; NDC 42023-115-10).

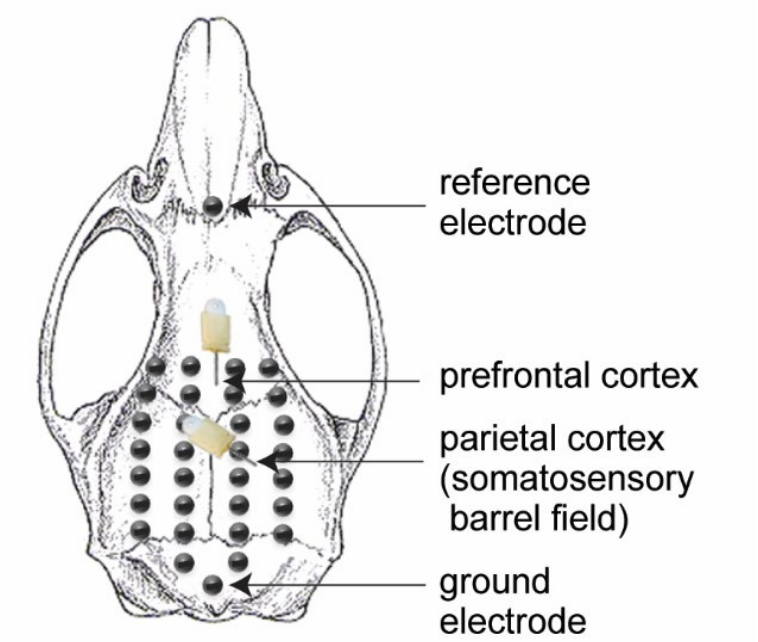

Figure 4.1 Schematic showing the EEG montage (30 screw electrodes) to record high-density intracranial monopolar EEG, and placement of microdialysis probes in prefrontal cortex and somatosensory barrel field region of the parietal cortex.
A single screw electrode on the nasal sinus served as a reference while another electrode over the cerebellum served as the ground.

4.2.3 Experimental design

Schematics depicting the design for ketamine and nitrous oxide experiments are illustrated in Figure 4.2A and 4.2B, respectively. The experiments were conducted after at least 10 days of post-surgical recovery. Equal sized cohorts of rats (n=12, 6 male, 6 female) were used for ketamine and nitrous oxide experiments. The sample size for the animals used in this study was based on similar studies from our laboratory[19,21,24,25]. EEG data were recorded continuously throughout the experiment while microdialysis samples were collected in 12.5 min epochs. The EEG was recorded and dialysis samples were first collected for 50 min (4 microdialysis epochs) during freely moving baseline wake condition. The EEG was monitored in real-time by the experimenter and gentle tapping on the recording chamber was used to maintain a constant state of wakefulness. Following baseline recording, rats were either connected to an intravenous catheter line to allow for sustained infusion of ketamine at 10 mg/kg/h, or were sealed in an air-tight chamber to allow for delivery of a mixture of 50% nitrous oxide and 50% oxygen into the recording chamber (12 L/min). EEG and dialysate samples were then collected for a period of 62.5 min (5 microdialysis epochs) during administration of subanesthetic ketamine or nitrous oxide. Ketamine infusion or nitrous oxide exposure was then stopped, and

data were collected for another 62.5 min (5 microdialysis epochs) during post-drug recovery period. At the conclusion of data collection, the sites of microdialysis were histologically verified (Figure 4.3).

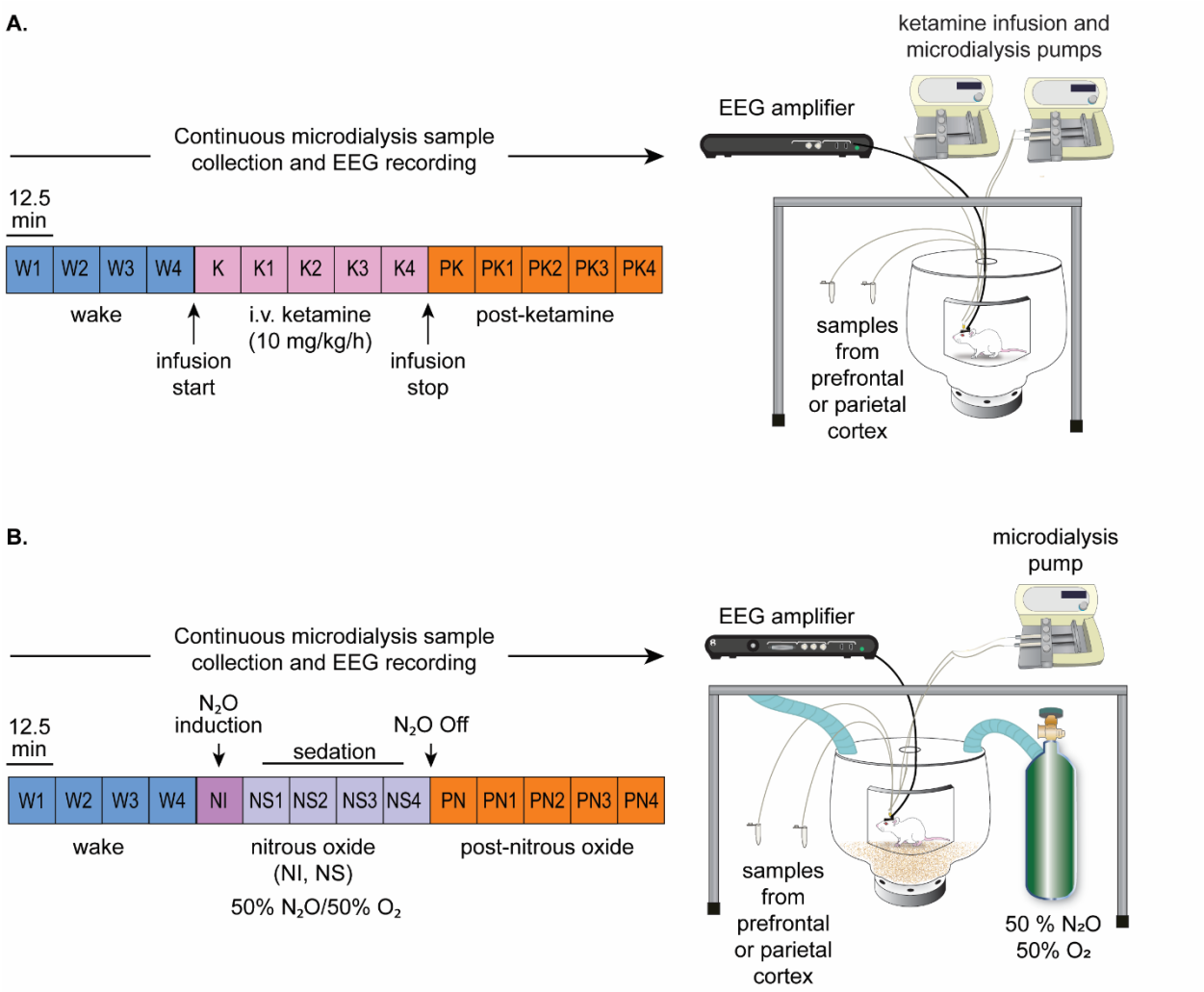

Figure 4.2 Schematics illustrating the experimental set-up and timeline for ketamine (A) and nitrous oxide (B) experiments. The EEG data and microdialysis samples from prefrontal and parietal cortices were collected simultaneously and continuously but the microdialysis samples were collected in 12.5 min bins. Each colored box represents one microdialysis epoch. Samples were collected during freely moving baseline wake (W) condition, continuous subanesthetic ketamine infusion at 10 mg/kg/h (K), or post-ketamine recovery period (PK). The data collection was performed similarly for the nitrous oxide (N_2O) cohort, with

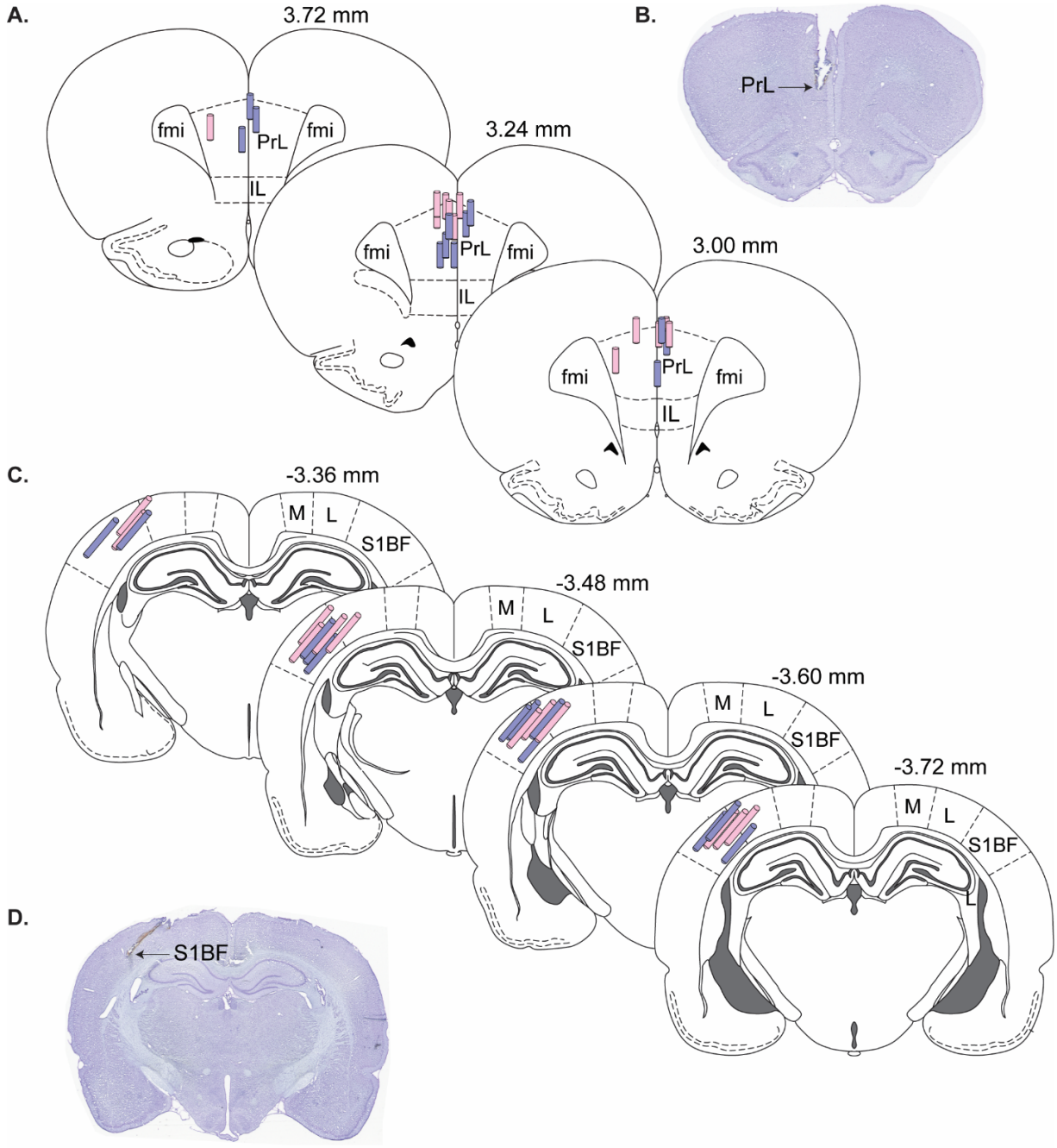

Figure 4.3 Histological verification of microdialysis probe placement in prefrontal and parietal cortices.
Stereotaxic maps from the rat brain atlas[177] show the location of microdialysis probes in the prelimbic (PrL) region of prefrontal cortex and somatosensory barrel field (S1BF) region of parietal cortex. Pink cylinders represent probes from ketamine experiments while purple cylinders represent probes from nitrous oxide experiments (A, C). B and D show cresyl violet-stained representative coronal brain sections (40 µm) through prefrontal cortex and parietal cortex, respectively. fmi – forceps minor corpus callosum, IL – infralimbic area, L – lateral parietal association cortex, M – medial parietal association cortex. The numbers on top right of the stereotaxic maps show the distance from Bregma; positive numbers are anterior to Bregma while negative numbers are posterior to Bregma.

4.2.4 EEG data acquisition

Monopolar EEG data, referenced to an electrode over the nasal sinus, were acquired using a 32-channel headstage (Cereplex µ, Blackrock Microsystems, Salt Lake City, UT). The signals were then digitized at 1 kHz and bandpass filtered between 0.1-500 Hz using a Cereplex Direct system paired with the Cereplex Direct Software Suite (Blackrock Microsystems, Salt Lake City, UT). Raw EEG signals were imported into MATLAB (version 2020b; MathWorks, Inc.; Natick, MA). Data segments with obvious noise or artifacts were identified and removed by visual inspection of both the raw waveform and spectrogram of the EEG signals. Prior to analyses, the EEG signals were detrended using a local linear regression method with a 10 s window at a 2 s step size in Chronux analysis software,[233] and subsequently lowpass filtered at 175 Hz via fifth-order Butterworth filter.

4.2.5 Lempel-Ziv complexity analysis

Lempel-Ziv complexity (LZs) was used to approximate temporospatial EEG complexity. LZs is a method of symbolic-sequence analysis that assesses the algorithmic complexity (i.e. diversity, compressibility) of finite sequences such as EEG time series.[90] LZs analysis was conducted as outlined in previous studies from our laboratory[79,159,217] and others.[75,76,80,83] To control for any potential bias in the resultant LZs values due to the frequency content of the EEG signal, we normalized LZs by the average of n=50 surrogate datasets in which the spectral profile were identical to the original signal, but the phase-information was maximally randomized.[80,83,159,217] This excludes the possibility that changes in complexity reflected in the normalized metric of LZs **(denoted LZs_N)** are attributable only to the spectral contents of the signal.

4.2.6 Frontoparietal directed connectivity: normalized symbolic transfer entropy analysis

To assess directed connectivity between frontal and parietal cortices, we used normalized symbolic transfer entropy (NSTE), which is an information theoretic measure. Transfer entropy has been proposed as a surrogate measure to estimate the directional exchange of information between two signals, such as those recorded from neural data.[108] More specifically, NSTE is a non-parametric, nonlinear, and model-free means by which one can approximate the degree of

statistical dependence between the EEG signals recorded from disparate brain regions. The precise method used is outlined in detail in a number of previous human[112,113,196] and rat studies[98,120,159,178] from our laboratory.

We used EEG data from ipsilateral frontal and parietal channels to assess feedback (frontal-to-parietal) and feedforward (parietal-to-frontal) connectivity before, during, and after subanesthetic ketamine or nitrous oxide administration. We focused on changes in directed connectivity in three gamma bandwidths: low gamma (25-55 Hz), mid gamma (85-125 Hz), and high gamma (125-175 Hz), as gamma oscillations have been implicated in arousal and previous studies from our laboratory have illustrated directed frontoparietal connectivity in high gamma bands to be a correlate of wakefulness.[98,120,178] We used a fourth-order Butterworth filter (butter.m and filtfilt.m, MATLAB Signal Processing Toolbox) to filter the respective gamma bandwidths of interest from the raw EEG signal and then segmented the filtered signal into non-overlapping 10 s windows. The calculation of NSTE is contingent upon three parameters: the embedding dimension, time delay, and prediction time. We set the embedding dimension at 3 across all analyses. The time delay was set at 5 (10 ms), 2 (4 ms), and 1 (2 ms) for the low, mid, and high gamma bandwidths, respectively. The prediction time was set by searching values between 1 and 50 (corresponding to 2–100 ms) and selecting the value that yielded maximum normalized symbolic transfer entropy in the feedback (frontal-to-parietal) and feedforward (parietal-to-frontal) directions.

4.2.7 Quantification of cortical acetylcholine in prefrontal and parietal cortices

CMA/11 microdialysis probes (CMA Microdialysis, Harvard Apparatus, Holliston, MA, USA) were inserted into the prefrontal cortex (1 mm cuprophane membrane, 0.24 mm diameter, 6 kDa membrane cutoff, 8309581) and somatosensory barrel field region of parietal cortex (2 mm cuprophane membrane, 0.24 mm diameter, 6 kDa membrane cutoff, 8309582). The probes were connected to a microsyringe pump (Model CMA/400, CMA Microdialysis, Harvard Apparatus, Holliston, MA, USA) and were continuously perfused with artificial cerebrospinal fluid (aCSF; 145 mM NaCl, Sigma Aldrich: S9888; 2.68 mM KCl, Sigma Aldrich: P9333; 1.40 mM CaCl2, • 2H2O, Sigma Aldrich: C8106; 1.01 mM MgSO4 • 7H2O, Sigma Aldrich: 63140; 1.55 mM Na2HPO4, Sigma Aldrich: S5136; 0.45 mM NaH2PO4 • H2O, Sigma Aldrich: 52074; 10 μM neostigmine, Sigma Aldrich: N2001; pH = 7.4) at a rate of 2 μL/min, allowing for sample

collection at a volume of 25 µL in epochs of 12.5 mins. To rule out the possibility of any potential change in probe membrane properties affecting the neurochemical analysis, we compared the recovery profile of the probes before and after the experiments using 3 pmol acetylcholine/choline standard.

Acetylcholine concentration was quantified via high-performance liquid chromatography (HPLC) coupled to an electrochemical detector (HTEC-510, Amuza Inc. San Diego, CA, USA). Mobile phase was perfused through the system at 175 µL/min and had a composition of 49.95 mM KHCO3 (Sigma Aldrich: 237205) ;148.72 µM Na2EDTA • 2H2O (Amuza/Dojindo: 111.114.91), and 1.23 mM decanesulfonate sodium salt (Amuza/TCI: 900.061.00) per 1 liter of ultrapure HPLC-grade water (Milli-Q, EMD Millipore, Burlington, MA, USA). We injected 20 µL from each microdialysis sample into a 50 µL sample loop connected to a polymer-based reverse phase separation column (AC-GEL, 2.0 mm ø x 150 mm, Amuza Inc., San Diego, CA, USA), allowing for the separation of acetylcholine and choline in the biological samples. Acetylcholine and choline are then broken down to produce hydrogen peroxide proportional to their relative concentrations (AC-ENZYMPAK II ACh enzyme reactor, 1 mm x 4 mm, Amuza Inc., San Diego, CA, USA). Hydrogen peroxide is oxidized at the platinum electrode surface (WE-PT platinum electrode, RE-500 Ag/Cl reference electrode, applied potential: +450 mV; Amuza Inc., San Diego, CA) and the generated current is detected by the electrochemical detector. A seven-point acetylcholine/choline standard curve (0.05 – 1.0 pmol) was generated prior to the start of each experiment, as outlined in previous experiments from our laboratory.[98,120,158]

4.2.8 Statistical Analysis

All statistical analyses were performed using R software[188] in consultation with the *Consulting for Statistics, Computing, and Analytics Research Core* at the University of Michigan, Ann Arbor. No a priori power analysis for sample size selection was performed. The sample size was informed by similar studies previously published by our laboratory[98,120,158,159] in which cortical acetylcholine, directed connectivity, or complexity were analyzed using identical analytic methodologies, and in which we found that sample sizes of $\leq$ 12 were sufficient in detecting significant differences in the outcome measures across experimental conditions. Our primary outcome measures were changes in cortical acetylcholine, Lempel-Ziv complexity, and

frontoparietal connectivity. The first ketamine infusion epoch was excluded from EEG and neurochemical analyses due to the time required for the drug to traverse dead space in the catheter and reach the blood circulation. For the rest of the epochs in ketamine experiments, a within-subjects design was utilized in which each rat contributed 4 wake datapoints, 4 ketamine infusion datapoints, and 4 post-ketamine datapoints for each measure. As opposed to intravenous administration of ketamine, which required 5-7 minutes to traverse the catheter, nitrous oxide exposure was quick, and the recording chamber was filled within 1 min of the start of nitrous oxide delivery. However, the rats showed an acute response to nitrous oxide, which was primarily limited to the first 12.5 min of nitrous oxide delivery and differed from the subsequent 50 mins of exposure. Therefore, we analyzed the first epoch (12.5 min) of nitrous oxide exposure separately as "nitrous induction" while the rest of the 4 epochs (50 min) were categorized as nitrous "sedation" and analyzed as a separate block. For nitrous oxide experiments, we implemented a within-subject design in which each rat contributed 4 wake datapoints, 1 nitrous oxide induction datapoint, 4 nitrous oxide sedation datapoints, and 4 post-nitrous oxide datapoints for each EEG measure and acetylcholine analysis. The statistical analyses for ketamine experiments were run on 5 min segments of noise-free EEG from each 12.5 min epoch, while for nitrous oxide experiments, 2 min segments of noise-free EEG were selected. The choice to use shorter EEG epochs for nitrous oxide experiments was due to the prevalence of noise in the EEG signal driven by sporadic chewing - or "bruxing" behavior. To exclude mixed states, the first post-ketamine and first post-nitrous oxide epochs were excluded from our analyses. Thus, each rat in the ketamine experiments contributed 12 EEG and microdialysis datapoints to the statistical analysis, while each rat in the nitrous experiments contributed 13 data points. A linear mixed model was utilized in which "Drug State" was treated as a fixed factor. We also included "Subject Sex" as a fixed factor to account for any influences of sex on drug response. "Subject" was treated as a random intercept in the model to account for inter-subject variability. An alpha threshold of $p<0.05$ was selected and Tukey's *post hoc* test was used to correct for multiple pairwise comparisons (paired t-test) between states. To assess correlations between cortical complexity, connectivity, and acetylcholine levels, we employed a Pearson correlation-based method, optimized for analysis of clustered repeated-measures data.[234] To assess correlations between cortical complexity, connectivity, and acetylcholine levels, a non-parametric Spearman rank correlation was used. This non-parametric means of assessing

correlation was selected due to the monotonic distribution of our LZs_N data, in which a narrow range of LZs_N values and a maximum value of "1" imposes a clear ceiling effect. The data are provided as box and whisker plots with median, interquartile range, minimum and maximum values, and the individual data points for each subject superimposed on the plots. The mean, standard deviation, and F-statistics for statistical comparisons are provided in Tables 4.1-4.8.

4.3 Results

4.3.1 Subanesthetic ketamine infusion produced a sustained increase in acetylcholine levels in prefrontal and parietal cortices

Intravenous infusion of subanesthetic ketamine resulted in a consistent increase in acetylcholine levels relative to wake state in both prefrontal [$t(130)=12.49$, $P < .001$, Fig. 4.4A] and parietal [$t(130)=13.72$, $P < .001$, Fig. 4.4B] cortices, lasting all 4 epochs. During subanesthetic ketamine infusion, rats displayed stereotypic head bobbing and circling behavior, interrupted by periodic bouts of ataxia. As compared to wake state, acetylcholine levels in both prefrontal and parietal cortices remained elevated during post-ketamine recovery period [prefrontal: $t(130)=3.54$, $P < .01$, Fig. 4.4A; parietal: $t(130)=2.546$, $P = .03$, Fig. 4.4B], with cortical acetylcholine progressively declining 12.5 min after the cessation of the infusion. The acetylcholine levels during the post-ketamine recovery period were significantly lower than that during subanesthetic ketamine infusion [prefrontal: $t(130)=-8.95$, $P < .001$, Fig. 4.4A; parietal: $t(130)=-11.17$, $P < .001$, Fig. 4.4B].

4.3.2 Nitrous oxide exposure produced state-dependent effects on acetylcholine levels in prefrontal and parietal cortices

Nitrous oxide exposure resulted in state-dependent effects on acetylcholine in prefrontal and parietal cortices that depended on the depth of sedation, which increased with the duration of exposure. During the first 12.5 min of nitrous oxide exposure – hereafter referred to as nitrous induction (NI) – rats showed active behavior such as grooming, stereotypic head bobbing, and uncoordinated locomotion. Acetylcholine levels were significantly elevated relative to wake in both prefrontal and parietal cortices [prefrontal: $t(141)=7.97$, $P < .001$, Fig. 4.4C; parietal: $t(141)=7.39$, $P < .001$, Fig. 4.4D]. The following 50 min of nitrous oxide exposure – hereafter

referred to as nitrous sedation (NS) – were marked by periodically quiescent behavior interrupted by active and purposeful behaviors such as slow locomotion, grooming, or pica-like consumption of bedding. The requirement to have a sealed recording chamber precluded any behavioral manipulation to assess the level of sedation. However, despite relatively quiescent behavior, rats clearly retained righting reflex throughout nitrous oxide treatment, displayed sporadic spontaneous behavior, and were easily aroused by tapping on the wall of recording chamber. This was accompanied by a progressive decline in prefrontal [$t(141)=-5.01$, $P < .001$, Fig. 4.4C] and parietal [$t(141)=-7.07$, $P < .001$, Fig. 4.4D] acetylcholine, relative to wake state. Despite significant attenuation in prefrontal and parietal acetylcholine levels and relatively quiescent behavior, rats retained righting reflex throughout nitrous oxide treatment and were easily aroused. Cortical acetylcholine showed a rapid return to pre-nitrous levels during post-nitrous recovery and did not statistically differ from the wake state [prefrontal: $t(141)=1.86$, $P = .2$, Fig 4.4C; parietal: $t(141)=0.01$, $P = 1$, Fig. 4.4D].

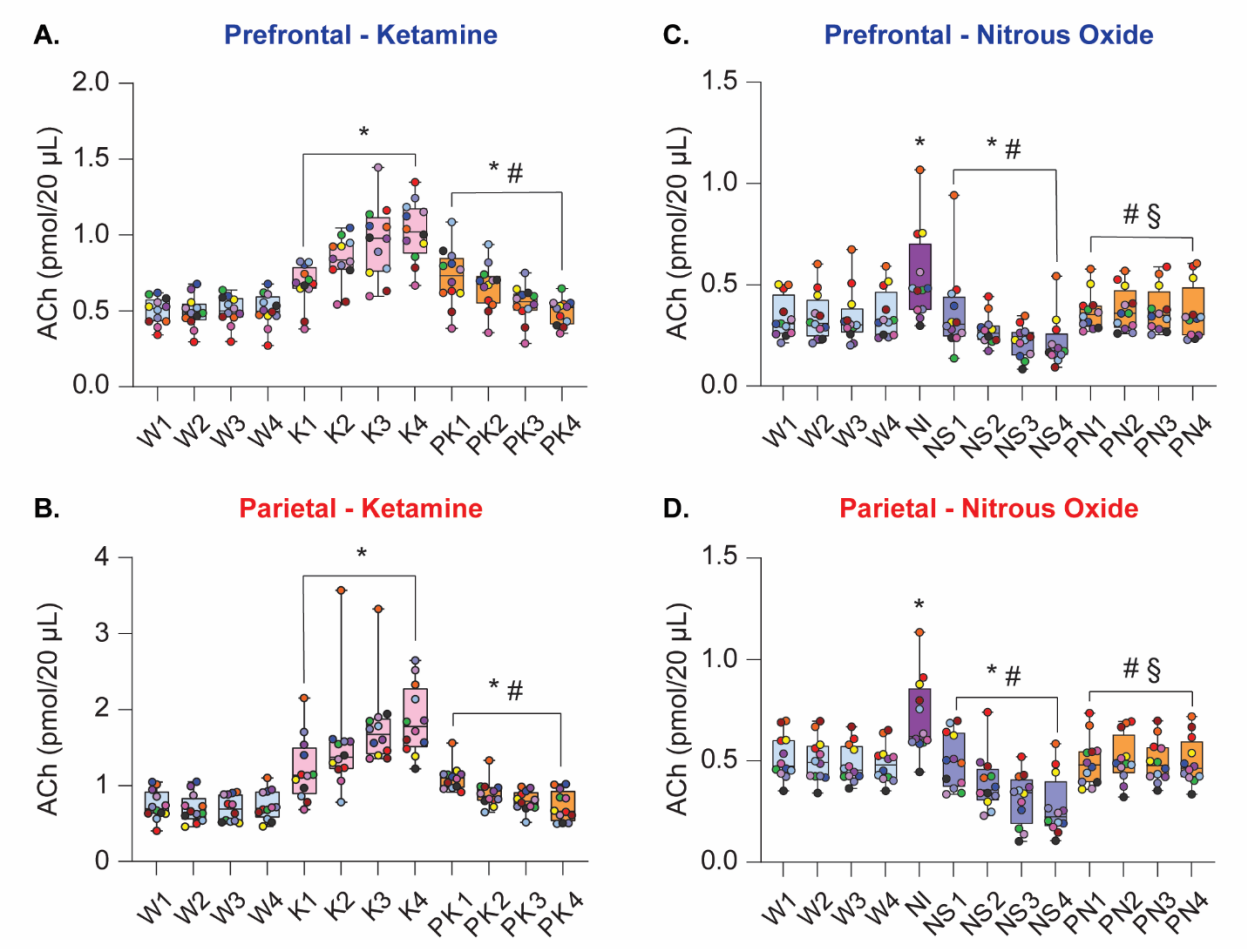

Figure 4.4 Subanesthetic ketamine and nitrous oxide administration produced differential effects on cortical acetylcholine levels. Subanesthetic ketamine infusion produced sustained increase in prefrontal (A) and parietal (B) acetylcholine levels. During post-ketamine recovery, cortical acetylcholine levels remained elevated compared to wakefulness, though this effect was largely driven by the first 2 post-ketamine epochs (A, B). In contrast, 50% nitrous oxide treatment transiently increased prefrontal and parietal acetylcholine levels during the first 12.5 min of exposure (nitrous induction), followed by a progressive decline in acetylcholine during nitrous oxide sedation phase (C, D). Cortical acetylcholine levels during post-nitrous oxide recovery did not significantly differ from those observed during baseline wake state (C, D). A linear mixed model with a random intercept for each rat was used for statistical comparisons. *Post hoc* pairwise tests between states were performed with single-step correction for multiple comparisons via Tukey's Test. The box plots show the median (horizontal bar) and interquartile range for averaged data over all 12 subjects at each epoch. The whiskers represent the minimum and maximum values within each epoch. The individual data for each subject is displayed by colored dots, with each color corresponding to a single subject across all epochs. ACh – acetylcholine, K – subanesthetic ketamine infusion, NI – nitrous oxide induction, NS – nitrous oxide sedation, PK – post-ketamine recovery, PN – post-nitrous oxide, W – wake. *Significant compared to wake, #significant compared to subanesthetic ketamine infusion or nitrous oxide induction, §significant compared to nitrous oxide sedation. The statistical comparisons are shown at $P < .05$. The exact P values are provided in the text in the results section. The mean, SD, and F-statistics for statistical comparisons are provided in Tables 4.1-4.2.

Prefrontal Cortex			
Wake	**Ketamine infusion**	**Post-ketamine recovery**	**F-Statistic**
0.5 ± 0.09 [0.42 - 0.58]	0.87 ± 0.15 [0.79 - 0.95] *P < .001	0.6 ± 0.12 [0.53 - 0.68] *P = .002; # P< .001	F(2,130)=82.92 *P < .001
Parietal Cortex			
Wake	**Ketamine infusion**	**Post-ketamine recovery**	**F-Statistic**
0.72 ± 0.17 [0.55 - 0.88]	1.59 ± 0.45 [1.43 - 1.75] *P < .001	0.88 ± 0.15 [0.72 – 1.04] *P = .03; #P < .001	F(2,130)=106.46 *P < .001

Table 4.1 Cortical acetylcholine before, during, and after intravenous infusion of subanesthetic ketamine.
Data are shown as mean ± standard deviation with 95% confidence interval in brackets. *Compared to Wake, #compared to Ketamine infusion.

Prefrontal Cortex				
Wake	**Nitrous induction**	**Nitrous sedation**	**Post-nitrous recovery**	**F-Statistic**
0.34 ± 0.11 [0.28 - 0.42]	0.54 ± 0.22 [0.46 - 0.61] *P < .001	0.27 ± 0.11 [0.20 - 0.33] *P < .001; #P < .001	0.37 ± 0.11 [0.31 - 0.44] *P = .247; #P < .001 §P < .001	F(3,141)=45.13 *P < .001
Parietal Cortex				
Wake	**Nitrous induction**	**Nitrous sedation**	**Post-nitrous recovery**	**F-Statistic**
0.5 ± 0.09 [0.45 - 0.55]	0.71 ± 0.19 [0.6 - 0.83] *P < .001	0.37 ± 0.105 [0.302 - 0.44] *P < .001; #P < .001	0.50 ± 0.11 [0.45 - 0.5] *P = 1; #P < .001 §P < .001	F(3,141)=52.72 *P < .001

Table 4.2 Cortical acetylcholine before, during, and after nitrous oxide administration.
Data are shown as mean ± standard deviation with 95% confidence interval in brackets.
*Compared to Wake, #compared to Nitrous induction, §compared to Nitrous sedation.

4.3.3 Subanesthetic ketamine infusion induced persistent increase in temporospatial EEG complexity

To assess the effect of subanesthetic ketamine infusion on temporospatial EEG complexity independent of the power spectrum, normalized Lempel-Ziv complexity (LZ_{SN}) was computed for EEG epochs before, during, and after ketamine infusion. As compared to baseline wake state, LZ_{SN} was significantly higher during subanesthetic ketamine [$t(130)=9.77$, $P < .001$,

Fig. 4.5A]. During post-ketamine recovery period, LZs_N values decreased relative to ketamine infusion [t(130)=-8.89, $P < .001$, Fig. 4.5A], returning to values comparable to those observed during wake state [t(130)=0.88, $P = .7$, Fig. 4.5A]. A topographic plot illustrating the degree of change in LZs_N during subanesthetic ketamine relative to wake in each EEG channel (as calculated by the t-statistic) is depicted in figure 4.5B, with regions colored red representing the areas with the greatest magnitude of change in LZs_N. EEG channels located within the frontal, posterior parietal, and occipital cortex showed the most statistically significant changes in LZs_N during subanesthetic ketamine infusion, as compared to wake state (Fig. 4.5B).

4.3.4 Nitrous oxide exposure caused state-dependent changes in temporospatial EEG complexity

Mirroring its effects on cortical acetylcholine, nitrous oxide exposure produced changes in EEG complexity that largely depended on the duration of exposure. The LZs_N during the first 12.5 min of nitrous oxide exposure (i.e., the induction phase) was found to be significantly higher than that observed during baseline wake state [t(141)=2.64, P = .04, Fig. 4.5C]. However, in the following 50 min of nitrous oxide exposure, the animals showed behavioral signs of sedation (i.e., reduced movement, slow stereotypic head bobbing, and sporadic grooming) accompanied with progressive decline in $\mathbf{LZs_N}$ values, which were significantly lower than that observed during both wakefulness [t(141=-7.34, P < .001, Fig. 4.5C] and nitrous oxide induction phase [t(141=-7.28, P < .001, Fig. 4.5C]. During post-nitrous recovery period, LZs_N values returned to levels that were significantly greater than nitrous-oxide sedation [t(141)=7.8, P < .001, Fig. 4.5C], but did not significantly differ from levels observed during baseline wake state [t(141)=0.45, P = 1, Fig. 4.5C]. Figures 4.5D and 4.5E illustrate topographic maps of the t-statistic representing changes in LZs_N relative to wake during nitrous oxide treatment within each EEG channel, with red regions representing channels with the most significant increases in LZs_N and the darkest blue regions representing the most significant decreases in LZs_N. Nitrous oxide induction caused a broad increase in neurophysiologic complexity across the EEG montage, with channels within the temporal, parietal, and occipital regions showing the most significant increases in LZs_N, as compared to wake (Fig. 4.5D). In contrast, nitrous oxide sedation in the following 50 min caused global suppression of LZs_N relative to wake state, with significant decreases in EEG complexity spanning the entirety of the cortex (Fig. 4.5E).

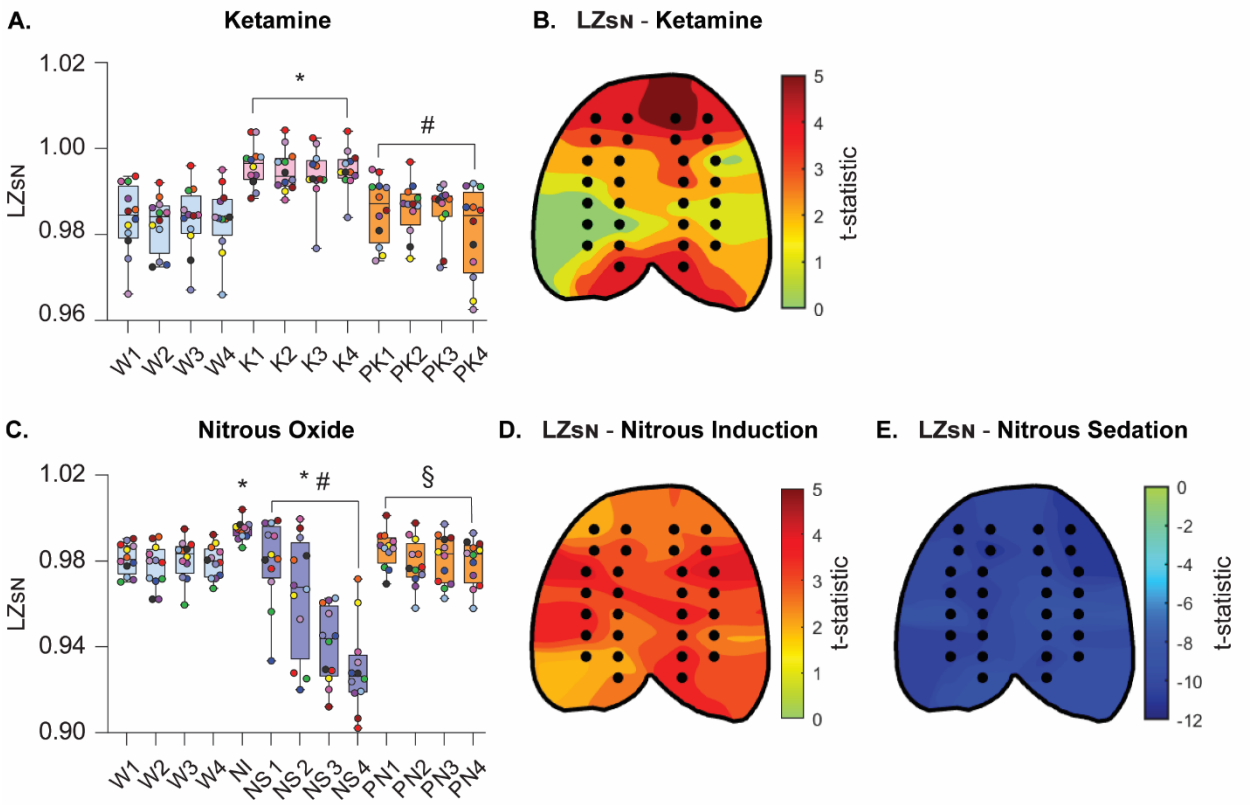

Figure 4.5 Changes in temporospatial EEG complexity during subanesthetic ketamine infusion and nitrous oxide exposure mirror concomitant changes in cortical acetylcholine levels.
Normalized Lempel-Ziv complexity (LZ_{SN}) was significantly increased during subanesthetic ketamine infusion, returning to wake levels after the infusion was stopped (A). Changes in LZ_{SN} during subanesthetic ketamine infusion were also quantified at the level of single channels (black dots in the topographic plots), demonstrating that the most pronounced changes in temporal complexity, relative to wake, occurred in frontal, posterior parietal, and occipital channel clusters (B). LZ_{SN} significantly increased during the first 12.5 min of nitrous oxide exposure (induction phase) as compared to baseline wake state (C). During the subsequent nitrous oxide sedation phase, the LZ_{SN} declined to levels significantly lower than that observed during baseline wake. LZ_{SN} returned to levels comparable to baseline wakefulness during post-nitrous oxide recovery (C). The most significant increases in temporal complexity during nitrous oxide induction, as compared to baseline wake state, were located in frontotemporal, parietal, and occipital regions (D). Nitrous oxide sedation was characterized by a significant decrease in temporal complexity across the entire cortical surface (E). A linear mixed model with a random intercept for each rat was used for statistical comparisons. Post hoc pairwise tests between states were performed with single-step correction for multiple comparisons via Tukey's Test. The box plots show the median (horizontal bar) and interquartile range for averaged data over all 12 subjects at each epoch. The whiskers represent the minimum and maximum values within each epoch. The individual data for each subject is displayed by colored dots, with each color corresponding to a single subject across all epochs. K – subanesthetic ketamine infusion, LZ_{SN} - normalized Lempel-Ziv complexity, NI – nitrous oxide induction, NS – nitrous oxide sedation, PK – post-ketamine recovery, PN – post-nitrous oxide, W – wake. *Significant compared to wake, #significant compared to subanesthetic ketamine infusion or nitrous oxide induction, §significant compared to nitrous oxide sedation. The statistical comparisons are shown at $P < .05$. The exact P values are provided in the text in the results section. The mean, standard deviation, and F-statistics for statistical comparisons are provided in Tables 4.3-4.4.

Wake	Ketamine infusion	Post-ketamine recovery	F-Statistic
0.983 ± 0.006 [0.979 - 0.986]	0.995 ± 0.004 [0.992 - 0.998] *P < .001	0.984 ± 0.005 [0.981 - 0.987] *P = .7; #P < .001	F(2,130)=58.4 *P < .001

Table 4.3 Normalized Lempel-Ziv complexity before, during, and after intravenous infusion of subanesthetic ketamine.
Data are shown as mean ± standard deviation with 95% confidence interval in brackets.
*Compared to Wake, #compared to Ketamine infusion.

Wake	Nitrous induction	Nitrous sedation	Post-nitrous recovery	F-Statistic
0.979 ± 0.007 [0.973 - 0.986]	0.993 ± 0.004 [0.982 – 1.006] *P = .04	0.953 ± 0.012 [0.947 - 0.96] *P < .001; #P < .001	0.981 ± 0.008 [0.974 - 0.987] *P = 1; #P = .09 §P < .001	F(3,141)=31.9 *P < .001

Table 4.4 Normalized Lempel-Ziv complexity before, during, and after nitrous oxide administration.
Data are shown as mean ± standard deviation with 95% confidence interval in brackets.
*Compared to Wake, #compared to Nitrous induction, §compared to Nitrous sedation.

4.3.5 Prefrontal and parietal acetylcholine levels correlate with the changes in cortical complexity

To assess the correlation between changes in prefrontal and parietal acetylcholine levels and temporospatial EEG complexity, the cluster-weighted marginal correlation was computed for both ketamine and nitrous oxide groups. Prefrontal and parietal acetylcholine levels for each microdialysis epoch were compared with the concomitant changes in LZs_N measured across all 144 individual datapoints in ketamine experiments, or all 156 datapoints in nitrous oxide experiments, with data dependencies based on individual rats factored into the analysis. Acetylcholine levels in the prefrontal and parietal cortices showed significant positive correlations with LZs_N both in the ketamine group [prefrontal: CW r(144)=0.42, P < .001, Fig. 4.6A; CW r(144)=0.49, P < .001, Fig. 4.6B] and the nitrous oxide group [prefrontal: CW r(156)=0.46, P < .001, Fig. 4.6C; parietal: CW r(156)=0.56, P < .001, Fig. 4.6D].

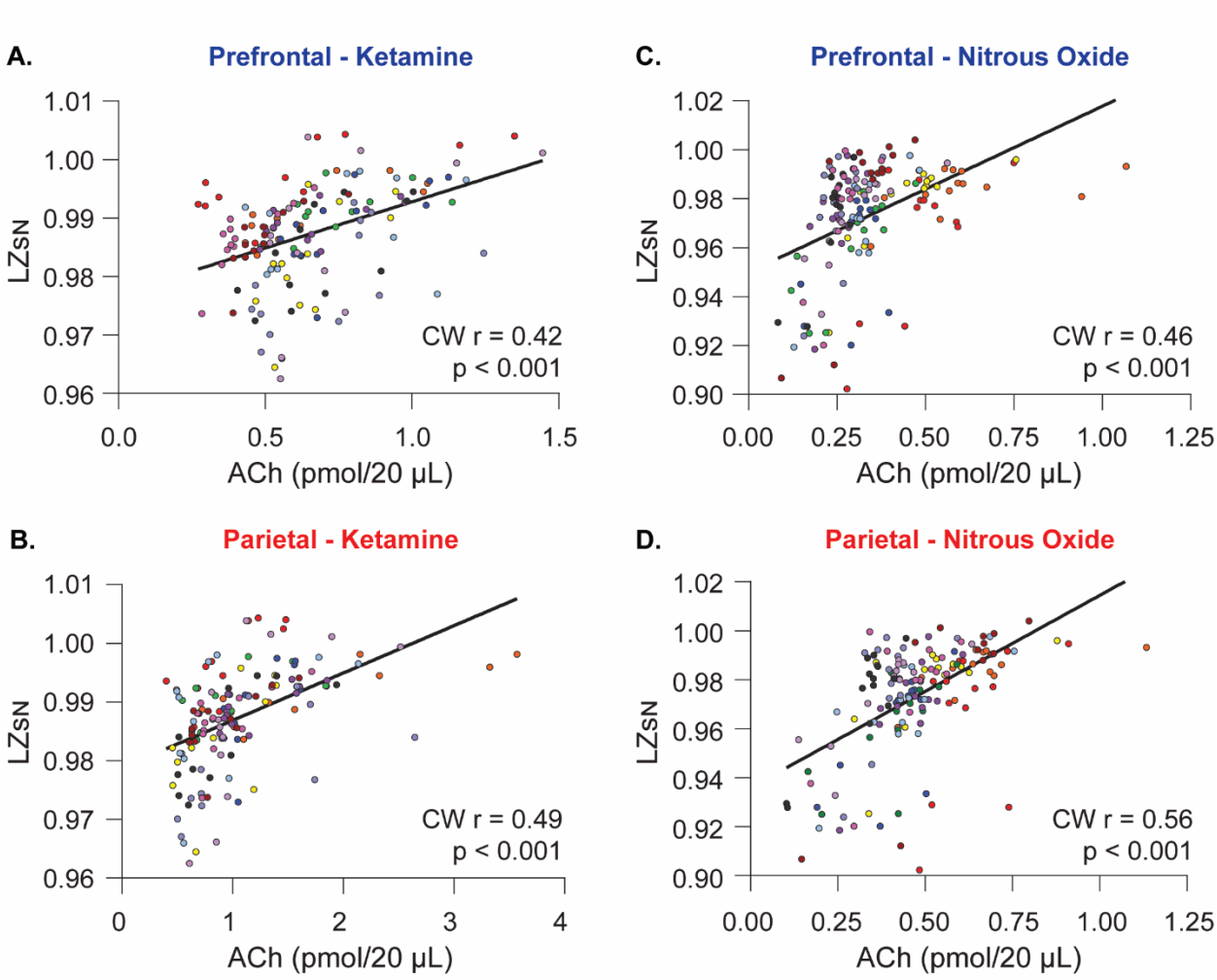

Figure 4.6 Relationship between cortical acetylcholine and temporospatial EEG complexity.
Relationship between cortical acetylcholine and temporospatial EEG complexity. Changes in prefrontal and parietal acetylcholine levels were significantly correlated with changes in temporospatial EEG complexity in the subanesthetic ketamine infusion **(A, B)** and nitrous oxide exposure **(C, D)** cohorts. The individual data for each subject is displayed by colored dots, with each color corresponding to a single subject across all epochs. To account for clustering of the data within each rat, we calculated the cluster-weighted marginal correlation. ACh – acetylcholine, LZ_{SN} – normalized Lempel-Ziv complexity, CW r – cluster-weighted marginal correlation. The line represents points of best fit.

4.3.6 Effects of subanesthetic ketamine on frontoparietal connectivity in gamma bandwidths

Normalized symbolic transfer entropy (NSTE) was computed across low (25-55 Hz), mid (85-125 Hz), and high gamma (125-175 Hz) bandwidths between ipsilateral frontal and parietal channels as an estimate of directed feedback (frontal to parietal) and feedforward (parietal to frontal) connectivity. Subanesthetic ketamine suppressed low and mid gamma frontoparietal connectivity in both feedback [low: t(130)=-6.89, $P < .001$, Fig. 4.7A; mid: t(130)=-15.12, $P < .001$, Fig. 4.7C] and feedforward directions [low: t(130)=-8.20, $P < .001$, Fig 4.7B; mid: t(130)=-

14.90, $P < .001$, Fig. 4.7D]. Conversely, high gamma frontoparietal connectivity was significantly increased during subanesthetic ketamine in both feedback [t(130)=17.59, $P < .001$, Fig. 4.7E] and feedforward [t(130)=17.24, $P < .001$, Fig. 4.7F] directions. As compared to wake state, post-ketamine recovery was characterized by reduced frontoparietal connectivity in the mid gamma band [feedback: t(130)=-10.54, $P < .001$, Fig. 4.7C; feedforward: t(130)=-12.79, $P < .001$, Fig. 4.7D] while the low and high gamma band connectivity returned to levels that did not significantly differ from those observed during the baseline wake state. In the low gamma band, feedback and feedforward connectivity were elevated relative to subanesthetic ketamine [feedback: t(130)=3.85, $P < .001$, Fig. 4.7A; feedforward: t(130)=6.24, $P < .001$, Fig 4.7B]. High gamma connectivity during post-ketamine recovery remained attenuated as compared to subanesthetic ketamine [feedback: t(130)=-18.02, $P < .001$, Fig. 4.7E; feedforward: t(130)=-17.89, $P < .001$, Fig. 4.7F]. The correlations between frontoparietal connectivity in gamma bandwidths and acetylcholine levels in prefrontal and parietal cortices are reported in Table 4.6.

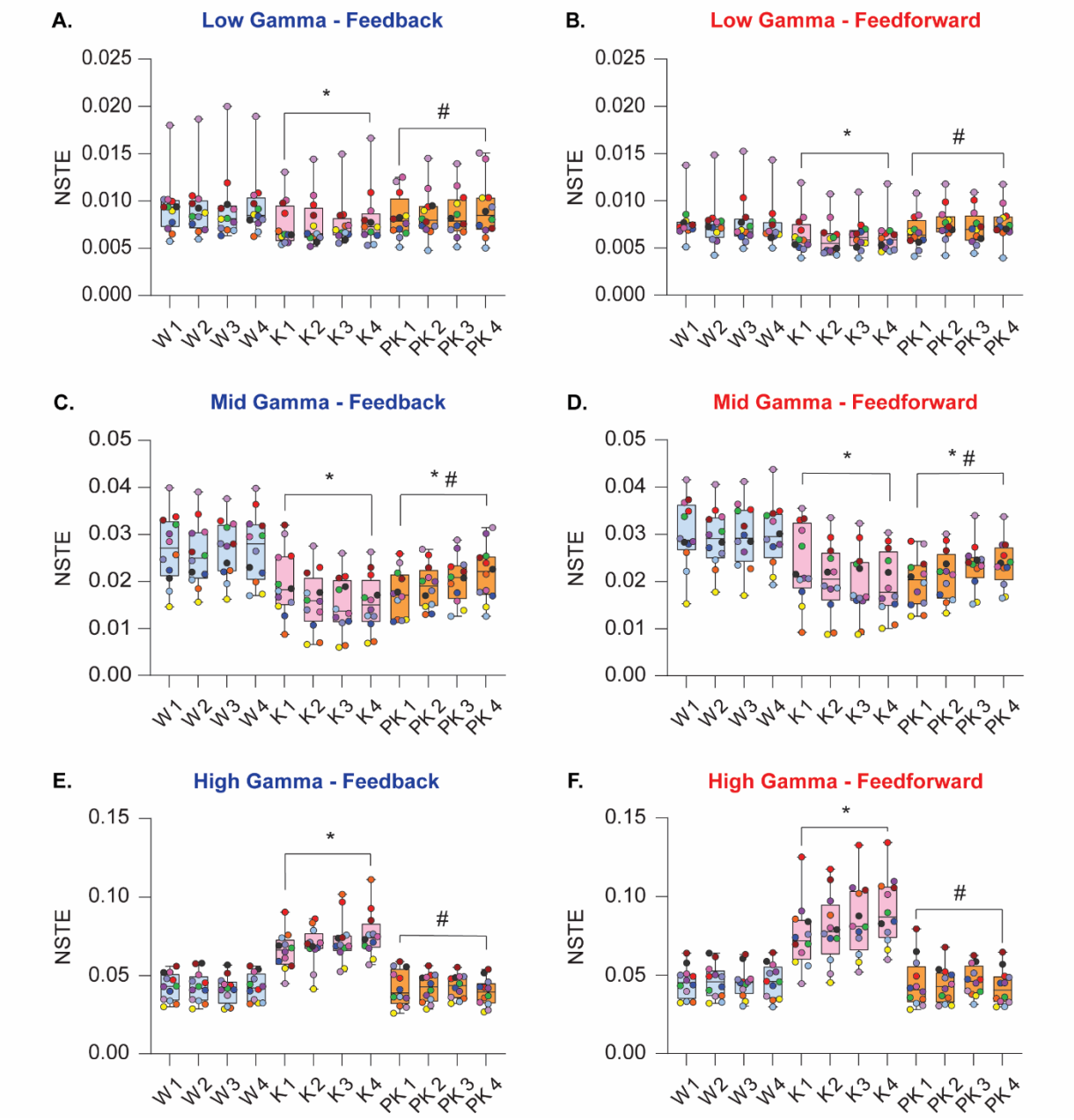

Figure 4.7 Effect of subanesthetic ketamine infusion on directed frontoparietal connectivity in gamma bandwidths. Subanesthetic ketamine infusion significantly decreased frontoparietal connectivity in the low gamma bandwidth (25-55 Hz) in both feedback and feedforward directions relative to baseline wake state (A, B). Frontoparietal connectivity in the mid gamma bandwidth (85-125 Hz) decreased in feedback and feedforward directions during subanesthetic ketamine and remained depressed relative to baseline wakefulness during post-ketamine recovery (C, D). Feedback and feedforward connectivity between frontal and parietal cortices was significantly increased in the high gamma bandwidth (125-175 Hz) during subanesthetic ketamine treatment, returning to levels comparable to baseline wakefulness during post-ketamine recovery (E, F). A linear mixed model with a random intercept for each rat was used for statistical comparisons. *Post hoc* pairwise tests between states were performed with single-step correction for multiple comparisons via Tukey's Test. The box plots show the median (horizontal bar) and interquartile range for averaged data over all 12 subjects at each epoch. The whiskers represent the minimum and maximum values within each epoch. The individual data for each subject is displayed by colored dots, with each color corresponding to a single subject across all epochs. K – subanesthetic ketamine infusion, PK – post-ketamine recovery, NSTE – normalized symbolic transfer entropy, W – wake. *Significant compared to wake, #significant compared to subanesthetic ketamine infusion. The statistical comparisons are shown at $P < .05$. The exact P values are provided in the text in the results section. The mean, SD, and F-statistics for statistical comparisons are provided in Table 4.5.

Feedback Connectivity				
Frequency (Hz)	**Wake**	**Ketamine infusion**	**Post-ketamine recovery**	**F-Statistic**
low γ (25–55)	0.009 ± 0.003 [0.008 - 0.011]	0.008 ± 0.002 [0.006 - 0.01] *P < .001	0.009 ± 0.002 [0.007 - 0.01] *P = .08; #P < .001	F(2,130)=23.84 *P < .001
mid γ (85–125)	0.027 ± 0.008 [0.023 - 0.030]	0.017 ± 0.006 [0.013 - 0.020] *P < .001	0.0196 ± 0.005 [0.016 - 0.023] *P < .001; #P < .001	F(2,130)=120.1 *P < .001
high γ (125–175)	0.042 ± 0.008 [0.037 - 0.048]	0.07 ± 0.013 [0.065 - 0.076] *P < .001	0.041 ± 0.009 [0.036 - 0.047] *P = 1; #P < .001	F(2,130)=211.5 *P < .001
Feedforward Connectivity				
Frequency (Hz)	**Wake**	**Ketamine infusion**	**Post-ketamine recovery**	**F-Statistic**
low γ (25–55)	0.008 ± 0.002 [0.006 - 0.009]	0.006 ± 0.002 [0.005 - 0.008] *P < .001	0.007 ± 0.002 [0.006 - 0.009] *P = .13; #P < .001	F(2,130)=36.67 *P < .001
mid γ (85–125)	0.03 ± 0.006 [0.026 - 0.034]	0.021 ± 0.007 [0.017 - 0.025] *P < .001	0.022 ± 0.005 [0.018 - 0.026] *P = .001; #P = .1	F(2,130)=130.01 *P < .001
high γ (125–175)	0.045 ± 0.01 [0.037 - 0.054]	0.08 ± 0.021 [0.074 - 0.091] *P < .001	0.044 ± 0.012 [0.036 - 0.053] *P = .796 #P < .001	F(2,130)=205.84 *P < .001

Table 4.5 Directed frontoparietal connectivity in gamma bandwidths before, during, and after intravenous infusion of subanesthetic ketamine.
Data are shown as mean ± standard deviation with 95% confidence interval in brackets.
*Compared to Wake, #compared to Ketamine infusion.

	Prefrontal acetylcholine		Parietal acetylcholine	
Frequency (Hz)	**Feedback connectivity**	**Feedforward connectivity**	**Feedback connectivity**	**Feedforward connectivity**
low γ (25–55)	CW r = -0.21 [-0.54 – 0.11] *P* = .18	CW r = -0.26 [-0.56 – 0.03] *P* = .08	CW r = -0.18 [-0.43 – 0.06] *P* = .14	CW r = -0.20 [-0.44 – 0.04] *P* = .09
mid γ (85–125)	CW r = -0.47 [-0.67 – -0.27] **P* < .001	CW r = -0.40 [-0.60 – -0.19] **P* < .001	CW r = -0.48 [-0.73 – -0.23] **P* < .001	CW r = -0.43 [-0.72 – -0.15] **P* < .01
high γ (125–175)	CW r = 0.54 [0.35 – 0.72] **P* < .001	CW r = 0.48 [0.25 – 0.70] **P* < .001	CW r = 0.64 [0.54 – 0.74] **P* < .001	CW r = 0.58 [0.46 – 0.70] **P* < .001

Table 4.6 Correlation between changes in cortical acetylcholine and directed frontoparietal connectivity in gamma bandwidths after intravenous infusion of subanesthetic ketamine.
Data are shown as the cluster-weighted marginal correlation with 95% confidence interval in brackets. *significant correlation.

4.3.7 Effects of nitrous oxide exposure on frontoparietal connectivity in gamma bandwidths

Nitrous oxide exposure produced no significant effect on low gamma frontoparietal connectivity in the first 12.5 min induction period [feedback: t(141)=0.44, *P* = 1, Fig. 4.8A; feedforward: t(141)=1, *P* = .7, Fig. 4.8B]. However, the following 50 min of nitrous oxide sedation significantly increased low gamma frontoparietal connectivity in both feedforward and feedback directions, as compared to wake state [feedback: t(141)=6.41, *P* < .001, Fig. 4.8A; feedforward: t(141)=6.84, *P* < .001, Fig. 4.8B]. As compared to nitrous oxide sedation, the post-nitrous recovery was characterized by significant attenuation of both feedback and feedforward low gamma frontoparietal connectivity [feedback: t(141)=-6.18, *P* < .001, Fig. 4.8A; feedforward: t(141)=3.33, *P* = .005, Fig. 4.8B]; no difference as compared to baseline wake levels [low gamma feedback: t(141)=0.24, *P* = 1, Fig. 4.8A; low gamma feedforward: t(141)=0.5, *P* = .9, Fig. 4.8B].

In the mid gamma bandwidth, nitrous oxide induction was characterized by increase in bidirectional frontoparietal connectivity [feedback: t(141)=6.43, *P* < .001, Fig 4.8C; feedforward: t(141) = 6.09, *P* < .001, Fig. 4.8D]. During nitrous sedation, mid gamma connectivity did not significantly differ from wake, but was significantly lower than nitrous

induction [feedback: t(141)=-7.15, $P < .001$, Fig. 4.8C; feedforward: t(141)=-7.72, $P < .001$, Fig. 4.8D]. As compared to wake state, the post-nitrous recovery period was characterized by a significant attenuation of mid gamma feedback connectivity [t(141)=-2.69, $P = .04$, Fig. 4.8C], with no significant difference as compared to baseline wake levels [t(141)=-2.50, $P = .06$, Fig. 4.8D].

High gamma frontoparietal connectivity during nitrous oxide induction increased in feedback [t(141)=3.90, $P < .001$, Fig. 4.8E] and feedforward [t(141)=4.52, $P < .001$, Fig. 4.8F] directions. During nitrous oxide sedation, high gamma connectivity returned to waking levels but were significantly attenuated as compared to that observed during nitrous oxide induction [feedback: t(141)=-4.19, $P < .001$, Fig. 4.8E; feedforward: t(141)=-4.02, $P < .001$, Fig. 4.8F]. Frontoparietal connectivity during post-nitrous oxide recovery wakefulness did not statistically differ from the baseline wake state [feedback: t(141)=-0.35, $P = 1$, Fig. 4.8E; feedforward: t(141)=-0.24, $P = 1$, Fig. 4.8F], and was significantly attenuated when compared with nitrous oxide induction [feedback: t(141)=-4.126, $P < .001$, Fig. 4.8E; feedforward: t(141)=-4.673, $P < .001$, Fig. 4.8F]. Correlations between frontoparietal connectivity in gamma bandwidths and acetylcholine levels in prefrontal and parietal cortices are reported in Table 4.8.

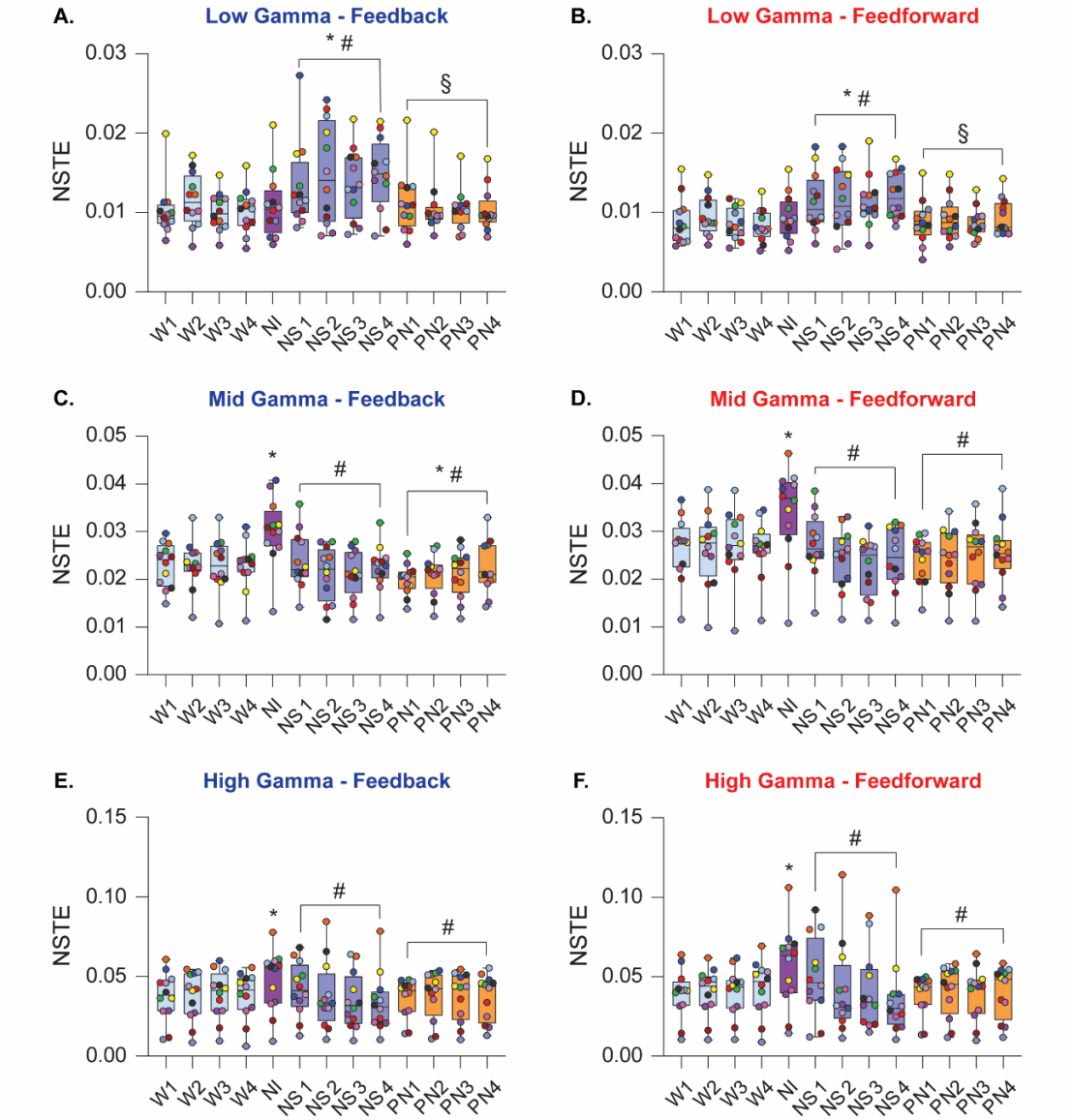

Figure 4.8 Effects of subanesthetic nitrous oxide exposure on directed frontoparietal connectivity in gamma bandwidths. During nitrous oxide induction, frontoparietal connectivity in the low gamma bandwidth (25-55 Hz) did not differ from wake (A, B). However, feedback and feedforward connectivity in low gamma frequencies was significantly increased during the following 50 min nitrous oxide sedation (A, B). Frontoparietal connectivity in feedback and feedforward directions was increased during nitrous oxide induction in the mid gamma bandwidth (85-125 Hz) (C, D) whereas nitrous oxide sedation was characterized by a decrease in connectivity as compared to wakefulness. During post-nitrous oxide recovery period, connectivity in the feedback direction showed a modest increase relative to baseline wakefulness, while feedforward connectivity did not statistically differ from wake. Nitrous oxide induction transiently increased the strength of connectivity between frontal and parietal cortices in the high gamma bandwidth (125-175 Hz) in feedback and feedforward directions (E, F) whereas the nitrous oxide sedation phase was characterized by decrease in both feedback and feedforward connectivity to wake levels. Frontoparietal connectivity did not differ between baseline wakefulness and post-nitrous oxide recovery. A linear mixed model with a random intercept for each rat was used for statistical comparisons. *Post hoc* pairwise tests between states were performed with single-step correction for multiple comparisons via Tukey's Test. The box plots show the median (horizontal bar) and interquartile range for averaged data over all 12 subjects at each epoch. The whiskers represent the minimum and maximum values within each epoch. The individual data for each subject is displayed by colored dots, with each color corresponding to a single subject across all epochs. NI – nitrous oxide induction, NS – nitrous oxide sedation, NSTE – normalized symbolic transfer entropy, PN – post-nitrous oxide, W – wake. *Significant compared to wake, #significant compared to nitrous oxide induction, §significant compared to nitrous oxide sedation. The statistical comparisons are shown at $P < .05$. The exact P values are provided in the text in the results section. The mean, SD, and F-statistics for statistical comparisons are provided in Table 4.7.

Feedback Connectivity					
Frequency (Hz)	**Wake**	**Nitrous induction**	**Nitrous sedation**	**Post-nitrous recovery**	**F-Statistic**
low γ (25–55)	0.011 ± 0.003 [0.008 - 0.013]	0.011 ± 0.004 [0.008 - 0.014] *P = 1	0.0141 ± 0.008 [0.012 - 0.016] *P < .001 #P = .002	0.011 ± 0.003 [0.009 - 0.013] *P = 1; #P = 1 §P < .001	F(3,141)=17.98 *P < .001
mid γ (85–125)	0.023 ± 0.004 [0.02 - 0.026]	0.03 ± 0.007 [0.027 - 0.034] *P < .001	0.022 ± 0.005 [0.019 - 0.025] *P = .66; #P < .001	0.021 ± 0.004 [0.018 - 0.024] *P < .04 #P < .001; §P = .4	F(3,141)=22.6 *P < .001
high γ (125–175)	0.038 ± 0.015 [0.028 - 0.047]	0.047 ± 0.019 [0.036 - 0.058] *P < .001	0.037 ± 0.016 [0.027 - 0.047] *P = .968 #P < .001	0.037 ± 0.014 [0.028 - 0.047] *P = .968 #P < .001 §P = .999	F(3,141) = 6.46 *P < .001
Feedforward Connectivity					
Frequency (Hz)	**Wake**	**Nitrous induction**	**Nitrous sedation**	**Post-nitrous recovery**	**F-Statistic**
low γ (25–55)	0.09 ± 0.003 [0.007 - 0.010]	0.009 ± 0.004 [0.008 - 0.011] *P = 1	0.012 ± 0.008 [0.01 - 0.013] *P < 0.001 #P = .002	0.009 ± 0.003 [0.008 - 0.011] *P = 1; #P = 1 §P < .001	F(3,141)=17.98 *P < .001
mid γ (85–125)	0.026 ± 0.006 [0.023 - 0.031]	0.034 ± 0.009 [0.03 - 0.039] *P < .001	0.024 ± 0.005 [0.021 - 0.029] *P = .05 #P < .001	0.025 ± 0.006 [0.021 - 0.029] *P = .06 #P < .001 §P = 1	F(3,141)=22.58 *P < .001
high γ (125–175)	0.040 ± 0.016 [0.03 - 0.05]	0.056 ± 0.025 [0.039 - 0.07] *P < .001	0.042 ± 0.023 [0.03 - 0.054] *P = .85 #P < .001	0.039 ± 0.015 [0.028 - 0.052] *P = 1; #P < .001 §P = .72	F(3,141) = 7.85 *P < .001

Table 4.7 Directed frontoparietal connectivity in gamma bandwidths before, during, and after nitrous oxide administration.
Data are shown as mean ± standard deviation with 95% confidence interval in brackets.
*Compared to Wake, #compared to Nitrous induction, §compared to Nitrous sedation.

	Prefrontal acetylcholine		Parietal acetylcholine	
Frequency (Hz)	**Feedback connectivity**	**Feedforward connectivity**	**Feedback connectivity**	**Feedforward connectivity**
low γ (25–55)	CW r = 0.13 [-0.11 – 0.37] *P* = .28	CW r = 0.11 [-0.11 – 0.34] *P* = .32	CW r = -0.11 [-0.29 – 0.08] *P* = .1	CW r = -0.07 [-0.229 – 0.093] *P* = .25
mid γ (85–125)	CW r = 0.18 [-0.03 – 0.40] *P* = .09	CW r = 0.35 [0.17 – 0.53] **P* < .001	CW r = 0.23 [0.02 – 0.42] **P* < .05	CW r = 0.25 [0.01 – 0.48] **P* < .05
high γ (125–175)	CW r = 0.42 [0.17 – 0.68] **P* < .01	CW r = 0.46 [0.20 – 0.71] **P* < .001	CW r = 0.16 [-0.18 – 0.49] *P* = .36	CW r = 0.20 [-0.13 – 0.54] *P* = .23

Table 4.8 Correlation between changes in cortical acetylcholine and directed frontoparietal connectivity in gamma bandwidths in the nitrous oxide group.
Data are shown as the cluster-weighted marginal correlation coefficient with 95% confidence interval in brackets. *significant correlation.

4.4 Discussion

The principal findings in our study demonstrate that changes in temporospatial EEG complexity during subanesthetic ketamine or 50% nitrous oxide exposure correlate with concomitant changes in prefrontal and parietal acetylcholine levels. Of note, the changes in EEG complexity showed distinct drug-dependent temporal and spatial profiles. Subanesthetic ketamine produced increases in signal complexity and cortical acetylcholine that lasted throughout the ketamine infusion (62.5 min), with the largest complexity changes occurring in frontal, posterior parietal, and occipital channel clusters. Conversely, nitrous oxide increased EEG complexity and cortical acetylcholine only during the first 12.5 min of nitrous administration (induction), with the largest magnitude of change in frontotemporal and parietal regions. The next 50 min of nitrous oxide exposure (sedation) were marked by periodically quiescent behavior, a gradual decline in prefrontal and parietal acetylcholine levels, and global suppression of EEG complexity that was most pronounced in frontal channel clusters. The topographic distribution of changes in EEG complexity during subanesthetic ketamine and nitrous oxide sedation in our study broadly mirrored recent magnetoencephalographic and EEG

data published during ketamine and nitrous oxide administration in humans,[83,235] suggesting a comparable dynamic landscape during the administration of dissociative anesthetics in rodents.

A previous study from our laboratory demonstrated that ketamine, in the absence of any behavioral arousal, can increase prefrontal acetylcholine.[98] A previous study quantifying the effect of nitrous oxide on cortical acetylcholine showed similar effects on acetylcholine as reported by us in the current study, i.e., a sharp increase after nitrous administration followed by a progressive decrease.[142] Cortical acetylcholine is also known to correlate with behavioral arousal.[207] Therefore, changes in cortical acetylcholine can result from a direct drug effect or changes in level of behavioral arousal. In the current study, it is difficult to ascribe the increase in cortical acetylcholine only to drug (ketamine/nitrous oxide) administration or only behavioral effects; it is likely that changes in cortical acetylcholine are a product of interaction between drug and behavioral effects. In contrast, previous findings suggest that increases in neurophysiologic complexity are likely due to increased cortical acetylcholine or EEG activation, rather than behavioral arousal. This conclusion was supported by prior studies from our laboratory in which we showed that a pharmacologically induced increase in prefrontal acetylcholine in sevoflurane-anesthetized rats was accompanied with EEG activation and an increase in complexity to baseline wake levels, with or without concomitant behavioral arousal.[158,159]

In addition to the relationship between neurophysiologic complexity and cortical acetylcholine, our study characterized changes in directed frontoparietal connectivity in low (25-55 Hz), mid (85-125 Hz), and high (125-175 Hz) gamma bandwidths. A previous study from our laboratory demonstrated that frontoparietal connectivity in high gamma bandwidth is a correlate of wakefulness, being reduced in conjunction with suppressed cortical levels of acetylcholine during general anesthesia.[120] Our data extend these findings to dynamics characteristic of psychedelic states, demonstrating that periods of elevated cortical acetylcholine and neurophysiologic complexity during subanesthetic ketamine or nitrous oxide induction were correlated with increased high gamma frontoparietal connectivity. Conversely, low gamma frontoparietal connectivity was reduced when cortical acetylcholine levels were high and increased when acetylcholine levels were suppressed. Our data relating to cortical complexity and connectivity are broadly supportive of studies demonstrating hyperfrontality during classical psychedelic and dissociative drug administration, wherein excessive glutamatergic or cholinergic

tone in frontal cortex accompanies aberrant cortical dynamics and alterations to the contents of consciousness.[236–239]

Reductions in measures of neurophysiologic complexity have been demonstrated across a broad range of pharmacologic and non-pharmacologic models of unconsciousness,[75,76,79,88,93,159,175,217] while an increase in neurophysiologic complexity during psychedelic states has been shown to correlate with subjective intensity of altered conscious contents.[80,83,240] Our finding of concomitant changes in cortical acetylcholine levels, neurophysiologic complexity, and high gamma frontoparietal connectivity during elevated and depressed states of consciousness is consistent with the purported role of acetylcholine in supporting cortical activation and arousal, expanding this relationship to dynamic neurophysiologic signatures related to the level of consciousness.[64,66,73] Heterogenous cell populations within the basal forebrain drive acetylcholine release at topographically specific targets across the cortex,[134,232,241] with cortical cholinergic transmission shaping the activity of pyramidal and GABAergic interneuron populations implicated in cortical activation and wakefulness.[242–244]Acetylcholine release within the cortex is thought to create conditions that are permissive of high levels of neurophysiologic complexity, such as the reduction of slow cortical oscillations,[245] thalamocortical desynchronization,[246] and the promotion of high frequency cortical gamma oscillations.[98,154,242] Thus, while further testing of this hypothesis is required, cortical cholinergic transmission is a plausible neuromodulatory mechanism by which dynamics such as complexity can be shaped within cortical networks.

Although an increase in cortical acetylcholine levels during subanesthetic ketamine and nitrous oxide in rats has been reported, there are key differences as compared to our study. First, to our knowledge, none of the previous studies recorded simultaneous changes in EEG, which in the current study has allowed us to bridge neurochemical events in the cortex with concurrent changes in neurophysiological complexity and corticocortical connectivity. Second, while previous studies in rodents have reported changes in complexity across altered states of arousal,[88,159,217] our use of high-density EEG allowed the application of temporospatial measures of complexity that more readily translate to those used in human studies.[75,76,79,80,83] Third, because of our carefully titrated and timed drug administration, we were able to clearly characterize neurochemical and neurophysiological changes before, during, and after drug administration.

There are limitations to our study. Given the poor temporal resolution of microdialysis, our results should only be interpreted as they relate to sustained tonic acetylcholine release. Alternative approaches such as cholinergic biosensors may be better suited to investigate phasic cholinergic dynamics as they relate to neurophysiologic complexity at finer scales such as spikes or event-related potentials. Although cortical acetylcholine appears to vary with the level of consciousness, neurophysiologic complexity is likely to be governed by a complex neurochemical milieu, and thus further research investigating the relationship between complexity and other neurotransmitter systems within the cortex is warranted. Finally, our data are correlative and further studies establishing a causal relationship between cholinergic neurotransmission and complexity are necessary.

In conclusion, we demonstrate that changes in cortical acetylcholine are correlated with measures of EEG complexity and frontoparietal connectivity in high-gamma bandwidths during subanesthetic ketamine and nitrous oxide. These findings expand our understanding of the relationship between neurochemical and neurophysiologic signatures purported to correlate with consciousness.

4.5 Summary and Conclusions

In Chapter 4, we explored the relationship between cortical acetylcholine and two computational measures purported to relate to the level of consciousness: neurophysiologic complexity and corticocortical connectivity between frontal and parietal cortices. Leveraging the unique pharmacological properties of the dissociative anesthetics ketamine and nitrous oxide, we modeled cortical dynamics characteristic of psychedelic and sedative states in rats and examined concurrent changes in cortical acetylcholine, EEG complexity, and directed frontoparietal connectivity in low (25-55 Hz), medium (85-125 Hz), and high gamma (125-175 Hz) bandwidths. We report that changes in cortical acetylcholine in prefrontal and parietal cortices are correlated with changes in neurophysiologic complexity and directed frontoparietal connectivity in high gamma bandwidths before, during, and after subanesthetic administration of ketamine or nitrous oxide.

Chapter 5 Conclusions and Future Directions

5.1 Complexity, Connectivity, and the Level of Consciousness: Where to Look Beyond Behavior?

Prevailing theories of consciousness have argued that the capacity for consciousness is related to dynamic features such as the complexity of brain state repertoire[64,66,68,228] or the strength of connectivity between frontal and parietal cortices.[101,102] In support of this, neurophysiologic and neuroimaging approaches have demonstrated reductions in cortical complexity and frontoparietal connectivity during physiologic,[76,88,120,187] pharmacologic,[69,73,75,98,112,120,161] and pathologic[93,126,169] loss of consciousness. However, the traditional approach to validating theoretically-proposed computational measures of consciousness has been to correlate such measures with the presence or absence of pretheoretical measures of consciousness, such as behavioral responsiveness or connection to external stimuli.[52,100] This approach has limitations when attempting to measure the level of consciousness during states in which conscious contents can become decoupled from behavioral responsiveness or the external environment, such as ketamine anesthesia or certain disorders of consciousness.[40,48,52,100] Furthermore, with only correlative data available – it is unknown if changes in complexity or corticocortical connectivity truly reflect the loss of consciousness, as opposed to drug-specific effects on the cortex.

A previous study from our laboratory[158] demonstrated that cholinergic (but not noradrenergic) stimulation of the prefrontal cortex was sufficient to reverse clinical levels of sevoflurane anesthesia in rats. In contrast, cholinergic or noradrenergic stimulation of parietal cortical regions was not able to restore wakefulness in sevoflurane-anesthetized rats, but was found to induce EEG activation, nonetheless. The finding of EEG activation in the absence of behavioral arousal in these conditions motivated our Chapter 2 study, as these data offered a unique experimental paradigm to test if changes in the level of consciousness induced by cholinergic stimulation of the prefrontal cortex were accompanied by a restoration of neurophysiologic complexity and large-scale connectivity to levels comparable to wakefulness.

We posited that if these computational measures were related to the level of consciousness as assessed by behavior, they should be selectively restored in the prefrontal cholinergic stimulation group that exhibited return of righting and a subsequent wake-like state, but not in the remaining noradrenergic or cholinergic stimulation conditions that remained unresponsive.

Given that previous studies from our laboratory have identified directed frontoparietal connectivity in the high gamma band to be a correlate of wakefulness,[98,120] we focused our investigation of corticocortical connectivity within low (25-55 Hz), medium (85-125 Hz), and high (125-155 Hz) gamma bandwidths. Counter to our expectations, we observed a bidirectional suppression of frontoparietal connectivity in all 3 gamma bandwidths across each cortical stimulation condition, irrespective of the presence or absence of wakefulness. While the results of the primary study by Pal and colleagues (2018)[158] demonstrate a role for prefrontal cholinergic transmission in the regulation of the level of consciousness, our subsequent analyses in Chapter 2 indicate that this is achieved independent of the regulation of frontoparietal connectivity. While our results warrant reconsideration of theories that propose large-scale corticocortical connectivity between frontal and parietal cortices to be a correlate of consciousness, they cannot refute a relationship between frontoparietal connectivity and the contents of consciousness. For example, while frontoparietal connectivity may be dissociable from the level of arousal, it is possible that animals exhibiting wakefulness following prefrontal cholinergic stimulation nonetheless experienced depreciated conscious contents. While this question cannot be addressed by the model utilized in our Chapter 2 study, future experiments in human or animal models could employ electrophysiological recordings and passive perceptual tasks involving pupillometry[247–249] or sensory-evoked plasticity[250–253] in the presence of progressively titrated concentrations of anesthetic to determine if conscious contents can be registered independent of frontoparietal connectivity.

In a separate cohort of rats, we employed high-density intracranial EEG and assessed spatiotemporal Lempel-Ziv complexity, a computational measure of signal diversity that is posited to reflect brain state repertoire.[69,73,75,76,83] An opposite dissociation between complexity and behavior was discovered following cholinergic or noradrenergic stimulation of the prefrontal and parietal cortices in sevoflurane-anesthetized rats, such that all stimulation conditions exhibited increases in complexity relative to the pre-stimulation anesthetized state, even in the absence of behavioral responsiveness. Rather, changes in complexity were found to correlate

with the presence of 1) broad spectral features of the signal such as EEG activation or slow oscillation power, and 2) periods of elevated levels of acetylcholine in the cortex.[158,159] Our finding of a dissociation between EEG complexity and behavior is not entirely surprising, given that past investigations of neurophysiologic complexity have demonstrated preserved brain state repertoire mirroring wakefulness during REM sleep and ketamine anesthesia,[69,73,76,88] states in which high cortical acetylcholine levels,[98,120,140] an activated cortex,[99,120,231,254] and the presence of conscious contents are decoupled from arousal. Our findings demonstrate a clear dissociation between neurophysiologic complexity and the level of consciousness as assessed by behavior, suggesting that changes in Lempel-Ziv complexity may instead index spectral aspects of cortical dynamics or the presence of arousal promoting neuromodulators, such as acetylcholine, in the cortex. While complexity was elevated even in stimulation groups that did not exhibit wakefulness, we cannot refute the possibility that conscious contents could have been present in these cortical stimulation groups, which each displayed an activated EEG. Indeed, studies administering psychedelic drugs in humans have demonstrated a relationship between changes in complexity and alterations to conscious contents,[80,83] and future studies utilizing dissociative psychedelics that decouple conscious contents from behavioral responsiveness – such as ketamine or salvinorin A – would make ideal pharmacological models to further examine the interaction between disconnected behavioral responsiveness, neural complexity, and conscious contents.

In summary, our Chapter 2 findings demonstrate that commonly employed computational measures of consciousness such as complexity or corticocortical connectivity are dissociable from the level of consciousness as assessed by behavior. Our finding of concomitant increases in cortical complexity and cortical acetylcholine levels across cholinergic or noradrenergic cortical stimulation groups[158] warrants further study of acetylcholine as a neurochemical correlate of complexity, the focus of our studies with ketamine and nitrous oxide in Chapter 4.

5.2 Measures of Complexity: State-Dependent, Frequency-Dependent, and Pharmacology-Dependent?

There has been an ongoing debate as to whether ketamine reduces neurophysiologic complexity at doses sufficient for surgical anesthesia. While previous studies of GABAergic anesthetics have revealed a reduction in brain state repertoire,[73,75,91,159,175] studies administering

ketamine have demonstrated both preserved and attenuated neural complexity at doses titrated to loss of responsiveness.[69,79,97] Studies showing a preservation of neurophysiologic complexity have attributed this phenotype to the reports of dream-like conscious contents following emergence.[69,97] Of critical importance, however, is that human studies investigating neurophysiologic complexity during ketamine anesthesia have used scalp EEG lowpass filtered at 55 Hz or lower. Prior studies have identified that Lempel-Ziv complexity outcomes correlate with broad spectral properties of the signal,[95,255] such as the presence of an activated EEG[158,159] or prominent slow-oscillatory signal components.[95,159,255] Ketamine anesthesia is known to promote periodic activations of the EEG signal with a preservation of wake-like 40 Hz gamma power,[231,256] a spectral property which has been posited to interfere with the detection of loss of consciousness using the Lempel-Ziv algorithm.[97] Studies have shown attenuated frontoparietal connectivity and a reduction in power in high gamma frequencies during ketamine anesthesia,[98,257] suggesting that the inclusion of higher gamma frequencies in analyses may be critical in assessing the level of consciousness during ketamine anesthesia. However, the frequency-dependent properties of Lempel-Ziv complexity are poorly characterized in vivo, and prior studies investigating complexity during ketamine anesthesia have left dynamics at higher gamma frequencies >55 Hz unexplored.

Therefore, in Chapter 3, we utilized intracranial EEG data from prior studies in our laboratory[98,120] to characterize Lempel-Ziv complexity at broadband (0.5-175 Hz), high gamma (65-175 Hz), and 0.5-55 Hz bandwidths, during, and after ketamine or propofol anesthesia in rats. Our results demonstrated that both ketamine and propofol anesthesia reduce broadband (0.5-175 Hz) EEG complexity. However, when isolating our analyses to frequencies of 65-175 Hz, we found that a reduction of complexity in the high gamma bandwidth was unique to ketamine anesthesia, suggesting that a reduction of neurophysiologic complexity in the high gamma bandwidth is a phenotype specific to dissociative anesthesia. To compare our data with results published in prior human studies,[69,75,79,97] we also performed an analysis of Lempel-Ziv complexity on signals lowpass filtered at 55 Hz. In line with our expectations, our results replicated prior human data utilizing scalp EEG,[69,75] demonstrating that propofol – but not ketamine anesthesia – reduced EEG complexity in the 0.5-55 Hz bandwidth. Following emergence from anesthesia, both ketamine and propofol promoted increases in time-shuffled (i.e. unnormalized) Lempel-Ziv complexity relative to wake in broadband and 0.5-55 Hz bandwidths,

characteristic of dynamics observed in brain states that are accompanied by hallucinations such as the psychedelic state[80,83] or in schizophrenia.[258,259]

To determine if changes in Lempel-Ziv complexity were dissociable from the spectral contents of the signal, we employed a phase-shuffling normalization technique previously described in studies from our laboratory[79,159] and others[75,80,83] across data from all three bandwidths. Normalization revealed that reductions observed in complexity during ketamine and propofol anesthesia occurred independent of the spectral contents of the signal, while increases in signal complexity observed following emergence from ketamine and propofol were largely frequency-dependent. Interestingly, prior studies examining neurophysiologic complexity during subanesthetic levels of ketamine have revealed increases in complexity relative to normal wakefulness that extend past the spectral contents of the signal following normalization.[79,83] While our rodent model cannot speak to the presence of delirium or dissociation, future studies in humans could examine neurophysiologic complexity during emergence from ketamine anesthesia to determine if 1) enhancements in raw Lempel-Ziv complexity are a correlate of emergence delirium and 2) if the frequency-dependency revealed by normalization reflects the lack of equivalence between the psychedelic state induced by subanesthetic administration of ketamine and delirium experienced upon emergence from ketamine anesthesia. The separation of spectral dynamics from Lempel-Ziv complexity through normalization was first implemented in work of Schartner and colleagues (2015),[75] and use of this normalized Lempel-Ziv complexity measure thereafter is relatively sparse,[76,79,80,83,159] thus it is unknown what distinct spectral and phasic components of complexity reflect and how changes in these distinct dynamics contribute to consciousness. While ketamine and propofol were administered at fixed dosing regimens in our Chapter 3 studies, future studies might characterize a dose-response curve of traditional and normalized metrics of Lempel-Ziv complexity across titrated doses of GABAergic anesthetics and glutamatergic dissociative anesthetics. These experiments would better describe how phase-specific or frequency-specific complexity dynamics evolve across differing depths of anesthesia, and how such changes might differ between pharmacologically disparate classes of anesthetics.

While the traditional Lempel-Ziv complexity algorithm used in our study demonstrates frequency-dependency,[95] there are recently developed measures, such as multi-scale Lempel-Ziv complexity,[96] that have shown improved accuracy and discriminative capability. The frequency-dependency of the traditional Lempel-Ziv complexity algorithm arises from the fact that it

focuses on a sliding window binarization approach at a single timescale, often failing to detect high-frequency components embedded within low frequency oscillations.[96,255] Multi-scale measures, by contrast, create multiple binarizations based on a range of timescales, allowing for the assessment of complexity across a broad spectrum of frequencies.[96] Multi-scale Lempel-Ziv complexity approaches have demonstrated superior sensitivity and discriminative capacity when compared with the broad contrastive qualities of the traditional algorithm, differentiating between eyes open and eyes closed conditions in healthy subjects[96], classifying aberrant brain dynamics in psychiatric patient populations,[255,259] and finding signs of wake-like complexity in children with Angelman syndrome,[260] a neurodevelopmental disorder characterized by prominent 1-4 Hz EEG power across the cortex despite the presence of wakefulness and volitional behavior.[261] Future studies might compare traditional and multi-scale implementations of Lempel-Ziv complexity through models in which neurophysiologic activity, conscious contents, and behavioral responsiveness become disconnected, such as dissociative psychedelic states, dissociative anesthesia, REM sleep dreaming, lucid dreaming, or minimally conscious states.[52,100,144,262] Validation of multi-scale approaches to measuring complexity through this approach could mark a significant advancement in the development of complexity-based approaches to measuring the level of consciousness, providing a tool with improved signal resolution and finer discriminative capability when compared with the application of the traditional Lempel-Ziv complexity algorithm to spontaneous neural data.

In summary, in Chapter 3 studies we built upon our Chapter 2 finding of a correlation between measures of neurophysiologic complexity and spectral characteristics of the EEG, characterizing distinct state-dependent and bandwidth-specific effects of ketamine and propofol on Lempel-Ziv complexity. We find that inclusion of higher gamma frequencies in the broadband signal or normalization for the spectral contents of the signal are necessary to detect a reduction in neurophysiologic complexity during ketamine anesthesia, a trait not shared with the traditional GABAergic anesthetic propofol. Our results warrant caution in the application of Lempel-Ziv complexity in measuring the level of consciousness, prompting consideration of the unique frequency-dependent effects that pharmacologically disparate anesthetics have on the EEG and how these distinct spectral profiles affect resultant complexity values.

5.3 Cortical Acetylcholine Is a Neurochemical Correlate of Cortical Dynamics Relating to Consciousness

Our Chapter 2[159] findings revealed a dissociation between neurophysiologic complexity, corticocortical connectivity, and the level of consciousness. However, we observed that elevations in neurophysiologic complexity following cholinergic or noradrenergic stimulation of the prefrontal and parietal cortices during sevoflurane anesthesia coincided with periods of heightened cortical acetylcholine in the original study conducted by Pal and colleagues (2018).[158] As discussed in our Chapter 1 introduction, neurochemical research has further supported the plausibility of a relationship between cortical cholinergic tone and neurophysiologic complexity, demonstrating that cortical acetylcholine levels track with the capacity for consciousness.[120,140,142,146,150,207] Thus, in Chapter 4 we posited that cortical dynamics thought to reflect the level of consciousness – such as neurophysiologic complexity – might reflect levels of extracellular acetylcholine in the cortex. To test this hypothesis, we developed a novel approach that allowed us to record high-density intracranial EEG (0.5-175 Hz) while measuring concomitant changes in cortical acetylcholine levels in prefrontal and parietal cortices. We then leveraged the unique properties of the dissociative NMDA-antagonists ketamine and nitrous oxide, which afforded us the ability to characterize cortical acetylcholine levels, neurophysiologic complexity, and frontoparietal connectivity in gamma bandwidths during periods of drug exposure that resembled both psychedelic and sedative states.

Our Chapter 4 data demonstrated that changes in temporospatial EEG complexity during a continuous intravenous subanesthetic infusion of ketamine or sustained 50% nitrous oxide exposure mirrored concomitant changes in cortical acetylcholine levels in frontal and parietal cortices. While ketamine and nitrous oxide share a pharmacological mechanism of NMDA-antagonism, they displayed differential state-dependent temporal and spatial patterns of changes in complexity. Subanesthetic ketamine induced a sustained increase in cortical acetylcholine levels and temporospatial EEG complexity that lasted during the entire 62.5 min infusion. When isolating changes in temporal complexity to individual channels across the EEG montage, it was revealed that ketamine induced the most significant changes in complexity in frontal, posterior parietal, and occipital regions. In contrast, 50% nitrous oxide exposure produced only a transient increase in cortical complexity and acetylcholine levels, lasting the first 12.5 minutes of exposure. During this induction period, frontotemporal and parietal regions showed the greatest magnitude of increase in temporal complexity, revealing a unique dynamic landscape of changes during nitrous oxide dissociation when compared to ketamine. During the remaining 50 minutes

of nitrous oxide exposure, rats displayed sporadic periods of quiescent behavior, a reduction in cortical acetylcholine levels, and a decrease in temporospatial EEG complexity found to span the entirety of the EEG montage. Of note, our use of high-density EEG in our Chapter 4 studies allowed us to be the first to characterize large-scale temporospatial complexity during subanesthetic ketamine or nitrous oxide in the rat. Interestingly, the topographic distribution of changes in EEG complexity observed during drug exposure in our study mirrored recent magnetoencephalographic and EEG data published during ketamine and nitrous oxide administration in humans,[83,235] suggesting a comparable dynamic landscape during dissociative states in rodents. While requiring replication and extension to classical serotonergic psychedelics, these results offer preliminary support for the utility of rat models in studying the neural correlates of dynamics which characterize the psychedelic state in humans, such as elevated brain state repertoire.[79,80,83]

Our Chapter 4 experiments also characterized changes in directed frontoparietal connectivity in low (25-55 Hz), mid (85-125 Hz), and high (125-175 Hz) gamma bandwidths before, during, and after ketamine or nitrous oxide exposure. Ketamine and nitrous oxide were again found to exert differential state-dependent – as well as bandwidth-specific – effects on directed frontoparietal connectivity. Periods of high cortical cholinergic tone and complexity during ketamine infusion or nitrous oxide induction coincided with a bidirectional increase in the strength of connectivity in high gamma frequencies from 125-175 Hz. In contrast, frontoparietal connectivity in low gamma bands showed an inverse correlation with cortical complexity and acetylcholine during ketamine and nitrous exposure, being suppressed when cholinergic tone in the cortex was high, and elevated when it was low. Mid gamma connectivity showed no clear relation to complexity or cortical acetylcholine levels during ketamine or nitrous oxide exposure. While dissociative anesthetics share common neurophysiologic mechanisms rooted in NMDA-antagonism such as the promotion of high frequency (>30 Hz) oscillations,[263] research supports the presence of unique spectral profiles induced in the electroencephalogram by ketamine, nitrous oxide, and xenon.[99,264–266] The differential state-dependent and bandwidth-specific effects of ketamine and nitrous oxide on directed frontoparietal connectivity suggest at least partially dissociable pharmacological drivers of large-scale corticocortical connectivity in gamma bandwidths, a topic worthy of future investigation.

Our data relating heightened cortical cholinergic tone, neurophysiologic complexity, and frontoparietal connectivity in the high gamma bandwidth draw parallels to human studies demonstrating "hyperfrontality" following the administration of classical serotonergic and dissociative drugs, wherein excessive glutamatergic (or in the case of our Chapter 4 studies, cholinergic) neurotransmission within the frontal cortex accompanies alterations to cortical dynamics and subjectively reported contents of consciousness.[236,237,239,267] Given that a comparable neurochemical and neurodynamic phenotype was observed in rats, future studies might employ localized inactivation or pharmacological challenge paradigms in the prefrontal cortex during psychedelic drug exposure, to determine 1) the necessity and sufficiency of the prefrontal cortex in promoting elevated complexity or connectivity in the brain and 2) if a causal relationship exists between acetylcholine release in the prefrontal cortex and cortical dynamics such as complexity thought to relate to consciousness.[79,80,83] However, the relationship between cortical cholinergic neurotransmission and neurophysiologic complexity is undoubtedly reflected by molecular mechanisms more specific than release, and thus future studies should test the role of specific cholinergic receptor subtypes and their relationship to changes in neurophysiologic complexity during anesthetic or psychedelic drug administration. Previous studies have implicated post-synaptic M1 receptors in the prefrontal cortex in the activation of the EEG,[244,268] while the systemic administration of muscarinic antagonists is known to cause a state of neurophysiologic and behavioral dissociation wherein prominent low frequency and high amplitude oscillations predominate the EEG despite the presence of wakeful behavior.[202,269] While nicotinic acetylcholine receptors have been implicated in the modulation of sleep-wake states[270,271] and neuronal synchronization,[272] evidence for a more direct role in the facilitation of cortical activation is less clear. Thus, cholinergic action at cortical muscarinic receptors is a possible molecular mechanism by which acetylcholine release could modulate neurophysiologic complexity in the cortex, prompting future study.

While our Chapter 4 data suggest an association between cortical acetylcholine levels and cortical dynamics related to consciousness, there are further limitations to our study that warrant consideration in the interpretation of our results. Our data are only correlative in nature and cannot rule out the possibility that changes in cortical acetylcholine are merely an epiphenomena of dissociative drug administration, as opposed to being a causal driver of neurophysiologic complexity. Causal data could come from circuit interrogation techniques such as optogenetics,

chemogenetics, or selective lesioning techniques, which could be employed to causally perturb cholinergic cell activity during altered states of consciousness such as the psychedelic or anesthetized state. While pedunculopontine and lateral dorsal tegmental cholinergic nuclei project to the cortex, tracing studies suggest the basal forebrain serves as the primary source of acetylcholine to the cortex.[134,136,232] Anatomical evidence has demonstrated a broad range of neuromodulatory influence for the basal forebrain. It is comprised of a constellation of regions including the ventral pallidum, vertical and horizontal diagonal band nuclei, medial septum, peripallidal regions, and substantia inominata.[273] In addition to its cortical targets, the basal forebrain shares projections with many major brainstem and hypothalamic arousal systems, including the dopaminergic ventral tegmental area, noradrenergic locus coeruleus, glutamatergic reticular neurons, serotonergic raphe nuclei, histaminergic tuberomammillary neurons, and orexinergic perifornical neurons.[134,136,274] Studies investigating the cytoarchitecture of the basal forebrain have also revealed GABAergic, glutamatergic, and peptidergic interneurons, which interact locally to modulate cholinergic neurotransmission and cortical cell firing, prompting a richer investigation of heterogenous basal forebrain interactions and their relationship to cortical cholinergic tone and dynamics.[232,273,275,276]

Evidence from neurophysiological, neuroimaging, and circuit interrogation studies have extensively supported a role for the basal forebrain cholinergic system in orchestrating cortical state dynamics. Optogenetic and chemogenetic studies in rodents have demonstrated that stimulation of basal forebrain cholinergic neurons fragments the sleep-wake cycle[277], increases the amount of time that animals spend in spontaneous wakefulness,[278] and decreases slow oscillation power during non-REM sleep.[279] Neurophysiologic investigations in freely behaving rodents have shown that the basal forebrain regulates gamma-band connectivity and oscillation power within large-scale resting state networks such as the default mode network.[280] An fMRI study in non-human primates further supported this finding, demonstrating that inactivation of the nucleus basalis decreased ipsilateral fluctuations in the global BOLD in areas known to be cortical cholinergic projection targets of the basal forebrain.[281]

While basal forebrain cholinergic neurons have been implicated in the regulation of cortical dynamics and wakefulness, recent work has demonstrated that non-cholinergic cell groups within the basal forebrain – such as GABAergic neurons – also possess a direct role in controlling cortical cholinergic dynamics and the level of consciousness.[277,282] In addition to an

established role in controlling sleep-wake states, basal forebrain GABAergic cell activity has been causally linked to the regulation of cortical gamma oscillations, which is hypothesized to occur through afferent projections from the basal forebrain that synchronize parvalbumin-containing GABAergic interneurons within the cortex.[283] Intriguingly, previous studies have demonstrated that subanesthetic ketamine administration promotes cortical gamma oscillations and alterations in visual-evoked responses through the antagonism of NMDA receptors on parvalbumin-containing interneurons.[284,285] Furthermore, transcriptional evidence suggests parvalbumin-containing interneurons are also a target of classical psychedelics, making these neurons a possible mechanism by which complexity or connectivity could be altered during altered states of consciousness.[286] Circuit-manipulation experiments targeting GABAergic basal forebrain cells during during anesthetic or psychedelic states are warranted, and could yield rich insights about the role of the basal forebrain in supporting cortical complexity, gamma band dynamics, and the level of consciousness.

Collectively, these studies suggest broad neuromodulatory influence for the basal forebrain cholinergic system, making it a plausible neurochemical mediator of the relationship between changes in cortical cholinergic tone and neurophysiologic complexity observed in our Chapter 2 and Chapter 4 findings. Forthcoming studies aimed at revealing a causal relationship between cholinergic nuclei, cortical cholinergic neurotransmission, and cortical dynamics will ultimately yield a richer understanding of the neurochemical correlates of dynamics purported to relate to consciousness.

5.4 Summary

This work expands our understanding of the neurochemical processes underlying changes in computational measures of complexity and directed frontoparietal connectivity. Taken together, our studies demonstrate that neurophysiologic complexity and corticocortical connectivity are dissociable from the level of consciousness as assessed by behavior, and that neurophysiologic complexity instead appears to correlate with extracellular levels of acetylcholine in the cortex. While a causal relationship remains to be demonstrated, this work offers preliminary evidence that cortical cholinergic neurotransmission may underlie the emergence of cortical dynamics thought to support the capacity for consciousness, such as cortical complexity or frontoparietal connectivity in high gamma bandwidth.

Bibliography

1. Walling, P. T. Consciousness: a brief review of the riddle. *Proc. Bayl. Univ. Med. Cent.* **13**, 376–378 (2000).
2. Van Gulick, R. Consciousness. in *The Stanford Encyclopedia of Philosophy* (ed. Zalta, E. N.) (Metaphysics Research Lab, Stanford University, 2018).
3. Mashour, G. A. Integrating the Science of Consciousness and Anesthesia: *Anesth. Analg.* **103**, 975–982 (2006).
4. LeDoux, J. E., Michel, M. & Lau, H. A little history goes a long way toward understanding why we study consciousness the way we do today. *Proc. Natl. Acad. Sci.* **117**, 6976–6984 (2020).
5. MORTON, W. T. G. THE FIRST USE OF ETHER AS ANESTHETIC.AT THE BATTLE OF THE WILDERNESS IN THE CIVIL WAR. *J. Am. Med. Assoc.* **XLII**, 1068–1073 (1904).
6. Ash, H. L. Anesthesia's dental heritage (William Thomas Green Morton). *Anesth. Prog.* **32**, 25–29 (1985).
7. Robinson, D. H. & Toledo, A. H. Historical Development of Modern Anesthesia. *J. Invest. Surg.* **25**, 141–149 (2012).
8. Haridas, R. P. Horace Wells' Demonstration of Nitrous Oxide in Boston. *Anesthesiology* **119**, 1014–1022 (2013).
9. CRAWFORD W. LONG (1815-1878) DISCOVERER OF ETHER FOR ANESTHESIA. *JAMA* **194**, 1008–1009 (1965).
10. Anaya-Prado, R. & Schadegg-Peña, D. Crawford Williamson Long: The True Pioneer of Surgical Anesthesia. *J. Invest. Surg.* **28**, 181–187 (2015).
11. Beecher, H. K. Anesthesia's Second Power: Probing the Mind. *Science* **105**, 164–166 (1947).
12. Ferrier, D. *The Functions of the Brain*. (Smith, Elder and Co., London, UK, 1876).
13. PENFIELD, W. & BOLDREY, E. SOMATIC MOTOR AND SENSORY REPRESENTATION IN THE CEREBRAL CORTEX OF MAN AS STUDIED BY ELECTRICAL STIMULATION1. *Brain* **60**, 389–443 (1937).
14. Rasmussen, T. & Penfield, W. Further studies of the sensory and motor cerebral cortex of man. *Fed. Proc.* **6**, 452–460 (1947).
15. Berger, H. Über das Elektrenkephalogramm des Menschen. *DMW - Dtsch. Med. Wochenschr.* **60**, 1947–1949 (1934).
16. Gloor, P. Hans Berger on Electroencephalography. *Am. J. EEG Technol.* **9**, 1–8 (1969).
17. İnce, R., Adanır, S. S. & Sevmez, F. The inventor of electroencephalography (EEG): Hans Berger (1873–1941). *Childs Nerv. Syst.* (2020) doi:10.1007/s00381-020-04564-z.
18. Loomis, A. L., Harvey, E. N. & Hobart, G. POTENTIAL RHYTHMS OF THE CEREBRAL CORTEX DURING SLEEP. *Science* **81**, 597 (1935).

19. Loomis, A. L., Harvey, E. N. & Hobart, G. A. Cerebral states during sleep, as studied by human brain potentials. *J. Exp. Psychol.* **21**, 127–144 (1937).
20. Moruzzi, G. & Magoun, H. W. Brain stem reticular formation and activation of the EEG. *Electroencephalogr. Clin. Neurophysiol.* **1**, 455–473 (1949).
21. Lindsley, D. B., Bowden, J. W. & Magoun, H. W. Effect upon the EEG of acute injury to the brain stem activating system. *Electroencephalogr. Clin. Neurophysiol.* **1**, 475–486 (1949).
22. LOEWI, O. CHEMICAL TRANSMISSION OF NERVE IMPULSES. *Am. Sci.* **33**, 159–174 (1945).
23. Fishman, M. C. Sir Henry Hallett Dale and acetylcholine story. *Yale J. Biol. Med.* **45**, 104–118 (1972).
24. Haas, L. F. Otto Loewi (1873–1961). *J. Neurol. Neurosurg. Psychiatry* **74**, 843–843 (2003).
25. Todman, D. Otto Loewi (1873–1961). *J. Neurol.* **256**, 291–292 (2009).
26. Hyman, S. E. Neurotransmitters. *Curr. Biol.* **15**, R154–R158 (2005).
27. López-Muñoz, F. & Alamo, C. Historical evolution of the neurotransmission concept. *J. Neural Transm. Vienna Austria 1996* **116**, 515–533 (2009).
28. Lashley, K. S. The behavioristic interpretation of consciousness ii. *Psychol. Rev.* **30**, 329–353 (1923).
29. Lashley, K. S. Basic neural mechanisms in behavior. *Psychol. Rev.* **37**, 1–24 (1930).
30. Pribram, K. H., Mishkin, M., Rosvold, H. E. & Kaplan, S. J. Effects on delayed-response performance of lesions of dorsolateral and ventromedial frontal cortex of baboons. *J. Comp. Physiol. Psychol.* **45**, 565–575 (1952).
31. Mishkin, M. & Pribram, K. H. Analysis of the effects of frontal lesions in monkeys: I. Variations of delayed alternations. *J. Comp. Physiol. Psychol.* **48**, 492–495 (1955).
32. Sperry, R. W. A modified concept of consciousness. *Psychol. Rev.* **76**, 532–536 (1969).
33. Eccles, J. C. The Brain and the Unity of Conscious Experience. in *Facing Reality: Philosophical Adventures by a Brain Scientist* (ed. Eccles, J. C.) 63–84 (Springer, 1970). doi:10.1007/978-1-4757-3997-8_5.
34. Penfield, W. *The Mystery of the Mind*. (Princeton University Press, 1975).
35. Pribram, K. H. & Carlton, E. H. Holonomic brain theory in imaging and object perception. *Acta Psychol. (Amst.)* **63**, 175–210 (1986).
36. Michel, M. Consciousness Science Underdetermined: A Short History of Endless Debates. *Open Access J. Philos.* **6**, (2019).
37. Crick, F. & Koch, C. Towards a neurobiological theory of consciousness. *Semin. Neurosci.* **2**, 263–275 (1990).
38. Lucignani, G. & Bastianello, S. Neuroimaging: a story of physicians and basic scientists. *Funct. Neurol.* **21**, 133–136 (2006).
39. Berlucchi, G. Chapter 13 The contributions of neurophysiology to clinical neurology: an exercise in contemporary history. in *Handbook of Clinical Neurology* (eds. Aminoff, M. J., Boller, F. & Swaab, D. F.) vol. 95 169–188 (Elsevier, 2009).
40. Owen, A. M. Detecting Consciousness: A Unique Role for Neuroimaging. *Annu. Rev. Psychol.* **64**, 109–133 (2013).
41. Crick, F. & Koch, C. A framework for consciousness. *Nat. Neurosci.* **6**, 119–126 (2003).
42. Odegaard, B., Knight, R. T. & Lau, H. Should a Few Null Findings Falsify Prefrontal Theories of Conscious Perception? *J. Neurosci.* **37**, 9593–9602 (2017).

43. Boly, M. *et al.* Are the Neural Correlates of Consciousness in the Front or in the Back of the Cerebral Cortex? Clinical and Neuroimaging Evidence. *J. Neurosci.* **37**, 9603–9613 (2017).
44. Raccah, O., Block, N. & Fox, K. C. R. Does the Prefrontal Cortex Play an Essential Role in Consciousness? Insights from Intracranial Electrical Stimulation of the Human Brain. *J. Neurosci.* **41**, 2076–2087 (2021).
45. Northoff, G. & Lamme, V. Neural signs and mechanisms of consciousness: Is there a potential convergence of theories of consciousness in sight? *Neurosci. Biobehav. Rev.* **118**, 568–587 (2020).
46. Icaza, E. E. & Mashour, G. A. Altered States: Psychedelics and Anesthetics. *Anesthesiology* **119**, 1255–1260 (2013).
47. Koch, C., Massimini, M., Boly, M. & Tononi, G. Neural correlates of consciousness: progress and problems. *Nat. Rev. Neurosci.* **17**, 307–321 (2016).
48. Overgaard, M. How can we know if patients in coma, vegetative state or minimally conscious state are conscious? in *Progress in Brain Research* (eds. Laureys, S., Schiff, N. D. & Owen, A. M.) vol. 177 11–19 (Elsevier, 2009).
49. Tobias, J. D. & Leder, M. Procedural sedation: A review of sedative agents, monitoring, and management of complications. *Saudi J. Anaesth.* **5**, 395–410 (2011).
50. Di Perri, C. *et al.* Measuring consciousness in coma and related states. *World J. Radiol.* **6**, 589–597 (2014).
51. Ishizawa, Y. *et al.* Dynamics of Propofol-Induced Loss of Consciousness Across Primate Neocortex. *J. Neurosci.* **36**, 7718–7726 (2016).
52. Bayne, T., Hohwy, J. & Owen, A. M. Are There Levels of Consciousness? *Trends Cogn. Sci.* **20**, 405–413 (2016).
53. Leslie, K. Dreaming during anesthesia. in *Consciousness, Awareness, and Anesthesia* (ed. Mashour, G. A.) 74–89 (Cambridge University Press, 2010). doi:10.1017/CBO9780511676291.005.
54. Neckelmann, D. & Ursin, R. Sleep Stages and EEG Power Spectrum in Relation to Acoustical Stimulus Arousal Threshold in the Rat. *Sleep* **16**, 467–477 (1993).
55. Aserinsky, E. & Kleitman, N. Regularly occurring periods of eye motility, and concomitant phenomena, during sleep. *Science* **118**, 273–274 (1953).
56. Dement, W. & Kleitman, N. The relation of eye movements during sleep to dream activity: an objective method for the study of dreaming. *J. Exp. Psychol.* **53**, 339–346 (1957).
57. Nir, Y. & Tononi, G. Dreaming and the brain: from phenomenology to neurophysiology. *Trends Cogn. Sci.* **14**, 88 (2010).
58. Boly, M., Sanders, R. D., Mashour, G. A. & Laureys, S. Consciousness and responsiveness: lessons from anaesthesia and the vegetative state. *Curr. Opin. Anesthesiol.* **26**, 444–449 (2013).
59. Markand, O. N. Electroencephalogram in “locked-in” syndrome. *Electroencephalogr. Clin. Neurophysiol.* **40**, 529–534 (1976).
60. Kübler, A. The history of BCI: From a vision for the future to real support for personhood in people with locked-in syndrome. *Neuroethics* **13**, 163–180 (2020).
61. Owen, A. M. *et al.* Detecting Awareness in the Vegetative State. *Science* **313**, 1402–1402 (2006).
62. Huang, Z. *et al.* Brain imaging reveals covert consciousness during behavioral unresponsiveness induced by propofol. *Sci. Rep.* **8**, 13195 (2018).

63. Tononi, G. An information integration theory of consciousness. *BMC Neurosci.* **5**, 42 (2004).
64. Tononi, G., Boly, M., Massimini, M. & Koch, C. Integrated information theory: from consciousness to its physical substrate. *Nat. Rev. Neurosci.* **17**, 450–461 (2016).
65. Carhart-Harris, R. *et al.* The entropic brain: a theory of conscious states informed by neuroimaging research with psychedelic drugs. *Front. Hum. Neurosci.* **8**, 20 (2014).
66. Carhart-Harris, R. L. The entropic brain - revisited. *Neuropharmacology* **142**, 167–178 (2018).
67. Oizumi, M., Albantakis, L. & Tononi, G. From the Phenomenology to the Mechanisms of Consciousness: Integrated Information Theory 3.0. *PLoS Comput. Biol.* **10**, e1003588 (2014).
68. Carhart-Harris, R. L. & Friston, K. J. REBUS and the Anarchic Brain: Toward a Unified Model of the Brain Action of Psychedelics. *Pharmacol. Rev.* **71**, 316–344 (2019).
69. Sarasso, S. *et al.* Consciousness and Complexity during Unresponsiveness Induced by Propofol, Xenon, and Ketamine. *Curr. Biol.* **25**, 3099–3105 (2015).
70. Zhang, X. S., Roy, R. J. & Jensen, E. W. EEG complexity as a measure of depth of anesthesia for patients. *IEEE Trans. Biomed. Eng.* **48**, 1424–1433 (2001).
71. Ferenets, R. *et al.* Comparison of Entropy and Complexity Measures for the Assessment of Depth of Sedation. *IEEE Trans. Biomed. Eng.* **53**, 1067–1077 (2006).
72. Li, L. & Wang, R. Complexity Analysis of Sleep EEG Signal. in *2010 4th International Conference on Bioinformatics and Biomedical Engineering* 1–3 (IEEE, 2010). doi:10.1109/ICBBE.2010.5515699.
73. Casali, A. G. *et al.* A Theoretically Based Index of Consciousness Independent of Sensory Processing and Behavior. *Sci. Transl. Med.* **5**, 198ra105-198ra105 (2013).
74. Bob, P. *et al.* Preictal Dynamics of EEG Complexity in Intracranially Recorded Epileptic Seizure: A Case Report. *Medicine (Baltimore)* **93**, e151 (2014).
75. Schartner, M. *et al.* Complexity of Multi-Dimensional Spontaneous EEG Decreases during Propofol Induced General Anaesthesia. *PloS One* **10**, e0133532 (2015).
76. Schartner, M. M. *et al.* Global and local complexity of intracranial EEG decreases during NREM sleep. *Neurosci. Conscious.* **2017**, (2017).
77. Eagleman, S. L. *et al.* Do Complexity Measures of Frontal EEG Distinguish Loss of Consciousness in Geriatric Patients Under Anesthesia? *Front. Neurosci.* **12**, (2018).
78. Eagleman, S. L., Chander, D., Reynolds, C., Ouellette, N. T. & MacIver, M. B. Nonlinear dynamics captures brain states at different levels of consciousness in patients anesthetized with propofol. *PloS One* **14**, e0223921 (2019).
79. Li, D. & Mashour, G. A. Cortical dynamics during psychedelic and anesthetized states induced by ketamine. *NeuroImage* **196**, 32–40 (2019).
80. Timmermann, C. *et al.* Neural correlates of the DMT experience assessed with multivariate EEG. *Sci. Rep.* **9**, 1–13 (2019).
81. Huels, E. R. *et al.* Neural Correlates of the Shamanic State of Consciousness. *Front. Hum. Neurosci.* **15**, 140 (2021).
82. Luo, Q. *et al.* Complexity Analysis of Resting State Magnetoencephalography Activity in Traumatic Brain Injury Patients. *J. Neurotrauma* **30**, 1702–1709 (2013).
83. Schartner, M. M., Carhart-Harris, R. L., Barrett, A. B., Seth, A. K. & Muthukumaraswamy, S. D. Increased spontaneous MEG signal diversity for psychoactive doses of ketamine, LSD and psilocybin. *Sci. Rep.* **7**, srep46421 (2017).

84. Moser, J. *et al.* Evaluating Complexity of Fetal MEG Signals: A Comparison of Different Metrics and Their Applicability. *Front. Syst. Neurosci.* **13**, 23 (2019).
85. Hudetz, A. G., Liu, X. & Pillay, S. Dynamic repertoire of intrinsic brain states is reduced in propofol-induced unconsciousness. *Brain Connect.* **5**, 10–22 (2015).
86. Sun, J. *et al.* Complexity Analysis of EEG, MEG, and fMRI in Mild Cognitive Impairment and Alzheimer's Disease: A Review. *Entropy* **22**, 239 (2020).
87. Varley, T. F. *et al.* Consciousness & Brain Functional Complexity in Propofol Anaesthesia. *Sci. Rep.* **10**, 1018 (2020).
88. Abásolo, D., Simons, S., Morgado da Silva, R., Tononi, G. & Vyazovskiy, V. V. Lempel-Ziv complexity of cortical activity during sleep and waking in rats. *J. Neurophysiol.* **113**, 2742–2752 (2015).
89. Dasilva, M. *et al.* Modulation of cortical slow oscillations and complexity across anesthesia levels. *NeuroImage* **224**, 117415 (2021).
90. Lempel, A. & Ziv, J. On the Complexity of Finite Sequences. *IEEE Trans. Inf. Theory* **22**, 75–81 (1976).
91. Hudetz, A. G., Liu, X. & Pillay, S. Dynamic Repertoire of Intrinsic Brain States Is Reduced in Propofol-Induced Unconsciousness. *Brain Connect.* **5**, 10–22 (2015).
92. Eagleman, S. L. *et al.* Do Complexity Measures of Frontal EEG Distinguish Loss of Consciousness in Geriatric Patients Under Anesthesia? *Front. Neurosci.* **12**, 645 (2018).
93. Bodart, O. *et al.* Measures of metabolism and complexity in the brain of patients with disorders of consciousness. *NeuroImage Clin.* **14**, 354–362 (2017).
94. Lin, M. A., Chan, H. L. & Fang, S. C. Linear and Nonlinear EEG Indexes in Relation to the Severity of Coma. in *2005 IEEE Engineering in Medicine and Biology 27th Annual Conference* 4580–4583 (IEEE, 2005). doi:10.1109/IEMBS.2005.1615489.
95. Aboy, M., Hornero, R., Abasolo, D. & Alvarez, D. Interpretation of the Lempel-Ziv Complexity Measure in the Context of Biomedical Signal Analysis. *IEEE Trans. Biomed. Eng.* **53**, 2282–2288 (2006).
96. Ibáñez-Molina, A. J., Iglesias-Parro, S., Soriano, M. F. & Aznarte, J. I. Multiscale Lempel–Ziv complexity for EEG measures. *Clin. Neurophysiol.* **126**, 541–548 (2015).
97. Wang, J. *et al.* Suppressed neural complexity during ketamine- and propofol-induced unconsciousness. *Neurosci. Lett.* **653**, 320–325 (2017).
98. Pal, D., Hambrecht-Wiedbusch, V. S., Silverstein, B. H. & Mashour, G. A. Electroencephalographic coherence and cortical acetylcholine during ketamine-induced unconsciousness. *Br. J. Anaesth.* **114**, 979–989 (2015).
99. Vlisides, P. E. *et al.* Neurophysiologic Correlates of Ketamine Sedation and Anesthesia: A High-density Electroencephalography Study in Healthy Volunteers. *Anesthesiology* **127**, 58–69 (2017).
100. Bayne, T., Seth, A. K. & Massimini, M. Are There Islands of Awareness? *Trends Neurosci.* **43**, 6–16 (2020).
101. Baars, B. J., Franklin, S. & Ramsoy, T. Z. Global workspace dynamics: cortical 'binding and propagation' enables conscious contents. *Front. Psychol.* **4**, 200 (2013).
102. Mashour, G. A., Roelfsema, P., Changeux, J.-P. & Dehaene, S. Conscious Processing and the Global Neuronal Workspace Hypothesis. *Neuron* **105**, 776–798 (2020).
103. Friston, K. J. *et al.* Granger causality revisited. *NeuroImage* **101**, 796–808 (2014).
104. Arsiwalla, X. D. & Verschure, P. Measuring the Complexity of Consciousness. *Front. Neurosci.* **12**, (2018).

105. Stefan, S. *et al.* Consciousness Indexing and Outcome Prediction with Resting-State EEG in Severe Disorders of Consciousness. *Brain Topogr.* **31**, 848–862 (2018).
106. Barnett, L., Barrett, A. B. & Seth, A. K. Granger Causality and Transfer Entropy Are Equivalent for Gaussian Variables. *Phys. Rev. Lett.* **103**, 238701 (2009).
107. Barrett, A. B. *et al.* Granger Causality Analysis of Steady-State Electroencephalographic Signals during Propofol-Induced Anaesthesia. *PLOS ONE* **7**, e29072 (2012).
108. McAuliffe, J. 14. The new math of EEG: Symbolic transfer entropy, the effects of dimension. *Clin. Neurophysiol.* **125**, e17 (2014).
109. Lindner, B., Auret, L., Bauer, M. & Groenewald, J. W. D. Comparative analysis of Granger causality and transfer entropy to present a decision flow for the application of oscillation diagnosis. *J. Process Control* **79**, 72–84 (2019).
110. Hudetz, A. G. & Mashour, G. A. Disconnecting Consciousness: Is There a Common Anesthetic End Point? *Anesth. Analg.* **123**, 1228–1240 (2016).
111. Boveroux, P. *et al.* Breakdown of within- and between-network Resting State Functional Magnetic Resonance Imaging Connectivity during Propofol-induced Loss of Consciousness: *Anesthesiology* **113**, 1038–1053 (2010).
112. Ku, S.-W., Lee, U., Noh, G.-J., Jun, I.-G. & Mashour, G. A. Preferential Inhibition of Frontal-to-Parietal Feedback Connectivity Is a Neurophysiologic Correlate of General Anesthesia in Surgical Patients. *PLoS ONE* **6**, e25155 (2011).
113. Lee, U. *et al.* Disruption of frontal-parietal communication by ketamine, propofol, and sevoflurane. *Anesthesiology* **118**, 1264–1275 (2013).
114. Moon, J.-Y., Lee, U., Blain-Moraes, S. & Mashour, G. A. General Relationship of Global Topology, Local Dynamics, and Directionality in Large-Scale Brain Networks. *PLOS Comput. Biol.* **11**, e1004225 (2015).
115. Bonhomme, V. *et al.* Resting-state Network-specific Breakdown of Functional Connectivity during Ketamine Alteration of Consciousness in Volunteers. *Anesthesiology* **125**, 873–888 (2016).
116. Barttfeld, P. *et al.* Signature of consciousness in the dynamics of resting-state brain activity. *Proc. Natl. Acad. Sci.* **112**, 887–892 (2015).
117. Uhrig, L. *et al.* Resting-state Dynamics as a Cortical Signature of Anesthesia in Monkeys. *Anesthesiology* **129**, 942–958 (2018).
118. Papadopoulou, M., Friston, K. & Marinazzo, D. Estimating Directed Connectivity from Cortical Recordings and Reconstructed Sources. *Brain Topogr.* **32**, 741–752 (2019).
119. Imas, O. A., Ropella, K. M., Ward, B. D., Wood, J. D. & Hudetz, A. G. Volatile anesthetics disrupt frontal-posterior recurrent information transfer at gamma frequencies in rat. *Neurosci. Lett.* **387**, 145–150 (2005).
120. Pal, D., Silverstein, B. H., Lee, H. & Mashour, G. A. Neural Correlates of Wakefulness, Sleep, and General Anesthesia: An Experimental Study in Rat. *Anesthesiology* **125**, 929–942 (2016).
121. Cohen, D., van Swinderen, B. & Tsuchiya, N. Isoflurane Impairs Low-Frequency Feedback but Leaves High-Frequency Feedforward Connectivity Intact in the Fly Brain. *eNeuro* **5**, ENEURO.0329-17.2018 (2018).
122. Haberkern, H. & Jayaraman, V. Studying small brains to understand the building blocks of cognition. *Curr. Opin. Neurobiol.* **37**, 59–65 (2016).
123. Kohl, J. & Jefferis, G. S. X. E. Neuroanatomy: decoding the fly brain. *Curr. Biol. CB* **21**, R19-20 (2011).

124. Laureys, S. *et al.* Impaired effective cortical connectivity in vegetative state: preliminary investigation using PET. *NeuroImage* **9**, 377–382 (1999).
125. Noirhomme, Q. *et al.* Brain Connectivity in Pathological and Pharmacological Coma. *Front. Syst. Neurosci.* **4**, 160 (2010).
126. Peran, P. *et al.* Functional and Structural Integrity of Frontoparietal Connectivity in Traumatic and Anoxic Coma. *Crit. Care Med.* **48**, e639–e647 (2020).
127. Sitt, J. D. *et al.* Large scale screening of neural signatures of consciousness in patients in a vegetative or minimally conscious state. *Brain* **137**, 2258–2270 (2014).
128. Demertzi, A. *et al.* Intrinsic functional connectivity differentiates minimally conscious from unresponsive patients. *Brain* **138**, 2619–2631 (2015).
129. Horovitz, S. G. *et al.* Decoupling of the brain's default mode network during deep sleep. *Proc. Natl. Acad. Sci. U. S. A.* **106**, 11376–11381 (2009).
130. Spoormaker, V., Gleiser, P. & Czisch, M. Frontoparietal Connectivity and Hierarchical Structure of the Brain's Functional Network during Sleep. *Front. Neurol.* **3**, 80 (2012).
131. Voss, U., Holzmann, R., Tuin, I. & Hobson, J. A. Lucid Dreaming: A State of Consciousness with Features of Both Waking and Non-Lucid Dreaming. *Sleep* **32**, 1191–1200 (2009).
132. Baird, B., Castelnovo, A., Gosseries, O. & Tononi, G. Frequent lucid dreaming associated with increased functional connectivity between frontopolar cortex and temporoparietal association areas. *Sci. Rep.* **8**, 17798 (2018).
133. Ljubojevic, V. *et al.* Cholinergic Modulation of Frontoparietal Cortical Network Dynamics Supporting Supramodal Attention. *J. Neurosci. Off. J. Soc. Neurosci.* **38**, 3988–4005 (2018).
134. Jones, B. E. Activity, modulation and role of basal forebrain cholinergic neurons innervating the cerebral cortex. in *Progress in Brain Research* vol. 145 157–169 (Elsevier, 2004).
135. Martinez-Gonzalez, C., Bolam, J. P. & Mena-Segovia, J. Topographical Organization of the Pedunculopontine Nucleus. *Front. Neuroanat.* **5**, 22 (2011).
136. Jones, B. E. Arousal systems. *Front. Biosci. J. Virtual Libr.* **8**, s438-451 (2003).
137. Celesia, G. G. & Jasper, H. H. Acetylcholine released from cerebral cortex in relation to state of activation. *Neurology* **16**, 1053–1063 (1966).
138. Szerb, J. C. Cortical acetylcholine release and electroencephalographic arousal. *J. Physiol.* **192**, 329–343 (1967).
139. Jasper, H. H. & Tessier, J. Acetylcholine Liberation from Cerebral Cortex during Paradoxical (REM) Sleep. *Science* **172**, 601–602 (1971).
140. Marrosu, F. *et al.* Microdialysis measurement of cortical and hippocampal acetylcholine release during sleep-wake cycle in freely moving cats. *Brain Res.* **671**, 329–332 (1995).
141. Nelson, C. L., Burk, J. A., Bruno, J. P. & Sarter, M. Effects of acute and repeated systemic administration of ketamine on prefrontal acetylcholine release and sustained attention performance in rats. *Psychopharmacology (Berl.)* **161**, 168–179 (2002).
142. Shichino, T. *et al.* Effects of inhalation anaesthetics on the release of acetylcholine in the rat cerebral cortex in vivo. *Br. J. Anaesth.* **80**, 365–370 (1998).
143. Shichino, T. *et al.* Effects of xenon on acetylcholine release in the rat cerebral cortex in vivo. *Br. J. Anaesth.* **88**, 866–868 (2002).
144. Siclari, F. *et al.* The neural correlates of dreaming. *Nat. Neurosci.* **20**, 872–878 (2017).

145. Steriade, M. Acetylcholine systems and rhythmic activities during the waking–sleep cycle. in *Progress in Brain Research* vol. 145 179–196 (Elsevier, 2004).
146. Shichino, T. *et al.* Effects of isoflurane on in vivo release of acetylcholine in the rat cerebral cortex and striatum. *Acta Anaesthesiol. Scand.* **41**, 1335–1340 (1997).
147. Kikuchi, T., Wang, Y., Sato, K. & Okumura, F. In vivo effects of propofol on acetylcholine release from the frontal cortex, hippocampus and striatum studied by intracerebral microdialysis in freely moving rats. *Br. J. Anaesth.* **80**, 644–648 (1998).
148. Kikuchi, T., Wang, Y., Shinbori, H., Sato, K. & Okumura, F. Effects of ketamine and pentobarbitone on acetylcholine release from the rat frontal cortex in vivo. *Br. J. Anaesth.* **79**, 128–130 (1997).
149. Nemoto, C. *et al.* Effects of dexmedetomidine, midazolam, and propofol on acetylcholine release in the rat cerebral cortex in vivo. *J. Anesth.* **27**, 771–774 (2013).
150. Pal, D. & Mashour, G. A. Consciousness, Anesthesia, and Acetylcholine. *Anesthesiology* **134**, 515–517 (2021).
151. Östberg, A. *et al.* Cholinergic dysfunction after traumatic brain injury: Preliminary findings from a PET study. *Neurology* **76**, 1046–1050 (2011).
152. Walker, C. O., Speeg, K. V., Levinson, J. D. & Schenker, S. Cerebral Acetylcholine, Serotonin, and Norepinephrine in Acute Ammonia Intoxication. *Proc. Soc. Exp. Biol. Med.* **136**, 668–671 (1971).
153. Parker, T. H., Roberts, R. K., Vorhees, C. V., Schmidt, D. E. & Schenker, S. The effect of acute and subacute ammonia intoxication on regional cerebral acetylcholine levels in rats. *Biochem. Med.* **18**, 235–244 (1977).
154. Howe, W. M. *et al.* Acetylcholine Release in Prefrontal Cortex Promotes Gamma Oscillations and Theta–Gamma Coupling during Cue Detection. *J. Neurosci.* **37**, 3215–3230 (2017).
155. McCormick, D. A. Cholinergic and noradrenergic modulation of thalamocortical processing. *Trends Neurosci.* **12**, 215–221 (1989).
156. McCormick, D. A. Neurotransmitter actions in the thalamus and cerebral cortex and their role in neuromodulation of thalamocortical activity. *Prog. Neurobiol.* **39**, 337–388 (1992).
157. Li, Q., Song, J.-L., Li, S.-H., Westover, M. B. & Zhang, R. Effects of Cholinergic Neuromodulation on Thalamocortical Rhythms During NREM Sleep: A Model Study. *Front. Comput. Neurosci.* **13**, 100 (2020).
158. Pal, D. *et al.* Differential Role of Prefrontal and Parietal Cortices in Controlling Level of Consciousness. *Curr. Biol.* **28**, 2145-2152.e5 (2018).
159. Pal, D. *et al.* Level of Consciousness Is Dissociable from Electroencephalographic Measures of Cortical Connectivity, Slow Oscillations, and Complexity. *J. Neurosci.* **40**, 605–618 (2020).
160. Dehaene, S. & Changeux, J.-P. Experimental and Theoretical Approaches to Conscious Processing. *Neuron* **70**, 200–227 (2011).
161. Lee, U. *et al.* The directionality and functional organization of frontoparietal connectivity during consciousness and anesthesia in humans. *Conscious. Cogn.* **18**, 1069–1078 (2009).
162. Schrouff, J. *et al.* Brain functional integration decreases during propofol-induced loss of consciousness. *NeuroImage* **57**, 198–205 (2011).
163. Boly, M. *et al.* Connectivity changes underlying spectral EEG changes during propofol-induced loss of consciousness. *J. Neurosci. Off. J. Soc. Neurosci.* **32**, 7082–7090 (2012).

164. Hudetz, A. G. General anesthesia and human brain connectivity. *Brain Connect.* **2**, 291–302 (2012).
165. Jordan, D. *et al.* Simultaneous electroencephalographic and functional magnetic resonance imaging indicate impaired cortical top-down processing in association with anesthetic-induced unconsciousness. *Anesthesiology* **119**, 1031–1042 (2013).
166. Ranft, A. *et al.* Neural Correlates of Sevoflurane-induced Unconsciousness Identified by Simultaneous Functional Magnetic Resonance Imaging and Electroencephalography. *Anesthesiology* **125**, 861–872 (2016).
167. Schroeder, K. E. *et al.* Disruption of corticocortical information transfer during ketamine anesthesia in the primate brain. *NeuroImage* **134**, 459–465 (2016).
168. Li, D., Hambrecht-Wiedbusch, V. S. & Mashour, G. A. Accelerated Recovery of Consciousness after General Anesthesia Is Associated with Increased Functional Brain Connectivity in the High-Gamma Bandwidth. *Front. Syst. Neurosci.* **11**, 16 (2017).
169. Bodart, O. *et al.* Global structural integrity and effective connectivity in patients with disorders of consciousness. *Brain Stimulat.* **11**, 358–365 (2018).
170. Sanders, R. D. *et al.* Propofol-induced unresponsiveness is associated with impaired feedforward connectivity in cortical hierarchy. *Br. J. Anaesth.* **121**, 1084–1096 (2018).
171. Lewis, L. D. *et al.* Rapid fragmentation of neuronal networks at the onset of propofol-induced unconsciousness. *Proc. Natl. Acad. Sci.* **109**, E3377–E3386 (2012).
172. Ní Mhuircheartaigh, R., Warnaby, C., Rogers, R., Jbabdi, S. & Tracey, I. Slow-wave activity saturation and thalamocortical isolation during propofol anesthesia in humans. *Sci. Transl. Med.* **5**, 208ra148 (2013).
173. Purdon, P. L. *et al.* Electroencephalogram signatures of loss and recovery of consciousness from propofol. *Proc. Natl. Acad. Sci. U. S. A.* **110**, E1142–E1151 (2013).
174. Warnaby, C. E., Sleigh, J. W., Hight, D., Jbabdi, S. & Tracey, I. Investigation of Slow-wave Activity Saturation during Surgical Anesthesia Reveals a Signature of Neural Inertia in Humans. *Anesthesiol. J. Am. Soc. Anesthesiol.* **127**, 645–657 (2017).
175. Hudetz, A. G., Liu, X., Pillay, S., Boly, M. & Tononi, G. Propofol anesthesia reduces Lempel-Ziv complexity of spontaneous brain activity in rats. *Neurosci. Lett.* **628**, 132–135 (2016).
176. Kilkenny, C., Browne, W. J., Cuthill, I. C., Emerson, M. & Altman, D. G. Improving Bioscience Research Reporting: The ARRIVE Guidelines for Reporting Animal Research. *PLOS Biol.* **8**, e1000412 (2010).
177. Paxinos, C. & Watson, G. *The Rat Brain in Sterotaxic Coordinates*. (London Academic Press, 1996).
178. Borjigin, J. *et al.* Surge of neurophysiological coherence and connectivity in the dying brain. *Proc. Natl. Acad. Sci. U. S. A.* **110**, 14432–14437 (2013).
179. Castro, S., Falconi, A., Chase, M. H. & Torterolo, P. Coherent neocortical 40-Hz oscillations are not present during REM sleep. *Eur. J. Neurosci.* **37**, 1330–1339 (2013).
180. Castro, S. *et al.* Inter-hemispheric coherence of neocortical gamma oscillations during sleep and wakefulness. *Neurosci. Lett.* **578**, 197–202 (2014).
181. Delorme, A. & Makeig, S. EEGLAB: an open source toolbox for analysis of single-trial EEG dynamics including independent component analysis. *J. Neurosci. Methods* **134**, 9–21 (2004).
182. Ziv, J. & Lempel, A. A universal algorithm for sequential data compression. *Ieee Trans. Inf. Theory* **23**, 337–343 (1977).

183. Ziv, J. & Lempel, A. Compression of individual sequences via variable-rate coding. *IEEE Trans. Inf. Theory* **24**, 530–536 (1978).
184. R Core Team (2016). R: a language and environment for statistical computing (R Foundation for Statistical Computing). doi:https://www. R-project.org/.
185. Kenny, J. D., Taylor, N. E., Brown, E. N. & Solt, K. Dextroamphetamine (but Not Atomoxetine) Induces Reanimation from General Anesthesia: Implications for the Roles of Dopamine and Norepinephrine in Active Emergence. *PloS One* **10**, e0131914 (2015).
186. Alkire, M. T., Hudetz, A. G. & Tononi, G. Consciousness and anesthesia. *Science* **322**, 876–880 (2008).
187. Massimini, M. *et al.* Breakdown of cortical effective connectivity during sleep. *Science* **309**, 2228–2232 (2005).
188. Ferrarelli, F. *et al.* Breakdown in cortical effective connectivity during midazolam-induced loss of consciousness. *Proc. Natl. Acad. Sci. U. S. A.* **107**, 2681–2686 (2010).
189. Boly, M. *et al.* Preserved feedforward but impaired top-down processes in the vegetative state. *Science* **332**, 858–862 (2011).
190. Cimenser, A. *et al.* Tracking brain states under general anesthesia by using global coherence analysis. *Proc. Natl. Acad. Sci.* **108**, 8832–8837 (2011).
191. Changeux, J.-P. G. Conscious processing: implications for general anesthesia. *Curr. Opin. Anaesthesiol.* **25**, 397–404 (2012).
192. Rosanova, M. *et al.* Recovery of cortical effective connectivity and recovery of consciousness in vegetative patients. *Brain J. Neurol.* **135**, 1308–1320 (2012).
193. Uhrig, L. *et al.* Resting-state Dynamics as a Cortical Signature of Anesthesia in Monkeys. *Anesthesiology* **129**, 942–958 (2018).
194. Hemmings, H. C. *et al.* Towards a Comprehensive Understanding of Anesthetic Mechanisms of Action: A Decade of Discovery. *Trends Pharmacol. Sci.* **40**, 464–481 (2019).
195. Mashour, G. A. & Hudetz, A. G. Bottom-Up and Top-Down Mechanisms of General Anesthetics Modulate Different Dimensions of Consciousness. *Front. Neural Circuits* **11**, (2017).
196. Li, D. *et al.* Dynamic Cortical Connectivity during General Anesthesia in Healthy Volunteers. *Anesthesiology* **130**, 870–884 (2019).
197. Vlisides, P. E. *et al.* Dynamic Cortical Connectivity during General Anesthesia in Surgical Patients. *Anesthesiology* **130**, 885–897 (2019).
198. Hudson, A. E., Calderon, D. P., Pfaff, D. W. & Proekt, A. Recovery of consciousness is mediated by a network of discrete metastable activity states. *Proc. Natl. Acad. Sci. U. S. A.* **111**, 9283–9288 (2014).
199. Brown, E. N., Lydic, R. & Schiff, N. D. General Anesthesia, Sleep, and Coma. *N. Engl. J. Med.* **363**, 2638–2650 (2010).
200. Hobson, J. A. REM sleep and dreaming: towards a theory of protoconsciousness. *Nat. Rev. Neurosci.* **10**, 803–813 (2009).
201. Sidorov, M. S. *et al.* Delta rhythmicity is a reliable EEG biomarker in Angelman syndrome: a parallel mouse and human analysis. *J. Neurodev. Disord.* **9**, 17 (2017).
202. Qiu, M.-H., Chen, M. C. & Lu, J. Cortical neuronal activity does not regulate sleep homeostasis. *Neuroscience* **297**, 211–218 (2015).

203. Gaskell, A. L. *et al.* Frontal alpha-delta EEG does not preclude volitional response during anaesthesia: prospective cohort study of the isolated forearm technique. *Br. J. Anaesth.* **119**, 664–673 (2017).
204. Sanders, R. D., Mostert, N., Lindroth, H., Tononi, G. & Sleigh, J. Is consciousness frontal? Two perioperative case reports that challenge that concept. *BJA Br. J. Anaesth.* **121**, 330–332 (2018).
205. Maksimow, A. *et al.* Increase in high frequency EEG activity explains the poor performance of EEG spectral entropy monitor during S-ketamine anesthesia. *Clin. Neurophysiol. Off. J. Int. Fed. Clin. Neurophysiol.* **117**, 1660–1668 (2006).
206. Tagliazucchi, E., Carhart-Harris, R., Leech, R., Nutt, D. & Chialvo, D. R. Enhanced repertoire of brain dynamical states during the psychedelic experience. *Hum. Brain Mapp.* **35**, 5442–5456 (2014).
207. Lydic, R. & Baghdoyan, H. A. Sleep, Anesthesiology, and the Neurobiology of Arousal State Control. *J. Am. Soc. Anesthesiol.* **103**, 1268–1295 (2005).
208. Pillay, S., Liu, X., Baracskay, P. & Hudetz, A. G. Brainstem Stimulation Increases Functional Connectivity of Basal Forebrain-Paralimbic Network in Isoflurane-Anesthetized Rats. *Brain Connect.* **4**, 523–534 (2014).
209. Alkire, M. T., McReynolds, J. R., Hahn, E. L. & Trivedi, A. N. Thalamic microinjection of nicotine reverses sevoflurane-induced loss of righting reflex in the rat. *Anesthesiology* **107**, 264–272 (2007).
210. Solt, K. *et al.* Electrical Stimulation of the Ventral Tegmental Area Induces Reanimation from General Anesthesia. *Anesthesiology* **121**, 311–319 (2014).
211. Taylor, N. E. *et al.* Optogenetic activation of dopamine neurons in the ventral tegmental area induces reanimation from general anesthesia. *Proc. Natl. Acad. Sci.* **113**, 12826–12831 (2016).
212. Alkire, M. T., Asher, C. D., Franciscus, A. M. & Hahn, E. L. Thalamic microinfusion of antibody to a voltage-gated potassium channel restores consciousness during anesthesia. *Anesthesiology* **110**, 766–773 (2009).
213. Solt, K. *et al.* Methylphenidate actively induces emergence from general anesthesia. *Anesthesiology* **115**, 791–803 (2011).
214. Chemali, J. J., Van Dort, C. J., Brown, E. N. & Solt, K. Active emergence from propofol general anesthesia is induced by methylphenidate. *Anesthesiology* **116**, 998–1005 (2012).
215. Muindi, F. *et al.* Electrical stimulation of the parabrachial nucleus induces reanimation from isoflurane general anesthesia. *Behav. Brain Res.* **306**, 20–25 (2016).
216. Gao, S., Proekt, A., Renier, N., Calderon, D. P. & Pfaff, D. W. Activating an anterior nucleus gigantocellularis subpopulation triggers emergence from pharmacologically-induced coma in rodents. *Nat. Commun.* **10**, 2897 (2019).
217. Brito, M. A., Li, D., Mashour, G. A. & Pal, D. State-Dependent and Bandwidth-Specific Effects of Ketamine and Propofol on Electroencephalographic Complexity in Rats. *Front. Syst. Neurosci.* **14**, (2020).
218. Mashour, G. A. The controversial correlates of consciousness. *Science* **360**, 493–494 (2018).
219. Seth, A. K., Izhikevich, E., Reeke, G. N. & Edelman, G. M. Theories and measures of consciousness: An extended framework. *Proc. Natl. Acad. Sci.* **103**, 10799–10804 (2006).
220. Gosseries, O., Di, H., Laureys, S. & Boly, M. Measuring consciousness in severely damaged brains. *Annu. Rev. Neurosci.* **37**, 457–478 (2014).

221. Ferenets, R., Vanluchene, A., Lipping, T., Heyse, B. & Struys, M. M. R. F. Behavior of entropy/complexity measures of the electroencephalogram during propofol-induced sedation: dose-dependent effects of remifentanil. *Anesthesiology* **106**, 696–706 (2007).
222. Sklar, G. S. Techniques and Instruments: Adverse reactions to ketamine anesthesia, abolition by a psychological technique. *Plast. Reconstr. Surg.* **68**, 843 (1981).
223. Leslie, K., Skrzypek, H., Paech, M. J., Kurowski, I. & Whybrow, T. Dreaming during anesthesia and anesthetic depth in elective surgery patients: a prospective cohort study. *Anesthesiology* **106**, 33–42 (2007).
224. Kelland, M. D., Soltis, R. P., Boldry, R. C. & Walters, J. R. Behavioral and electrophysiological comparison of ketamine with dizocilpine in the rat. *Physiol. Behav.* **54**, 547–554 (1993).
225. Hunt, M. J., Raynaud, B. & Garcia, R. Ketamine Dose-Dependently Induces High-Frequency Oscillations in the Nucleus Accumbens in Freely Moving Rats. *Biol. Psychiatry* **60**, 1206–1214 (2006).
226. Hakami, T. *et al.* NMDA Receptor Hypofunction Leads to Generalized and Persistent Aberrant γ Oscillations Independent of Hyperlocomotion and the State of Consciousness. *PLoS ONE* **4**, (2009).
227. Pal, D. *et al.* Propofol, Sevoflurane, and Ketamine Induce a Reversible Increase in Delta-Gamma and Theta-Gamma Phase-Amplitude Coupling in Frontal Cortex of Rat. *Front. Syst. Neurosci.* **11**, 41 (2017).
228. Tononi, G. & Edelman, G. M. Consciousness and Complexity. *Science* **282**, 1846 (1998).
229. Laureys, S. The neural correlate of (un)awareness: lessons from the vegetative state. *Trends Cogn. Sci.* **9**, 556–559 (2005).
230. Mateos, D. M., Guevara Erra, R., Wennberg, R. & Perez Velazquez, J. L. Measures of entropy and complexity in altered states of consciousness. *Cogn. Neurodyn.* **12**, 73–84 (2018).
231. Akeju, O. *et al.* Electroencephalogram Signatures of Ketamine-Induced Unconsciousness. *Clin. Neurophysiol. Off. J. Int. Fed. Clin. Neurophysiol.* **127**, 2414–2422 (2016).
232. Záborszky, L. *et al.* Neurons in the Basal Forebrain Project to the Cortex in a Complex Topographic Organization that Reflects Corticocortical Connectivity Patterns: An Experimental Study Based on Retrograde Tracing and 3D Reconstruction. *Cereb. Cortex* **25**, 118–137 (2015).
233. Bokil, H., Andrews, P., Kulkarni, J. E., Mehta, S. & Mitra, P. Chronux: A Platform for Analyzing Neural Signals. *J. Neurosci. Methods* **192**, 146–151 (2010).
234. Lorenz, D. J., Datta, S. & Harkema, S. J. Marginal association measures for clustered data. *Stat. Med.* **30**, 3181–3191 (2011).
235. Vrijdag, X. C. E., van Waart, H., Mitchell, S. J. & Sleigh, J. W. An Electroencephalogram Metric of Temporal Complexity Tracks Psychometric Impairment Caused by Low-dose Nitrous Oxide. *Anesthesiology* **134**, 202–218 (2021).
236. Vollenweider, F. X. *et al.* Metabolic hyperfrontality and psychopathology in the ketamine model of psychosis using positron emission tomography (PET) and [18F]fluorodeoxyglucose (FDG). *Eur. Neuropsychopharmacol. J. Eur. Coll. Neuropsychopharmacol.* **7**, 9–24 (1997).
237. Vollenweider, F. X. *et al.* Positron emission tomography and fluorodeoxyglucose studies of metabolic hyperfrontality and psychopathology in the psilocybin model of psychosis. *Neuropsychopharmacol. Off. Publ. Am. Coll. Neuropsychopharmacol.* **16**, 357–372 (1997).

238. Abdallah, C. G. *et al.* The effects of ketamine on prefrontal glutamate neurotransmission in healthy and depressed subjects. *Neuropsychopharmacology* **43**, 2154–2160 (2018).
239. Mason, N. L. *et al.* Me, myself, bye: regional alterations in glutamate and the experience of ego dissolution with psilocybin. *Neuropsychopharmacology* **45**, 2003–2011 (2020).
240. Varley, T. F., Carhart-Harris, R., Roseman, L., Menon, D. K. & Stamatakis, E. A. Serotonergic psychedelics LSD & psilocybin increase the fractal dimension of cortical brain activity in spatial and temporal domains. *NeuroImage* **220**, 117049 (2020).
241. Benarroch, E. E. Acetylcholine in the cerebral cortex: Effects and clinical implications. *Neurology* **75**, 659–665 (2010).
242. Liljenstrom, H. & Hasselmo, M. E. Cholinergic modulation of cortical oscillatory dynamics. *J. Neurophysiol.* **74**, 288–297 (1995).
243. Poulet, J. F. A. & Crochet, S. The Cortical States of Wakefulness. *Front. Syst. Neurosci.* **12**, (2019).
244. Yi, F. *et al.* Direct excitation of parvalbumin-positive interneurons by M1 muscarinic acetylcholine receptors: roles in cellular excitability, inhibitory transmission and cognition. *J. Physiol.* **592**, 3463–3494 (2014).
245. Chen, L. *et al.* Basal Forebrain Cholinergic Neurons Primarily Contribute to Inhibition of Electroencephalogram Delta Activity, Rather Than Inducing Behavioral Wakefulness in Mice. *Neuropsychopharmacology* **41**, 2133–2146 (2016).
246. Colangelo, C., Shichkova, P., Keller, D., Markram, H. & Ramaswamy, S. Cellular, Synaptic and Network Effects of Acetylcholine in the Neocortex. *Front. Neural Circuits* **13**, (2019).
247. Mathot, S. Pupillometry: Psychology, Physiology, and Function. *J. Cogn.* **1**, 16 (2018).
248. Turi, M., Burr, D. C. & Binda, P. Pupillometry reveals perceptual differences that are tightly linked to autistic traits in typical adults. *eLife* **7**, e32399 (2018).
249. Montes-Lourido, P., Kar, M., Kumbam, I. & Sadagopan, S. Pupillometry as a reliable metric of auditory detection and discrimination across diverse stimulus paradigms in animal models. *Sci. Rep.* **11**, 3108 (2021).
250. Kirkwood, A., Rioult, M. G. & Bear, M. F. Experience-dependent modification of synaptic plasticity in visual cortex. *Nature* **381**, 526–528 (1996).
251. Normann, C., Schmitz, D., Fürmaier, A., Döing, C. & Bach, M. Long-Term Plasticity of Visually Evoked Potentials in Humans is Altered in Major Depression. *Biol. Psychiatry* **62**, 373–380 (2007).
252. Cambiaghi, M. *et al.* Flash visual evoked potentials in mice can be modulated by transcranial direct current stimulation. *Neuroscience* **185**, 161–165 (2011).
253. You, Y., Thie, J., Klistorner, A., Gupta, V. K. & Graham, S. L. Normalization of Visual Evoked Potentials Using Underlying Electroencephalogram Levels Improves Amplitude Reproducibility in Rats. *Invest. Ophthalmol. Vis. Sci.* **53**, 1473–1478 (2012).
254. Mishra, A. & Colgin, L. L. The High Energy Cost of Theta–Gamma Activity during REM Sleep. *Trends Neurosci.* **42**, 239–241 (2019).
255. Kalev, K., Bachmann, M., Orgo, L., Lass, J. & Hinrikus, H. Lempel-Ziv and multiscale Lempel-Ziv complexity in depression. in *2015 37th Annual International Conference of the IEEE Engineering in Medicine and Biology Society (EMBC)* 4158–4161 (2015). doi:10.1109/EMBC.2015.7319310.

256. Garwood, I. C. *et al.* A hidden Markov model reliably characterizes ketamine-induced spectral dynamics in macaque local field potentials and human electroencephalograms. *PLOS Comput. Biol.* **17**, e1009280 (2021).
257. Nicol, A. U. & Morton, A. J. Characteristic patterns of EEG oscillations in sheep (Ovis aries) induced by ketamine may explain the psychotropic effects seen in humans. *Sci. Rep.* **10**, 9440 (2020).
258. Li, Y. *et al.* Abnormal EEG complexity in patients with schizophrenia and depression. *Clin. Neurophysiol.* **119**, 1232–1241 (2008).
259. Ibáñez-Molina, A. J. *et al.* EEG Multiscale Complexity in Schizophrenia During Picture Naming. *Front. Physiol.* **9**, (2018).
260. Frohlich, J. *et al.* Emergence of consciousness and complexity amidst diffuse delta rhythms: the paradox of Angelman syndrome.
261. Sidorov, M. S. *et al.* Delta rhythmicity is a reliable EEG biomarker in Angelman syndrome: a parallel mouse and human analysis. *J. Neurodev. Disord.* **9**, 17 (2017).
262. Konkoly, K. R. *et al.* Real-time dialogue between experimenters and dreamers during REM sleep. *Curr. Biol.* **31**, 1417-1427.e6 (2021).
263. Carlén, M. *et al.* A critical role for NMDA receptors in parvalbumin interneurons for gamma rhythm induction and behavior. *Mol. Psychiatry* **17**, 537–548 (2012).
264. Rampil, I. J., Kim, J.-S., Lenhardt, R., Negishi, C. & Sessler, D. I. Bispectral EEG Index during Nitrous Oxide Administration. *Anesthesiology* **89**, 671-677. (1998).
265. Hirota, K. Special cases: ketamine, nitrous oxide and xenon. *Best Pract. Res. Clin. Anaesthesiol.* **20**, 69–79 (2006).
266. Pelentritou, A. *et al.* Source-level Cortical Power Changes for Xenon and Nitrous Oxide–induced Reductions in Consciousness in Healthy Male Volunteers. *Anesthesiology* **132**, 1017–1033 (2020).
267. Anticevic, A. *et al.* N-Methyl-D-Aspartate Receptor Antagonist Effects on Prefrontal Cortical Connectivity Better Model Early Than Chronic Schizophrenia. *Biol. Psychiatry* **77**, 569–580 (2015).
268. Douglas, C. L., Baghdoyan, H. A. & Lydic, R. Postsynaptic Muscarinic M1 Receptors Activate Prefrontal Cortical EEG of C57BL/6J Mouse. *J. Neurophysiol.* **88**, 3003–3009 (2002).
269. Castro-Zaballa, S. *et al.* EEG dissociation induced by muscarinic receptor antagonists: Coherent 40 Hz oscillations in a background of slow waves and spindles. *Behav. Brain Res.* **359**, 28–37 (2019).
270. Léna, C. *et al.* Beta2-containing nicotinic receptors contribute to the organization of sleep and regulate putative micro-arousals in mice. *J. Neurosci. Off. J. Soc. Neurosci.* **24**, 5711–5718 (2004).
271. Madrid-López, N. *et al.* The Sleep–Wake Cycle in the Nicotinic Alpha-9 Acetylcholine Receptor Subunit Knock-Out Mice. *Front. Cell. Neurosci.* **11**, 302 (2017).
272. Djemil, S. *et al.* Activation of nicotinic acetylcholine receptors induces potentiation and synchronization within in vitro hippocampal networks. *J. Neurochem.* **153**, 468–484 (2020).
273. Záborszky, L. *et al.* Specific Basal Forebrain–Cortical Cholinergic Circuits Coordinate Cognitive Operations. *J. Neurosci.* **38**, 9446–9458 (2018).
274. Semba, K. Multiple output pathways of the basal forebrain: organization, chemical heterogeneity, and roles in vigilance. *Behav. Brain Res.* **115**, 117–141 (2000).

275. Gritti, I., Manns, I. D., Mainville, L. & Jones, B. E. Parvalbumin, calbindin, or calretinin in cortically projecting and GABAergic, cholinergic, or glutamatergic basal forebrain neurons of the rat. *J. Comp. Neurol.* **458**, 11–31 (2003).
276. Záborszky, L. *et al.* Chapter 19 - Organization of the Basal Forebrain Cholinergic Projection System: Specific or Diffuse? in *The Rat Nervous System (Fourth Edition)* (ed. Paxinos, G.) 491–507 (Academic Press, 2015). doi:10.1016/B978-0-12-374245-2.00019-X.
277. Anaclet, C. *et al.* Basal forebrain control of wakefulness and cortical rhythms. *Nat. Commun.* **6**, 8744 (2015).
278. Zant, J. C. *et al.* Cholinergic Neurons in the Basal Forebrain Promote Wakefulness by Actions on Neighboring Non-Cholinergic Neurons: An Opto-Dialysis Study. *J. Neurosci. Off. J. Soc. Neurosci.* **36**, 2057–2067 (2016).
279. Chen, L. *et al.* Basal Forebrain Cholinergic Neurons Primarily Contribute to Inhibition of Electroencephalogram Delta Activity, Rather Than Inducing Behavioral Wakefulness in Mice. *Neuropsychopharmacology* **41**, 2133–2146 (2016).
280. Nair, J. *et al.* Basal forebrain contributes to default mode network regulation. *Proc. Natl. Acad. Sci.* **115**, 1352–1357 (2018).
281. Turchi, J. *et al.* The Basal Forebrain Regulates Global Resting-State fMRI Fluctuations. *Neuron* **97**, 940-952.e4 (2018).
282. Manns, I. D., Mainville, L. & Jones, B. E. Evidence for glutamate, in addition to acetylcholine and GABA, neurotransmitter synthesis in basal forebrain neurons projecting to the entorhinal cortex. *Neuroscience* **107**, 249–263 (2001).
283. Kim, T. *et al.* Cortically projecting basal forebrain parvalbumin neurons regulate cortical gamma band oscillations. *Proc. Natl. Acad. Sci.* **112**, 3535–3540 (2015).
284. Ng, L. H. L. *et al.* Ketamine and selective activation of parvalbumin interneurons inhibit stress-induced dendritic spine elimination. *Transl. Psychiatry* **8**, 1–15 (2018).
285. Picard, N., Takesian, A. E., Fagiolini, M. & Hensch, T. K. NMDA 2A receptors in parvalbumin cells mediate sex-specific rapid ketamine response on cortical activity. *Mol. Psychiatry* **24**, 828–838 (2019).
286. Martin, D. A. & Nichols, C. D. Psychedelics Recruit Multiple Cellular Types and Produce Complex Transcriptional Responses Within the Brain. *EBioMedicine* **11**, 262–277 (2016).